ADDIS ABABA UNIVERSITY

ADDIS ABABA INSTITUTE OF TECHNOLOGY

SCHOOL OF MECHANICAL AND INDUSTRIAL ENGINEERING

Numerical Simulation of Passenger Train Aerodynamics in Tunnels

By

Gizachew Endale

A thesis Submitted to the School of Graduate Studies of Addis Ababa University in Partial Fulfillment of the Requirements for the Degree of Masters of Science in Mechanical Engineering (Under Railway Engineering)

Advisor

Mr. Habtamu Tkubet

September, 2017

Addis Ababa, Ethiopia

ADDIS ABABA UNIVERSITY

ADDIS ABABA INSTITUTE OF TECHNOLOGY

SCHOOL OF MECHANICAL AND INDUSTRIAL ENGINEERING

Master's Program Final Thesis Acceptance Approval Form

Thesis Title: - Numerical Simulation of Passenger Train Aerodynamics in Tunnels

By

Gizachew Endale

September, 2017

Approved by Board of Examiners

Dr. Daniel Tilahun A/Head, Railway Center	Signature	04/10/2017 Date
Habtamu Tkubet (M.Sc.) Advisor	Signature	04/10/17 Date
Dr. Yilma Tadesse Internal Examiner	Signature	04/10/2017 Date
Dr. Solomon T/Mariam External Examiner	Signature	29/09/17 Date

DECLARATION

I hereby declare that this thesis paper entitled "**Numerical Simulation of Passenger Train Aerodynamics in Tunnels**" is the result of my own original work carried out under the supervision of Mr. Habtamu Tkubet. I solemnly declare that this thesis is not submitted to any other institution and universities anywhere for the awards of any certificate and that all sources of material that are used for this thesis have been duly acknowledged and that I have used no other sources and aids other than those indicated.

Gizachew Endale Signature: -____________________

[Author] Date: - ____________________

This is to certify that the above declaration made by the candidate is correct to the best of my knowledge.

Habtamu Tkubet Signature: - ____________________

[Advisor] Date: - ____________________

Place: - Addis Ababa, Ethiopia

DEDICATION

To

Almighty God

For his immeasurable love and encouragement!

ACKNOWLEDGMENT

All praises and thanks be to GOD who guided me to this, never could I have go far this, were it not that GOD had helped me!

I gratefully acknowledge my advisor Mr.Habtamu Tkubet (Addis Ababa University) for his valuable guidance and continuous encouragement throughout the time. I would like to express my gratitude to the staff of the Ethiopian Railway Corporation (ERC) for kindly providing detailed data's and available resources of Weldia-Mekelle railway line. I would like to thank AAiT and all stuff of Department of Mechanical and Industrial Engineering for their great supports on completion of the courses and for their contribution to this work.

Finally I would like express my gratitude and heartfelt thanks to friends and peoples who were next to me for their devotion and support during this master's thesis and also during those study times, cannot find the appropriate words that could properly describe my appreciation.

Without your help this project would not have been possible!

ABSTRACT

In the present study, an analysis to investigate the aerodynamic drag and related pressure characteristics of the passenger train traveling in tunnel is performed. In particular, the effect of aerodynamic loads on the Ethiopian National passenger train at speed of 120 km/hr operating in open field and as it travels through in currently constructing Addi-onfito tunnel with 179m length is analyzed. The aerodynamic drag and pressure loads developed on the train are estimated and compared; while the train is moving in open field and while the train travels in the tunnel. In addition the study also investigated the effect of the blockage ratio of an underground train upon the aerodynamic drag and pressure developed on a train body, by altering the train-tunnel gaps. The investigation uses computational fluid dynamics techniques (CFD). First a numerical simulation was developed to estimate the aerodynamic drag and peak pressures on operational passenger train operating in open filed and underground railway with existing tunnel cross-sectional area and blockage ratio which is currently under construction. The results of the study show that in existing high blockage ratio underground railways, the pressure acting on the train body experienced huge fluctuations as the train moved along the current Addi-onfito tunnel. The maximum pressure change (ΔP_{max}) on the train body reaches around the value of 4.36 kPa, which exceeds the maximum admissible limit of change in pressure on train body travelling in tunnel. There is significant increment of the aerodynamic drag approximately 3.65 times that of the train in open field. Peak-pressures experienced are also greater on all train position when the train travels in the tunnel as compared to the train travelling in open field. Then the blockage ratio of the underground railway is varied (by increasing the train-tunnel gaps) to evaluate the effects upon aerodynamic drag and pressure developed. The simulation results shows that due to reduction of the blockage ratio by 12.19% of train in tunnel the value of maximum pressure change (ΔP_{max}) on the train body reduced to around 3.20 kPa, which satisfy the maximum admissible limit of change in pressure on train body travelling in tunnel. Due to reduction of blockage ratio; the magnitude of the drag force decreased by 28.46% at constant train speed and tunnel length. These results of reduction of aerodynamic drag and pressure is enormous indicating that without affecting the shape and speed of the train one can save 28.48% of aerodynamic power requirements by little modification of the blockage ratio.

Key words: *Train, Tunnel, Blockage ratio, Aerodynamic drag, Pressure, Velocity.*

Contents

LIST OF FIGURES

LIST OF TABLES

NOMENCLATURES

Symbol

A_{tr} Cross-sectional area of the train

A_{tu} Cross-sectional area of the tunnel

β Blockage ratio

β_1 Blockage ratio for tunnel 1

β_2 Blockage ratio for tunnel 2

$C(a)$ Speed of sound

CFD Computational Fluid Dynamics

C_1 Rolling resistance

$C_2 v_{tr}$ Momentum resistance

C_L Coefficient of Lift

C_D Coefficient of Drag

C_{D1-max} Maximum drag coefficient on blockage ratio β_1

C_{D2-max} Maximum drag coefficient on blockage ratio β_2

C_M Coefficient of Moment

C_P Coefficient of Pressure

C_{P1-max} Maximum pressure coefficient on blockage ratio β_1

C_{P2-max} Maximum pressure coefficient on blockage ratio β_2

C_q Specific Heat Capacity

cvt^2 Aerodynamic drag

C_d Coefficient of Aerodynamic drag

D Equivalent diameter of tunnel

D_h Hydraulic diameter of tunnel

F_D Drag force

F_L Lift force

F_{PX} Pressure drag

F_R Total drag

$F_{\tau x}$ Friction drag

g Gravity constant

$k-\varepsilon$ K-epsilon turbulent model

K Coefficient of thermal conductivity

k Turbulent kinetic energy

L The characteristics length of the train

L_{tr} Length of the train

L_{tu} Length of the tunnel

M Moment

Ma Mach number

P Pressure

$P_{sta1-max}$ Maximum static pressure on blockage ratio β_1

$P_{sta2-max}$ Maximum static pressure on blockage ratio β_2

Δp_{comp} Compression wave

Re Reynolds number

Re_x Reynolds number along a position x

t Time frame

T_f Tunnel factor

T Temperature

V_{tr} Train velocity

Y_a Vertical upper gap between the train and tunnel

Y_{tr} Height of train

Y_{tu} Height of tunnel

Z_a Horizontal gap between the train and tunnel

Z_{tr} Width of train

Z_{tu} Width of tunnel

X_p Distance between the entrance portal and the train head

Greek letter

α Leakage ratio

ρ Density

τ Shear stress

α Angle of attack

γ Ratio of specific heat

λ Friction wall factor

λ' Friction factor of the train

$\lambda_{m'}$ Friction factor of the train model

µ Static viscosity

μ_t Turbulence viscosity

ϑ Dynamic viscosity

φ Energy dissipation

ϕ Cross-sectional area ratio

Φ Viscose dissipation

ν Kinetic viscosity

Ɛ Turbulent energy dissipation rate

ABBREVIATIONS

AALR Addis Ababa Light Rail Transit

$AAiT$ Addis Ababa institute of technology

CFD Computational fluid dynamics

ERC Ethiopian Railway Corporation

FEM Finite element method

HST High speed train

LES Large eddy simulation

NWF Non-equilibrium wall function

$NRNE$ National Railway Network of Ethiopia

$RANS$ Reynolds-Average Navier-strokes

RSM Reynolds stress model

UIC International union of railway

$URANS$ Unsteady Reynolds-average nervier-strokes

CHAPTER 1: - INTRODUCTION

1.1 Background

Geographical limitations have always been a major concern in constructing transportation lines. In order to have sufficient land for industries, infrastructures, water catchments and military needs, underground spaces have been put into good use. In Ethiopia, as demand for a more efficient railway transport system to accommodate the rising population increases, alternatives such as underground spaces have been explored and made available.

The development of new transportation technologies and the improvement of the existing systems in the railway field have led to the increase of the commercial speed and reduce the geographical effect, and therefore to the design and building of new underground lines is an interest. Examples include the tunnels to be built in Ethiopia through the newly introduced Weldia – Mekelle railway line which consists of 6 tunnels with total 9 km.[1] A series of other planned railway lines are also aggressively setting up new underground transit systems. With the transport lines built underground, the trains are expected to operate in confined spaces over a long period of time. These new lines need straighter tracks and thus require longer and more numerous tunnel sections in order to avoid obstacles and to reduce environmental impacts.

Traditionally, train aerodynamic problems were not considered a priority except for drag reduction. However, with the increasing the speed of trains, aerodynamic effects became a major issue for both train operators and train manufacturers. The aerodynamic phenomena are of interests, such as the pressure variation while the train is driving in a tunnel, the study of the consequences of a crosswind, the study of the train rollover or the slipstream. When a train runs, a strong head pressure pulse is created at the very front of the train which leads to a change of pressure in the surrounding. A low pressure bubble is also created at the rear part of the train but is less strong than the first one, and is mostly a problem for people or objects standing near to the track when the train travels in open air. [2]

When a train moves in open-air, it generates region of highly turbulent flow known as a slipstream. The slipstream is generally associated with high air velocities and rapidly-changing pressure fields. These two effects can create significant problems for passengers on platforms, trackside workers and also for the stability of high-speed trains if running in strong side winds. However, when a train passes a confined space such as a tunnel, additional aerodynamic issues appear, which are different than those in the open air. This can be explained through the underlying phenomena such as the compressibility of the air around high-speed trains due to running in a confined space, which produces pressure transients along the tunnel. When train enters a tunnel the air at the train nose is compressed which creates an overpressure wave that migrates at the speed of sound. When this waves reaches the end of the tunnel a part of the wave is reflected and goes back as an under-pressure wave. These pressure waves cause relevant aerodynamic loads on vehicle and tunnel structures. Aerodynamic noise, forces and moments acting on the train, and especially the aerodynamic drag, grow due to the confinement of the surrounding space. With the transport lines built underground, the trains are expected to operate in confined spaces over a long period of time. Drag, velocity, pressure variation and direction of the flow inside tunnels are different and greater than those around a train in open air. According to the previous works, the blockage ratio (ratio of the cross-sectional areas of train to tunnel) has been known to be one of the most important parameters influencing the aerodynamics of train/tunnel systems [5].

The focus of this paper is to estimate the aerodynamic loads on passenger train operating at speed of 120km/hr in open field and while operating in presented Addi-onfito tunnel configuration, which is one of the tunnels in Weldia-Mekelle railway line. In addition numerical simulation and theory analysis are adopted to study the effect of blockage ratio on the aerodynamic drag and pressure characteristics on the train. The numerical predictions are conducted using a commercial CFD code ANSYS Fluent.

1.2 Statements of the problem

Aerodynamic loads represent an integral part of general loads that effect on operating rail vehicles. The aerodynamic problems occurring when train travels in tunnel are more complicated and serious, compared with the open air traveling. This aerodynamic problems are due to generation of compression and expansion of pressure waves when the train moves through the tunnel, and as travels inside the tunnel. These pressure waves cause relevant aerodynamic loads on vehicle and tunnel structures; aerodynamic noise, forces and moments acting on the train, and especially the aerodynamic drag, grow due to the confinement of the surrounding space. These aerodynamic phenomena gain in complexity and importance as the train speed and the blockage ratio (ratio of vehicle to free tunnel cross-section area) increase.

Aerodynamic drag is by far the major contribution to the total drag for trains travelling in tunnels; the entity of this drag [4, 5] depends on primarily on the train speed and the blockage ratio. Other secondary factors include the length of the tunnel (compared to the train), the configurations of the tunnel network geometry and surface (existence of airshafts and portal shaping etc.), and the presence of multiple trains in the tunnel (especially the crossing of trains). If the estimation and tests on the aerodynamic loads developed on train is underestimated during design, either the required operating speed cannot be attained, or the maximum pressure change resulting can exceed safety limits.

Whilst designing new trains and underground lines, simulations to estimate the aerodynamic drag, pressure difference and air velocity have proved to be mandatory to remain safety. Otherwise the amplitude of waves and pressure difference grows and pressurized vehicles could be required; the air flow velocity increases and unsteady compressible effects become dominant; moreover, the train drag rises, leading to extremely high power requirements for high-speed motion, eventually limiting the maximum speed allowed by the power supply system.

In this paper numerical simulation were conducted to estimate the aerodynamic loads on passenger train while operating in open field and in present Addi-onfito tunnel. The study also investigate the effect of the blockage ratio (by altering train-tunnel gaps) with a particular emphasis on the influence of the aerodynamic drag and pressure developed when the train travels in tunnel. Simulations on several positions of the train with respect to the tunnel were performed using CFD methods.

1.3 Research objective

1.3.1 General objective

The objective of this paper is to estimate the aerodynamic loads of a passenger train travelling through a tunnel using Computational Fluid Dynamics (CFD) method. The study also covers the effect of the blockage ratio (by altering train-tunnel gaps) with a particular emphasis on the influence of the aerodynamic drag and peak-pressure developed on the train as it travels in tunnel.

1.3.2 Specific objectives

The specific objective of this paper is to study on:

- Estimation of extreme peak pressures and aerodynamic drag that could potentially be generated during a passenger train moves through the tunnel.
- Variation of pressure and aerodynamic drag acting on the passenger train, when the train is moving in open field and as it travels through the tunnel.
- The relationship between the blockage ratio and the aerodynamic loads of; pressure peaks and aerodynamic drag developed on train.
- The variation of values of peak pressure, aerodynamic drag, and air flows around the train on different intersecting location of train inside the tunnel.
- Effect of aerodynamic drag on the energy efficiency (in terms of traction power reduction) of a train travelling in a tunnel.

1.4 Delimitations/Scope of the Research

This research studies is mainly concerned on the study of the aerodynamic behavior of drag, pressure and air flow developed on a passenger train operating in open field and as it travels in confined spaces (tunnels). Numerical simulation were also conducted to investigate the effect of blockage ratio on the aerodynamic loads acting on the train. The paper study particularly in the passenger train traveling in the tunnel at constant speed of 120km/hr, therefore effect of train speed on the aerodynamic loads is not considered. The simulation were conducted based on a single track tunnel (not a double track), therefore there will be no attempt to investigate the effect of passing of multiple trains inside tunnel. The study don't demonstrate full-scale experiment to investigate the aerodynamics of the train in tunnels. However a brief review of literatures on mechanisms of investigating the aerodynamics loads on passenger railway vehicle will be presented.

1.5 Significance of the research

Aerodynamic phenomena in confined spaces such as tunnels have received the attention of researchers, especially with issues of aerodynamic drag, vibration and pressure variations of trains in tunnels. The train aerodynamics plays an influential role for achieving the design train speed. Whilst designing new train tunnels; simulations to estimate the aerodynamic drag, peak-pressure and air velocity have proved to be mandatory to remain safety of rail equipment's in the tunnels, to achieve the desired speed and to fulfill increasing demand of customers' comfort during their journey. [6]

This research tries to investigate and estimate the aerodynamics resistance, pressure loads and air flow generated on the passenger railway vehicles operating in tunnels. The paper also investigate the effect of blockage ratio on the aerodynamic loads acting on the train. Since there are a lot has to be done studies in the area, it will give a comprehensive starting point for more advanced researches. The study also enhances our understanding on the aerodynamics of railway vehicles operating in tunnels, and it will provide a guideline for the manufacturing of trains and construction of the new underground railway lines built in Ethiopian railway transportation projects.

1.6 Research Methodology

The present work used Computational Fluid Dynamics (CFD) techniques in order to investigate the aerodynamic properties of drag, pressure and velocity fields around a train. To simulate the air flow around trains in tunnels, the Reynolds Averaged Navier-Stokes (RANS) method was used. The actual vehicle body dimension has been taken from ERC specification for the analysis. Details of the methodology will be presented in Chapter 3.

1.7 Structure/Outline of the paper

This report is divided into 5 chapters, starting with Chapter 1 as an introduction to the background of the study and the general rationale of the research. In chapter 2, starting out with background of train aerodynamics in tunnel, a critical literature review is carried out with a focus on the aerodynamics of trains in tunnels. Chapter 3 will introduce the reader to the work procedure and methodology of this study and also briefly explain the fundamental fluid dynamics and theory behind the computational fluid dynamics used in this study. This chapter will then be followed up by the Numerical simulation methods , introducing the reader to the model geometry of the train and tunnel, mesh and simulation settings. In the Chapter 4 the obtained and processed data will be presented and the results of simulations are analyzed and discussed. Furthermore, the findings are concluded in Chapter 5. Lastly, the paper finishes off with recommendations and indication for future works.

CHAPTER 2: - LITERATURE REVIEW

2.1 Introduction-Aerodynamics of train

The aerodynamics of railway vehicles covers a wide range topics reaching from the aerodynamic loads acting on structure and components of the train, the flow characteristics around the train influencing the efficiency of mechanical components and the aerodynamic influence of the train and its infrastructure. All these effects need to be investigated to ensure an efficient layout of the train in manufacturing, maintenance and operation. The specific description of the aerodynamic loads on a railway vehicle is one of the most relevant tasks for the construction and operation of modern trains. [8]

With the increase of the train speed, aerodynamics has become an important key in the rail vehicles field. The study of the aerodynamics of a train can lead to substantial cost savings and more environmental friendly trains. The most studied phenomenon in the realization of a train is the drag generated by the displacement of the train in the air flow. Reducing the drag leads to a reduction of the amount of energy needed. But some others aerodynamic phenomena are of interests, such as the pressure variations while the train is driving in a tunnel, the study of the consequences of a crosswind, the study of the train rollover or the slipstream. [7]

2.1.1 Aerodynamic problems of train

For the purpose of development of a faster and safer train system with lower air pollution and noise, many researchers are paying much attention on the aerodynamics of high-speed railway train. These works have attention to the development of new-generation train body, rail and tunnel systems. The aerodynamic phenomena with regard to high-speed railway train are strongly dependent on the train speed. Thus, the aerodynamic problems become more important as the train speed increases.

In general, the train aerodynamics are related to aerodynamic drag, pressure variations inside train, train-induced flows, cross-wind effects, ground effects, pressure waves inside tunnel, impulse waves at the exit of tunnel, noise and vibration, etc. The aerodynamic drag is dependent on the cross-sectional area of train body, train length, shape of train fore- and after-bodies, surface roughness of train body, and geographical conditions around the traveling train. The train-induced flows can influence passengers on the platform and is also associated with the cross-sectional area of train body, train length, shape of train fore- and after-bodies, surface roughness of train body, etc. The pressure variations, occurring as two trains intersecting each other, are related to passenger's comfort and safe traveling of train. These are dependent on the shape of train fore- and after-bodies, train width, and the distance between track lines. The cross-wind can also influence the safe traveling of the train, relating to train height and perimeter, bridge system, etc. [5]

Table 2-1, lists these major aerodynamic problems of high speed trains and associated factors. All of these aerodynamic problems are closely related to the train and tunnel shape, which is required to produce aerodynamically good characteristics.

Table 2-1: Aerodynamics problems and there related matter

	Aerodynamic problem	**Related matters**
1	Aerodynamics drag of train	Maximum speed, energy consumption
2	Aerodynamics characteristics of train due to cross winds	Safety in Strong cross-winds
3	Aerodynamics force due to passing-by of two trains	Running stability, Quality of comfort for passengers
4	Winds induced by train	Safety for passengers on platforms, safety for maintenance workers.
5	Pressure variation in tunnels	Quality of comfort for passengers, (Ear discomfort), Airtightness of vehicle, stress upon vehicle, ventilating system of vehicle
6	Micro-pressures waves radiating from tunnel exit	Environmental problems near tunnel exit
7	Ventilation and heat transfer in underground station and tunnel	Quality of comfort passengers, prevention of disaster (fire)
8	Aerodynamics noise	Environmental problems

2.2 Aerodynamics of railway train/tunnel systems

The aerodynamic problems occurring when train travels at high speed in tunnel are more complicated and serious, compared with the open air traveling. The aerodynamic drag and noises on the train are strongly dependent on the pressure waves in the tunnel. The aerodynamic drag on a train traveling in a tunnel can significantly increase, compared with that in the open air. [9, 10, 11]

2.2.1 Aerodynamic resistance

In general, a desirable train system should be aerodynamically stable and have low aerodynamic forces. These aerodynamic characteristics are closely associated with the aerodynamic drag of the running train. The aerodynamic drag on the traveling train is largely divided into mechanical and aerodynamic ones. Of both, the aerodynamic drag can influence the energy consumption of train. Thus, detailed understanding on the aerodynamic drag and its precise evaluation are of practical importance.

The train drag is divided into the aerodynamic drag, the sliding force between the wheel and rails, and the friction force caused by the pantograph system. The total drag of train was composed of the sum of each carriage drag [63].

Compared with the mechanical drag, the portion of the aerodynamic drag becomes larger as the train speed increases. Thus, reduction of the aerodynamic drag on high-speed railway train is one of the essential issues for the development of the desirable train system. In the open air without any cross-wind effects, the total drag on the traveling train can be expressed by a sum of the aerodynamic and mechanical ones [5]:

$$D = D_M + D_A = (a + bV)W + cV^2 \tag{2.1}$$

Where D_A and D_M are the aerodynamic and mechanical drags, respectively, a, b and c are the constants to be determined by the experiment, V the train speed and W the train weight.

In Eq. (6), the mechanical drag, being proportional to the train weight, includes the sliding drag between rails and train wheels, and the rotating drag of the wheels. The measurement of the total drag on train and its precise prediction are not straightforward. The total drag can be obtained by using a deceleration speed of train or the consumed electric power.

In the open air traveling, the aerodynamic drag on train can be divided into two contributions; one is dependent on train length and the other is independent of it. Therefore, the aerodynamic drag of the train is the sum of the tangential forces (skin friction drag) and the normal forces (pressure drag), both of which are parallel to the opposition direction of vehicle's velocity vector of positive x-axis direction. The pressure drag comes from the integral of the skin pressure of the train [63].

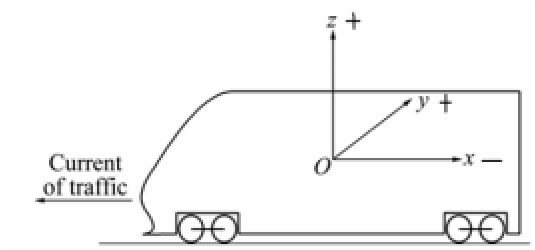

Figure 2-1 Coordinate definition of train [63]

The drag formula for the train in the open air can be expressed as:

$$F_x = F_{px} + F_{\tau x} \tag{2.2}$$

Where F_x is the aerodynamic drag, F_{px} is the pressure drag, and $F_{\tau x}$ is the friction drag. Therefore, the aerodynamic drag on the traveling train is divided into pressure drag and friction drag. That is, in real both pressure drag and friction drag are in the same direction, the sign of positive and negative does not have change for the value of total aerodynamic drag.

The drag independent of the train length is the pressure drag caused by the fore- and after-bodies of train. When the train runs there will be a stagnation region with high pressure on the windward face of the train nose, and the flow speed will decrease. At the same time, the flow moves at high velocity along the tail car and the pressure decreases. The pressure drag stems from the pressures due to the abrupt change in the cross-sectional area of the train.

The pressure drag can be obtained by integrating along the whole car.

$$F_{px} = \oint_{S_f} P_{bx} dS_f \tag{2.3}$$

Where P_{bx} is the skin pressure of the train along x axis, and S_f is the area of the train wall surface. For the high-speed train, the pressure drag comes from the pressure due to the shape of fore-body and after-body of the train, the connecting parts between trains, the train wall surfaces, the pantograph system, the bogie, and underneath structure of the train.

Friction drag of the train is the sum of shear stress, which is in the reverse direction of the train running direction. Friction drag can be obtained by integrating along the whole train:

$$F_{\tau x} = \oint_{s_f} \tau_{ix} dS_f \tag{2.4}$$

Where: τ_{ix} is the shear stress on the train along x axis.

The shear stress is proportional to the viscosity of the air (µ) and the velocity gradient. The velocity is related to the height of boundary layer. However, the boundary is closely related to the shape of the train, the smooth of the train wall, the running velocity and the ambient surround. It is not easy to estimate the drag dependent on the train length. This is because the friction drag on the train body should involve all kinds of the drags occurring in the connecting parts between trains, photographs, the structures under the train, etc

In this case, the aerodynamic drag can be expressed as [7]

$$D = \frac{1}{2}\rho A_{tr} V^2 (C_{dp} + \frac{\lambda'}{d'} l) \tag{2.5}$$

Where V is the train speed, ρ the density of air, A_{tr} the cross-sectional area of train, C_{dp} the coefficient of the pressure drag caused by the fore- and after-bodies of train, d' the hydraulic diameter of train, l the train length, and λ' the hydraulic friction coefficient caused by the connecting parts between trains, photographs, the structures under the train, etc.

When a train enters a tunnel, a compression wave is formed ahead of the train which propagates along the tunnel at a nearly sonic speed. A part of the compression wave is reflected back from the exit of the tunnel as an expansion wave. A complex wave interaction occurs inside the tunnel due to successive reflections of the pressure waves at the exit and entry to the tunnel. These pressure waves cause large pressure transients resulting in fluctuating loads on the train causing discomfort to passengers. It is necessary to predict these pressure transients to design trains and tunnels, and to improve the passenger comfort.

There is a simple analytical approach to understand such complicated aerodynamic problems occurring inside tunnel. Assume that the cross-sectional areas of train and tunnel are constant, and their equivalent diameters are much larger than tunnel length, and train speed Vis very low compared with the speed of sound corresponding to the atmospheric conditions, and the propagation speed of pressure wave is the same as the speed of sound. Under these assumptions, it is reasonable to prescribe that the continuity equation involves variable density of air but the compressibility effect is not considered in the momentum and energy equations.

Assuming that V is the air velocity, and P the pressure, the continuity equation is written as [17]

$$a^2 \frac{\partial u}{\partial x} + \frac{1\partial p}{\rho \partial t} = (y-1)\varphi \tag{2.6}$$

And the momentum equation is given by

$$\frac{\partial u}{\partial t} + \frac{1\partial p}{\rho y x} = f \tag{2.7}$$

Where a is the speed of sound, the density ρ is assumed to be constant, x the distance along tunnel, t the time, y the ratio of specific heats (y=1.4) and f and φ are the frictional force and energy dissipation.

For the sake of simplicity, the flows divided into three regions: ahead of train, behind train, and in train. For the regions ahead of and behind train, the frictional forces are generated on tunnel walls:

$$f = -\frac{\lambda}{2d} u/u/ \tag{2.8}$$

$$\varphi = \frac{\lambda}{2d} /u/^3 \tag{2.9}$$

For the region in train, the frictional forces stem from both train body and tunnel wall surfaces. Thus, the frictional force and energy dissipation can be expressed as

$$f = -\frac{\lambda}{2d}\frac{1}{1-R} u'/u'/ - \frac{\lambda'}{2d'}\frac{1}{1-R}(u'-V)[u'-V] \tag{2.10}$$

$$\varphi = \frac{\lambda}{2d}\frac{1}{1-R}[u']^3 + \frac{\lambda'}{2d'}\frac{R}{1-R}[u'-V]^3 \tag{2.11}$$

Where d and d' are, respectively, the hydraulic diameters of tunnel and train, and λ and λ' the friction coefficients of tunnel wall and train body surfaces, respectively, R or β the ratio of the cross-sectional areas of train to tunnel, and u' the flow velocity occurring between train and tunnel. [5]

The compatibility conditions should be used to connect the flow fields in the three regions. Using the coordinate system moving with train, the conservation laws of mass and energy are given by

$$u - V = (1 - R)(u' - V) \tag{2.12}$$

$$p + \rho(u - V)^2 = p'(1 - R)\rho(u' - V)^2 - C_{dp}R\frac{1}{2}\rho(u' - V)^2 \tag{2.13}$$

Where C_{dp} is the coefficient of the pressure drag on train in the open air. At the entrance and exit of tunnel, it is assumed that the flow discharges at atmospheric pressure and when the flow comes into tunnel, it is also assumed that the pressure reduces as much as the dynamic pressure. At the entrance and exit of tunnel, the boundary conditions can be given by

Tunnel entrance $\quad p = \frac{1}{2}\rho u^2, \quad u \geq 0, \quad (2.14)$

$p = 0, \quad u < 0,$

Tunnel exit $\quad p = 0, \quad u \geq 0, \quad (2.15)$

$p = -\frac{1}{2}\rho u^2, \quad u < 0,$

The aerodynamic drag on the train traveling in the tunnel is given by

$$\frac{D}{A_{tr}} = \frac{1}{2}\rho \begin{Bmatrix} R \\ o \end{Bmatrix} (u' - V)^2 + \frac{1}{2}\rho C_{dp} \begin{Bmatrix} (u' - V)^2 \\ u^2 \end{Bmatrix} +$$

$$\frac{1}{2}\rho\frac{\lambda'}{d'}\left\{\int_{in}(V - u') \parallel V - u \parallel dx + V^2\int_{out} dx\right\} + \Delta p' \tag{2.16}$$

Where D is the aerodynamic drag and A_{tr} the cross sectional area of train. R and 0 in the first term on the right side are, respectively, taken for the fore-body of train to be inside and outside tunnel. In similarly $(u' - V)^2$ and u^2 in the second term are selected for the after-body of train to be inside and outside tunnel, respectively. The integral of the third term is performed along train length, and the subscripts in and out indicate the inside and outside tunnel, respectively. The last term p' on the right side is the pressure difference between the fore- and after-bodies of train. In the case where the train is fully outside tunnel, Eq. (2.16) reduces to Eq. (2.5) mentioned previously. Before train enters tunnel, the flow velocity and pressure both remain zero. Using these initial conditions, the equations above can be solved after some calculations.

According to the previous work, the ratio of the cross-sectional areas of train to tunnel (=blockage ratio β) has been known to be one of the most important parameters influencing the aerodynamics of train/tunnel systems [5]. As β increases, the pressure variation, flow velocity and aerodynamic drag increase. Additionally, the coefficients of friction forces on tunnel wall and train body can significantly influence the aerodynamics of train/tunnel systems. The increase of drag in a tunnel depends on many factors; the blockage ratio B of the train in the tunnel is by far the most important of them:

$$\beta = \frac{A_{tr}}{A_{tu}} \tag{2.17}$$

Where A_{tr} is the cross sectional area of the train and A_{tu} is the cross sectional area of the tunnel. But the type of the train and its length also have to be considered, as well as, at least for short tunnels (< 2000 m), the tunnel length and the train speed. [6]

2.2.2 Pressure transients

When a train enters a tunnel, a compression wave is induced propagating along the tunnel with sonic speed. This wave is reflected at the opposite portal as a rarefaction wave. When the rear of the train enters the tunnel, a rarefaction wave is produced again propagating along the tunnel relative to the moving air with sonic speed. This wave is reflected at the opposite tunnel end as a compression wave. These two waves are the main waves and they are always reflected at portals with opposite sense. Minor waves are caused by the passage of these waves over the train head and the train tail and so a very complex wave pattern is generated. Depending on the location in the tunnel, the pressure histories can be very different. Further localized pressure changes are caused when the train head passes (pressure drop) and when the rear of the train passes (pressure increase) [6]

The intensity of the head entrance wave is a typical measure for the pressure history of a train passage. For aerodynamically well-shaped trains and small values of β the loss coefficient ζ_h(depending on the shape of the train head) can be neglected. For this case the pressure increase is function of the train speed V_{tr} and the blockage ratio β only:

$$P = P - P_o = \frac{\rho V_{tr}^2}{2} - \frac{2\beta}{1-2\beta} \tag{2.18}$$

2.2.2.1 Pressure wave due to the train entering into tunnel

The train entering into tunnel at high speed plays a role of the piston motion against the air inside tunnel and thus compresses the air in front of the train. The resulting compression wave propagates along tunnel at a nearly sonic speed. The compression wave will be distorted or attenuated by viscous actions and heat transfer inside tunnel [18].

When a train with a cross-sectional area of A_{tr} enters a tunnel (cross-sectional area: A_{tu}) at speed V_{tr}, a compression wave is formed at the vicinity of the entrance of tunnel, as schematically shown in Figure 2-2. [5]

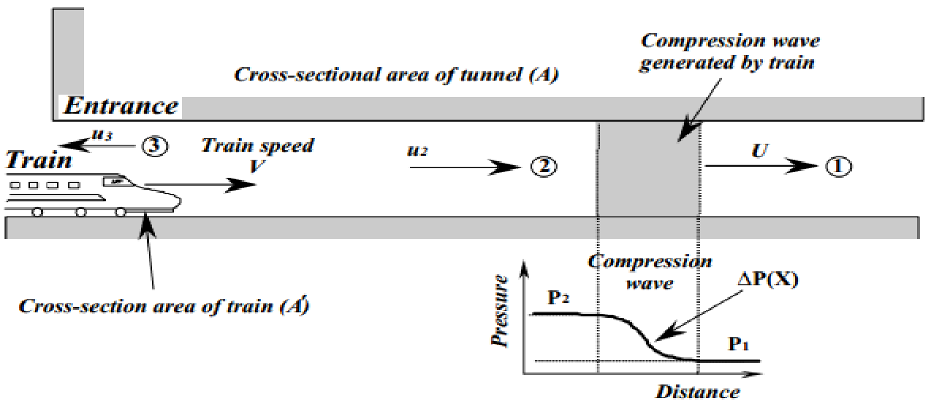

Figure 2-2: One-dimensional flow model of compression wave in the tunnel [5]

It is assumed that the compression wave form and the resulting pressure rise are expressed as $\Delta p_{(x)}$ and $\Delta p_{21}(=p_2 - p_1)$; respectively. Here p_1 and Δp_2 are the static pressures just upstream and downstream of the compression wave, respectively. Assuming that the value of Δp_{21} is very small, compared with the atmospheric pressurep1; and that isentropic flow is formed between states 2 and 3 [19], Δp_{21} can be given as a function of the train Mach number M_a and the cross-sectional area ratio ϕ :

$$\Delta p_{21} = \frac{1}{2}\gamma p_1 M_a^2 \frac{1-\phi^2}{\phi^2+(1-\phi^2)^2 M_t - M_t^2} \tag{2.19}$$

Where γ is the ratio of specific heats of air, and ϕ is (*A* - *A*')/ *A*. If we want to use the blockage ratio *R* of train to tunnel instead of ϕ ;   is replaced with $(1 - \phi$).

It can be deduced from the above results that the strength Δp_{21} of the compression wave formed at the entrance of tunnel is almost independent of the shape of the fore-body of train. However, it is expected that the compression wave form $\Delta p_{(x)}$ should be dependent on train velocity, blockage ratio, etc. [20–22]. From some computational and experimental works it is found that the compression wave form is a function of train velocity, Δp_{21}; and the equivalent diameter of tunnel *D*; as indicated in an empirical. [41]:

$$\Delta p_{comp} = \Delta p_{21}[\frac{1}{2} + \frac{1}{\pi} tan^{-1}\left(\frac{V_0 t}{0.3D}\right)] \quad (2.20)$$

Where t is the time frame the center of the compression wave from. This equation is often employed to simulate the compression wave produced at the entrance of real tunnels.

2.2.3 Flow Velocities

The propagating pressure waves induce a flow in a tunnel. The head wave of the train causes a flow in the direction of train motion between the front of the wave and the train head. In the gap between the tunnel wall and the train wall there is a flow to the entrance portal during the entrance phase of the train. Due to the reflections of the pressure waves a very complex flow field in space, especially if the track is not in the center of the tunnel cross section. The induced flow velocity depends on the train speedV_{tr}, the blockage ratio β, the length of the train L_{tr} and of the tunnel L_{tu} respectively, the roughness of the train and the tunnel wall respectively and on the initial air speed in the tunnel. The highest value of the flow speed is normally caused by the wake of the train after the main end has passed. [6]

2.3 Related Literatures

Flow around high speed trains has received considerable attention from researchers in the last three decades. Investigations have been performed using different experimental and computational techniques, including full-scale, physical modelling and numerical simulations. In what follows, a brief review of the literature regarding each method will be presented.

2.3.1 Full-Scale measurements

The first attempt to investigate the aerodynamic issues in tunnels was carried in central Japan on the Shinkansen high-speed railway. Later investigations were conducted in Europe. In the UK, the situation was more complicated due to the existing narrow Victorian tunnels having smaller loading gauges [31]

“Field measurement of aerodynamic pressures in tunnels induced by high speed trains” by Chen et al., (2012): studied the nature of pressure waves inside tunnels by means of full scale experiment on the Taiwan high-speed line. Several operating speeds with a maximum of 300 km/h were considered for obtaining pressure time histories. These histories were measured by positioning pressure sensors at different locations in a 7 km long tunnel using tunnel hood portals. The results showed that the entry and exit of the nose of the train cause a significant positive pressure which propagates along the tunnel while the entry and exit of the tail cause negative pressures. The results showed that the wave propagates within the tunnel at nearly the speed of sound. The study also showed that, in such a long tunnel, the peak pressure remains constant during the passing of a train in locations far enough from the exit (around 50 m for this tunnel portal). It was hypothesized that the positive peak pressure inside the tunnel is related to the square of operating speed, which is in agreement with the theoretical models. However, it has been found that relating pressure troughs to train speed is not as straightforward as relating the pressure peaks. Although there are different parameters that can affect the pressure inside the tunnel such as train length, train nose and under-body blockage, these have not been included in their experimental study. In addition, although the tunnel included a high numbers of shafts along its length, there was no clear interpretation of their effects on pressure waves.[32]

'Full-scale measurement and numerical simulation of flow around high-speed train in tunnel', by Suzuki et al., (2008) studied the aerodynamic forces on a Shinkansen train passing through a tunnel. The train experienced lateral vibrations noticeably greater than those in open air. The main aim of the study was to clarify the mechanism of the unknown aerodynamic forces around the train in the Shinkansen high-speed line and their effect on the lateral vibrations generated during operation. Four pressure gauges were installed on each side of a 16-car set Shinkansen train. Also a number of accelerometers were installed in order to measure the lateral acceleration on the car bodies. The train operating speed was 267 km/h and the tunnel was more than 2000 m in length. The results showed that when the nose of the train entered the tunnel, a compression wave was generated which was followed by an expansion wave generated inside the tunnel when the tail entered the tunnel. These pressure waves propagated ahead of the train at the speed of sound and reflected back at the tunnel exit. The waves continued travelling and reflecting between the two portals (entrance and exit) although a portion of the compression wave radiated as a pulse from the tunnel in the form of micro pressure waves. The paper concluded that the lateral vibration of the Shinkansen train running through tunnels originates from the development of the pressure fluctuation along the first 8 cars of the train between the train sides and the tunnel wall. [33]

2.3.2 Physical Modeling

Using full-scale experiments to investigate the velocity and pressure generated by high speed trains in confined spaces such as tunnels is very difficult and expensive. It is more practical and economical for researchers to carry out model-scale experiments due to the more controlled environment and the possibility of investigating different parameters in a short time.

"Nature of pressure waves induced by a high speed train travelling through a tunnel" by Baron et al, (2007) investigated, numerically and experimentally, the pressure waves generated by a train passing through a tunnel. They noted that the size of a separation bubble at the train nose increases the effective blockage ratio of the train, which in turn increases pressure peaks, and is influenced by the shape of the nose. Their work of numerical analysis indicated that the pressure rise as the train nose approaching is from the overpressure positioned just in front of the train nose, and the sudden pressure drop as the train nose passing by is due to the suction positioned aside the train nose.[35]

Gilbert et al., (2012) in the paper ''Aerodynamics of high-speed trains in confined spaces" studied the pressure and velocity variations in the tunnels of different lengths. Cobra probes were used to measure the velocity at different locations inside the tunnels. The probes were fixed in space and thus measure the slipstream and wake flow as would be experienced by a static observer. A Moving-model aerodynamic experiments were undertaken to identify the fundamental changes to train-induced air movements by firing a 1/25th scale high-speed train past instrumented walls and through box-shaped tunnels. The paper analyzed train-induced air flow in a confined space and, in line with previous findings, observed occurrence of compression and expansion waves in front of and behind the train, respectively. However, it is well known that the Cobra probes are not capable of measuring reversed flow and thus a detailed description of the flow cannot be achieved. [36]

2.3.3 Analytical methods

Although computational and experimental tools offer detailed ways of investigations for train aerodynamics, in some circumstances straightforward analytical methodologies are adequate. Especially in cases of investigating pressure transients in tunnels one dimensional analyses are quite sufficient for practical issues. [38]

In the paper "Review of the theory of the compression wave generated when a high speed train enters a tunnel" Howe (1999) indicated that the pressure rise (exclusive of the atmosphere pressure, i.e., the gauge pressure) generated by the compression wave, which is produced from the entry of a train into the tunnel is proportional to the square of the train speed and proportional to the cross-sectional area ratio of the train to the tunnel (the blockage ratio) based on a simplified analytical model. Therefore, the train speed and the blockage ratio are the two primary factors influencing the magnitude of the train-induced pressure transient in the tunnel. Other secondary factors include the length of the tunnel (compared to the train), the configurations of the tunnel (existence of airshafts and adits, portal shaping etc.), and the presence of multiple trains in the tunnel (especially the crossing of trains). [39]

There are a number of studies investigating the train aerodynamic in tunnels mainly by using one dimensional analytical methods. For instance, Howe et al., (2000), [40] studied the compression waves generated by a high-speed train passing a tunnel theoretically. The study showed that the pressure rise across the wave is directly proportional to mean air density, train speed and the cross sectional area of the train. Furthermore, Howe et al., (2003), [41] studied a theoretical prediction of compression waves for a train passing a tunnel with unvented entrance hood. Some experiments have also been conducted and the theoretical predictions are found to be in an excellent agreement with the experimental data.

2.3.4 Numerical Modeling

As previously mentioned, full-scale experiments are often expensive and time-consuming to conduct. A potential solution to overcome this problem is to use model-scale experiments. However, there are limitations when conducting physical modelling such as the amount of data that can be obtained is limited by the measurement equipment and campaign length. Alternatively, train aerodynamics investigations can be conducted using numerical techniques in which both the flow and pressure fields can be obtained for both full- and model-scales. Numerical simulations have been used extensively to study the flow around trains subjected to crosswinds, slipstream investigations and drag reduction tests. [37] However, due to the complexities associated with the moving train simulations in CFD, few researches have been carried out to study the flow around trains in tunnels.

“A validated numerical investigation of the effects of high blockage ratio and train and tunnel length upon underground railway aerodynamics.” A paper by Cross et al. (2015); investigated the effect of altering the blockage ratio of an underground train upon the ventilating airflows driven by a train. First a computational model was developed and validated with experimental data from literature. The model was scaled to represent an operational underground railway with high blockage ratio and the blockage ratio varied to evaluate the effects upon ventilation. The results of the study show that ventilating air flows can be increased significantly during periods of constant train motion and acceleration, by factors of 1.4 and 2 respectively, but that the train drag will increase at the same rate. During deceleration negligible increases in ventilation flows are found but drag increases by a factor of 4. Considered the air flows and drag generated in high blockage ratio underground railways, finding that increasing the blockage ratio by 30% will double the air flow but also the drag on the train by the same amount. The changes in pressure throughout the train motion do not indicate that unsafe pressure changes are created at any blockage ratio. The safe level of pressure change is given by the *International Union of Railways (2005*) as 4 KPa in a 4 s period. Since, the model used in this work is idealized and lacks any geometrical changes, in practice unsafe pressure changes may be generated. However, the study is based on the model scaled investigation and lacks a comprehensive actual visualization of the movement of the train in the tunnel. [66]

"CFD simulation of train aerodynamics: Train-induced wind conditions at an underground railroad passenger platform", a paper by Khayrullina et al., (2015); studied the flow around Dutch passenger and freight trains running through underground tunnels using transient CFD simulations. The research considered factors influencing the strength of pressure waves inside a tunnel such as blockage ratio, train speed, portal shape, tunnel length and roughness. The study found that the passenger train caused higher velocities than the freight train because of a higher operating speed and lower blockage ratio. A slipstream velocity exceeding 5m/s was considered a discomfort wind speed, while, any slipstream velocity exceeding 12 m/s as a dangerous wind speed. Hence, the investigation of the velocity in the tunnel showed that exceeding the discomfort threshold normally occurs at distances between 1.2 m to 2.9 m from the platform edge in the case of the passenger train. The results of the study show that passengers standing on a platform can experience strong wind effects when passenger trains or freight trains are passing at speeds of 140 and 100 km/h, respectively. The study mainly focused on the investigating the danger and discomfort zones in Dutch underground stations and lacks a comprehensive visualization of the flow.[42]

“Effect of Aerodynamic Drag on Performance of High Speed Train” a paper by Solomon Asmamaw, 2016, the paper investigate the effect of aerodynamic drag resistance of passenger rolling stock of two high speed train models with leading car, middle coach, and tail car. The first train model is existing European ICE-2 Regional Train and the second modified train model is called Ehio-HST-250+. The aerodynamic investigation is done using CATIA V5R20 modeling software and ANSYS Fluent V 17.0 Computational Fluid Dynamics (CFD) simulation software. The numerical method used on Fluent solver is viscous-incompressible steady state Reynolds Average Navier Stock (RANS) and two equation turbulence model of Realizable k - ε model (RKE) with Non-equilibrium wall function (NWF) of near wall treatment for the simulation of the system in an open air condition. The paper conclude with the reduction of coefficient of aerodynamic drag percentage amount of 49.01% of enormous aerodynamic drag is reduced and 636.13 kW traction power is saved with new train model called Ehio-HST-250. However, as the paper studies only focused on the analysis of the train operation on open field, the aerodynamic effects of the train while it is travelled in the tunnel is not analyzed.[61]

“Single train passing through a tunnel” paper by Jakub Novák et al, (2006). The paper examine aerodynamic impact created by tunnels as the loads represent an integral part of general loads that effect on operating rail vehicles. the paper deals with numerical solution of a complex problem of aerodynamic loads evoked by a train motion while entering and passing through a double track tunnel. The train set consists of an electrical loco and three coaches. The loco model shape closely corresponds with a real three-system electrical locomotive developed and produced by ŠKODA. The train performs a straight movement of 200 km/h speed rate. The realizable k-ε turbulent model with the default values of model constants was used to compute turbulent kinetic energy and turbulent energy dissipation rate. The paper used Computational Fluid Dynamics (CFD) software, ANSYS Fluent to monitor both the train motion aerodynamic effects on environment (tunnel wall surface) and backward effects of surrounding objects especially on loco body. Most of the results represent time variations of pressure, aerodynamic drag and velocities monitored both on tunnel and loco surfaces and in specified locations in the domain. Some of the values computed are compared with admissible limits published in adjacent standards. [6]

"Numerical Simulation of Train Aerodynamics" by Yeo Zhuan Lun et al, (2015); The paper analyzes the aerodynamics behavior of the airflow when the train is traveling through the tunnel by the means Commercial Computational Fluid Dynamics (CFD) software, ANSYS Fluent of solving the steady state Navier-Stoke's equations. The methodology was validated by experimental data of a reduced model-scale train running through a tunnel. The train simulated to travel at a velocity of 38.9 m/s (140km/h). The simulations were done with the train positioned at different locations with respect to the tunnel. Whilst a direct validation was not conducted (given the different operating conditions and train geometry), a similar trend in the pressure variation along the train body could be observed. The results from the paper simulations using CFD ANSYS had provided a good appreciation of the aerodynamic patterns around and on the train. However, as the paper studies only focused on the first train cabin, the effects of the turbulent flow at the rear of the train can be reduced with the presence of other cabins (increasing the length of the train). [43]

''Stability of High Speed Train under Aerodynamic Excitations'' by E. Bjerklund and M. Ohman; the paper examines aerodynamic effects on high speed trains and its impact on both comfort of the passenger and stability of the trains. The paper is performed on Swedish high speed trains that are aiming to go at a speed of 250 km/h. The authors tried to closely connects the aerodynamic effects with the vibration dynamics within the train. The authors chose two scenarios to be simulated. The scenario are when two trains meeting each other and a train leaving a tunnel and is hit by a strong wind gust (35 m/s). From the aerodynamic part, computational fluid dynamics (CFD) is used. To simulate both scenarios a moving mesh needs to be used. From the CFD the moments and forces from the pressure and traction on the train body are calculated, and these loads are taking into a low order mathematical model that simulates the vibration dynamics in the train. The paper conclude for the scenario with meeting trains the train experiences some slight vibrations, causing discomfort, but has no impact on the stability of the train, but for the scenario with the tunnel and side wind the train has a very high risk of derailment. From the results it can be seen that the aerodynamic drag and other aerodynamic loads on the train are strongly dependent on the pressure waves in the tunnel. [44]

In the paper entitled “Stability of trains under aerodynamics excitation for AALRT” by Abel Demissie, 2015**,** in his Master’s thesis paper investigate the aerodynamic impact on a lightweight railway vehicle used in A.A.LRT. The performed simulation allows measuring the aerodynamic forces on the vehicles. Numerical prediction of incompressible flow has been performed in AALRT train moving at a speed of 22.2m/s (80k/hr). The software CFD ANSYS Fluent used which incorporates turbulence model and segregated implicit solver was used for the computation. The aerodynamic analysis was performed to study the flow behavior of the air over the train body. The analysis includes the study of contours of pressure and velocity. The peak pressure difference along the train is analyzed which is exhibited for trains passing each other. The two scenarios conducted for a train exiting and entering the tunnel shows that the pressure deviation is addressed. However the paper is focused mainly on the aerodynamic analysis of the AALRT train operation on open field. [45]

2.3.5 Conclusions

From the aforementioned literature review, it can be concluded that aerodynamic phenomena in confined spaces such as tunnels have received the attention of researchers, especially with issues of aerodynamic drag and pressure variations of trains in tunnels; and also the effect of the blockage ratio on the influence of the aerodynamic drag and peak-pressure generated on the train as it travels in tunnel. Whilst designing new train tunnels, simulations to estimate and examine aerodynamic drag, pressure, and air velocity have proved to be mandatory to understand the aerodynamic effects upon the structural perspective of the design of train and with the issues of reducing aerodynamic drag power demand of trains and; thus limiting drag and maximizing stability also increases acceleration, which reduces travelling time. This research aims to examine and investigate the aerodynamics impact of passage of a passenger railway vehicle in tunnels.

CHAPTER 3: - METHODOLOGY

3.1 Background

There are different ways to obtain the aerodynamic drag, velocities and pressures around a moving train body. These include full-scale measurements, physical modeling, analytical solutions and computational fluid dynamics. The analytical solution is possible only for very simplified two dimensional laminar cases, which are not of engineering interest. For many cases the full-scale measurements are difficult and/or expensive to perform. Although physical modelling is feasible for many engineering cases it also suffers from many drawbacks which include scaling problems and measurement constraints. For instance, measuring the entire three-dimensional velocity field around a moving body is impossible because data can only be obtained from a limited number of points due to time-constraints. The alternative is to use the computational fluid techniques, in which the full three dimensional velocity and pressure field can be obtained in an affordable way.

3.1.1 Computational Fluid Dynamics (CFD)

Fluid flow around moving bodies is normally turbulent, in which case the velocity and pressure fields are fluctuating in both time and space. There is no analytical solution for the governing equations of turbulent flows, instead one needs to simplify these equations to be able to solve them numerically. Computational fluid dynamics (CFD) is a numerical method to compute and analyze the dynamics of a fluid and to solve the governing equations of the fluid flow using complex numerical algorithms.

According to this definition, CFD is not a science by itself but a way to apply methods of one discipline (numerical analysis) to another (heat and mass transfer). In retrospect, it is integrating not only the disciplines of fluid mechanics with mathematics but also with computer science as illustrated in Figure 3.1. The physical characteristics of the fluid motion can usually be described through fundamental mathematical equations, usually in partial differential form, which govern a process of interest and are often called governing equations in CFD. [54]

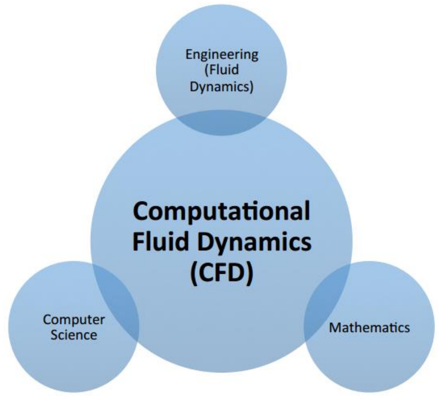

Figure 3-1: The different disciplines contained within computational fluid dynamics

ANSYS FLUENT is Computational Fluid Dynamics (CFD) software that allows users to simulate flow problems of ranging complexity. It contains broad physical modeling capabilities needed to model flow, turbulence, heat transfer, and reactions over objects designed by the user. Thousands of companies around the world benefit from the use of CFD software as a main part of their design phases in their product development. It uses the finite-volume method to solve the governing Navier-Stokes equations for a fluid which are derived from the conservation mass equation , the conservation of momentum and the conservation of energy equations. [46]

The difficulty arises from the fact that the conservation of mass, momentum and energy are coupled and non-linear set of differential equations making them practically impossible to solve analytically for practical engineering problems. Hence CFD software such as FLUENT is utilized to provide very reasonable approximation upon solving the specified governing equations. The approach for a CFD simulation is to divide the physical domain into small finite elements where the governing equations are solved numerical.

3.1.1.1 The CFD Process

CFD codes are structured around the numerical algorithms that can handle fluid flow problems. All the CFD commercial packages available in the market have three basic elements, which divide the complete analysis of the numerical experiment to be performed on the specific domain or geometry. Since the CFD process has been the core of this study, this will be further explained and the software used introduced in this subsection. The CFD process have three basic elements; [52]

i. Pre-processing,
ii. Solving and
iii. Post-processing.

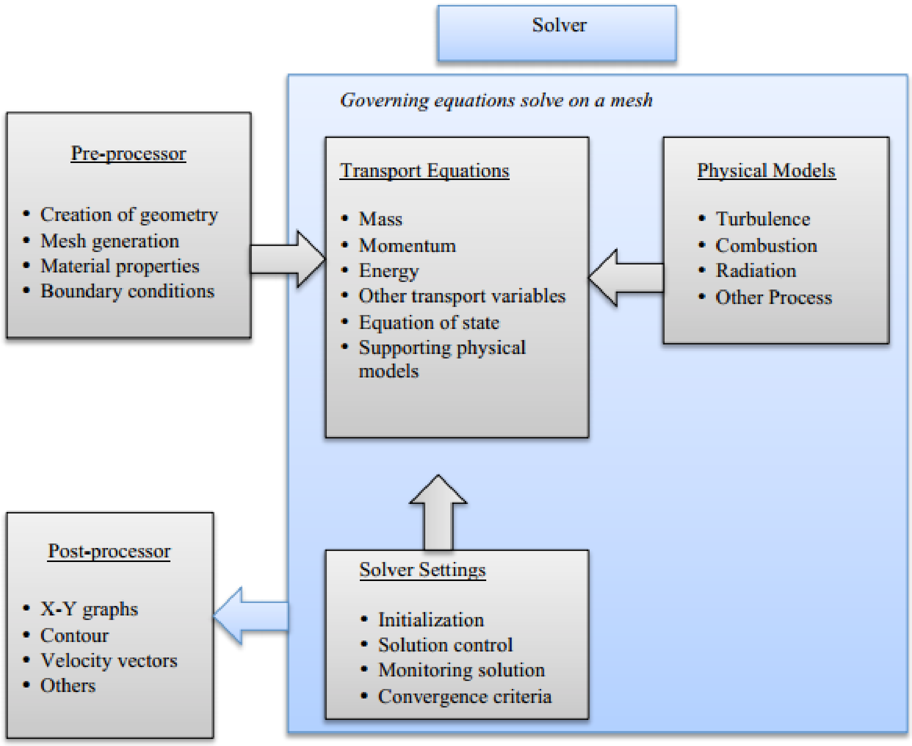

Figure 3-2: The inter-connectivity functions of the three main elements within a CFD analysis framework.

i. Pre-Processing

Pre-processor consists of input of a flow problem by means of a user-friendly interface and subsequent transformation of this input into form of suitable for the use by the solver. The pre-processor is the link between the user and the solver.

ii. Solving of the equations

After pre-processing the model, the computational mesh that was generated was imported into the solver software. As mentioned earlier in the Theory chapter, the solver used for this paper is a RANS (Reynolds Averaged Navier Stokes) steady state solver employing the k-epsilon realizable turbulence model. In the solver all boundary conditions and solver settings where specified before initializing the solution.

The appropriate usage of either an in-house or a commercial CFD code commands the core understanding of the underlying numerical aspects inside the CFD solver. This section focuses on the treatment of the solver element. A CFD solver can usually be described and envisaged by the solution procedure presented in Figure 3.3. [54]

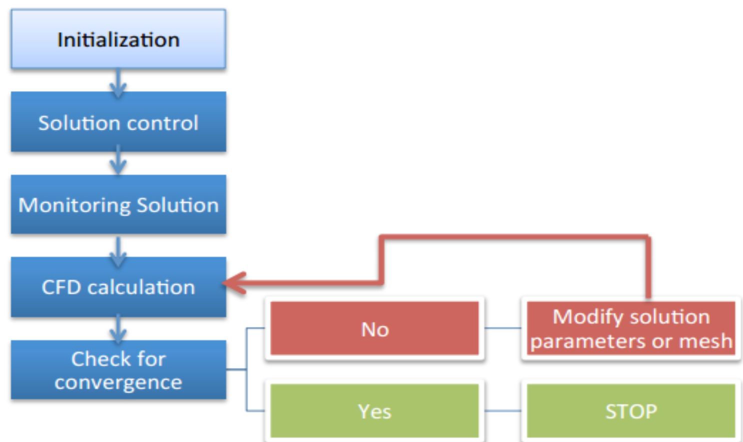

Figure 3-3: An overview of the solution procedure

In the current market, the solvers usually use three distinct ways of calculating the solutions, namely, the finite difference method, finite element method and the finite volume method. The finite difference and finite element method are usually suitable for stress and structure analysis. On the other hand the finite volume method is the most suitable method for the CFD process. As the name implies, finite volume method is the numerical algorithm calculation process involving the use of finite volume cells. In this study numerical simulations were performed using ANSYS Fluent, the general setup for this simulation will be further specified in the next part of this chapter

iii. Post-Processing

After finalizing a simulation, the physical quantities where exported to a post processing software to enable visualization of the results. Commercial CFD codes such as ANSYS® Inc., CFX®, ANSYS Fluent®, STARCD®, and others often incorporate impressive visualization tools within their user friendly GUIs to allow users to graphically view the results of a CFD calculation at the end of a computational simulation. Those data visualization tools of the CFD solver to observe the following results of the simulation: [54]

1) Domain geometry and Grid display
2) Vector plots

3) Line and shaded contour plots
4) 2D and 3D surface plots
5) Particle tracking
6) XY plots and graphs of results

The results could be displayed in many different ways and in this study the most interesting parameters to visualize were aerodynamic drag, pressure and velocity distribution.

3.1.2 Research Design Procedures

The general methodology procedure to achieve the aim of the present paper is depicted as follows.

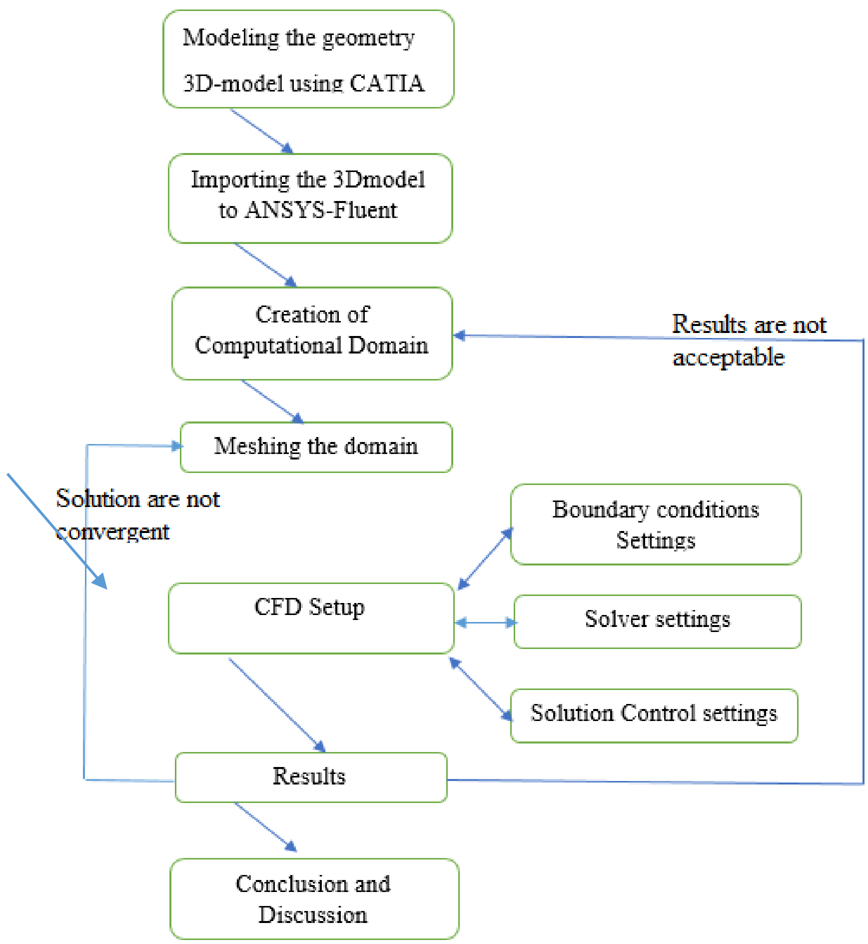

Figure 3-4: The design procedure for the methods of study.

3.2 Data Analysis and Numerical Modeling

The study is concerned with the analysis of aerodynamic loads on passenger train while operating in open field and in tunnel. Numerical simulation and theory analysis were conducted to study aerodynamic loads and pressure waves around the passenger caused by passing of passenger train within currently built Addi-onfito tunnel at speed of 120Km/hr. Addi-onfito is one of the six tunnels constructed in Weldia-Mekelle railway line. The effect of tunnel cross-section on the aerodynamic properties of air and pressure developed on the train body is also investigated. The study used the actual passenger train body and tunnel dimensions taken from ERC specification.

3.2.1 Data Analysis

The analysis is done using computational fluid dynamics (CFD) method of ANSYS Fluent simulation software and the physical modeling is developed collected data from ERC standards and papers. This process involves several computer aided design (CAD) software like CATIA®, Solid-works®, Pro-E® and many more. The help of CATIA software defines the topology of the fluid flow region of interest.

In this paper, the models of passenger train used in the numerical analysis have been 3D printed using the software called CATIA-V5®. The passenger train used for simulation is selected among the passenger trains that are used in National Railway Network of Ethiopia (ERNE), which is "HDX1C locomotive and hard seat passenger car".

1. Train Geometry Preparation

The passenger train consists of two locomotives and one passenger car. The car-body structure consists of different steel structure, mainly of carbon steel material [57] [65] In order to be able to use a CATIA model for ANSYS-Fluent simulations, the first step is to reduce the level of detail so that only the surfaces that will have a possible impact on the flow are left. This is done in order to decrease the amount of cells and hence reduce the simulation time. This will also enable better mesh quality and it is important to remove details with care and be sure that they do not influence the flow in the tunnel.

Table 3.1: Technical description of YZ25G Hard seat passenger car [65]

	Parameters	**Dimensions**
1	Carbody length	25500mm
2	Carbody width	3105mm (Approx)
3	Height between rail top to car top(empty car)	4433mm
4	Vehicle center distance	18000mm
5	Height from rail top to coupler center (empty car)	880+10-5 mm
6	Vehicle center distance	18000mm

The full size of the passenger train is 70m long, width of 3.105m and height of 4433m including wheel. However, due to the confidentiality issues, the fine details of the train and the tunnel (train door, gearbox assembly and wheels at the bottom of the train and train tracks etc.) are not available and hence neglected at the current stage of the study. The distance (gap) between each three carriages, which is included in the model, assumed as 0.3m.

Table 3.2: The overall size of the passenger train used in simulation

Passenger Train	**Parameters**	**Dimensions**
Two Electric powered Locomotive and One Passenger Car	Length	70m
	Width	3.105m
	Height	4.433m

The CATIA model of the train geometry used for the analysis is shown in Figure 3.5 below. The dimensions are taken from ERC technical department [Appendix 1], some of the detailed dimensions are taken by assumption because of the unavailability.

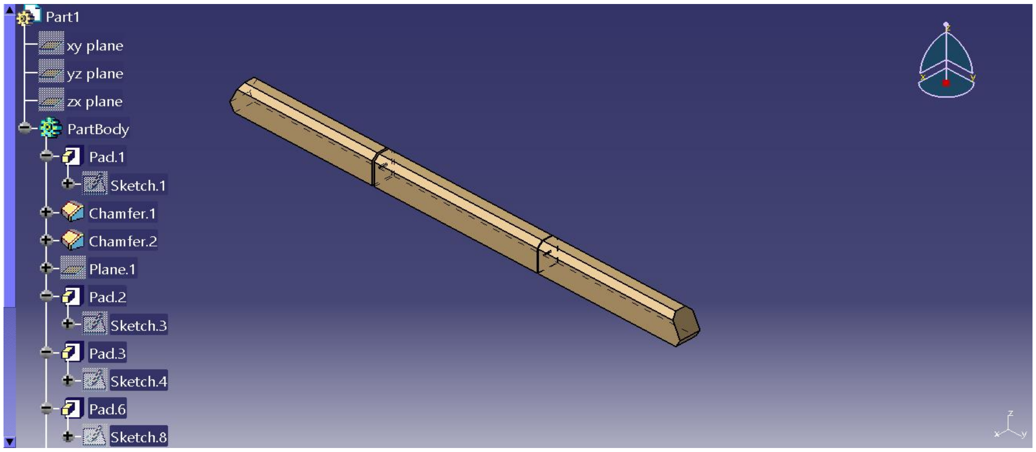

Figure 3-5: Assembly 3D CATIA model of HDXIC locomotive and hard seat passenger car

2. Tunnel Geometry preparation

Currently in National Railway Network of Ethiopia (ERNE) there are many underground tunnel systems in addition to the normal railway lines. The most recent example is the newly introduced Weldia – Mekelle railway line which consists of 6 tunnels with total 9 Km.

Table 3.3: Schedule of tunnels (Preliminary design) between railway line of Weldia and Mekelle [1]

	Name of Tunnel	Tunnel mid –point	Tunnel entrance	Tunnel exit	Tunnel length (m)
1	Aroley 1	DIK165+605	DIK164+615	DIK166+595	1980
2	Aroley 2	DIK169+395	DIK168+898	DIK169+892	994
3	Addi onfito	DIK176+553	DIK176+463	DIK176+642	179
4	Serghiem	DIK178+571	DIK178+510	DIK178+631	121
5	Maiceflo	DIK188+344	DIK186+513	DIK190+175	3662
6	Kokele	DIK194+590	DIK193+555	DIK195+625	2070
Sub total		L<=1000		3	1294
		1000<L<=2000		1	1980
		2000<L<=3000		1	2070
		3000<L<=4000		1	3662
Total				6	9006

The Addi onfito tunnel is chosen as a base model of the simulation. The cross-sectional area of the tunnel is 31.61m^2 with 179m tunnel length, and is of rectangular cross section with no portal at the entrance or exit. A schematic diagram of the full scale model of the present Addi-onfito tunnel structure is shown in Figure 3-6.

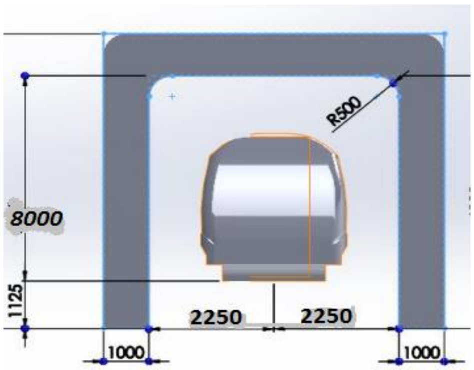

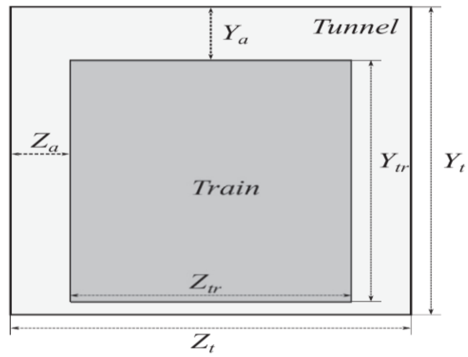

Figure 3-6: The cross-section of the Addi-onfito tunnel dimensions for the original design [1]

The train-tunnel cross-sections have a vertical upper gap between the train and tunnel gap of Y_a as 2.973 m and a horizontal gap between the train and tunnel of Z_a as 0.5812 m, while the passenger train have the same dimensions as of the passenger train of National Railway Network of Ethiopia (ERNE) with height Y_{tr} as 4.433 m and width as Z_{tr} as 3.105 m. In this work a value of 0.25 m is used to represent a gap under the train without reducing the height of the train significantly. Table 3.4 shows the dimension parameters used in the train-tunnel analysis.

Table 3.4: Dimension parameters of the Addi-onfito tunnel [1]

Tunnel	Train-Tunnel cross-sections (m)							
	Y_a	Z_a	Y_{tr}	Z_{tr}	Y_{tu}	Z_{tu}	A_{tu} (m^2)	L_{tu}
Addi-onfito Tunnel	2.973	0.5812	4.433	3.105	7.406	4.268	31.61	179

3.2.2 Numerical Modeling

Computation Fluid Dynamics (CFD) is the use of computer simulations to compute and analyze the dynamics of a fluid and the method is used in various areas such as ventilation, internal combustion engines, and vehicle aerodynamics as in this study. Fluid dynamics describes the motion of fluid (gas & liquid) in terms of energy, momentum and mass.

In this paper the flow around the train is solved by using a commercial CFD tool. CFD simulations are carried out by dividing the physical domain into small finite volume elements and numerically solved by the governing equations that describe the behavior of the flow. The governing equations are derived from the laws of conservation, which become very complex, almost impossible to solve analytically and therefore requires numerical simulations. The ANSYS-Fluent software is used in this study in order to solve the governing equations of fluid flow for a finite number of cells in generated grid domain.

A first approach for describing the flow field is to state the three laws of conservation and assuming incompressible and isothermal flow, the energy equation can then be neglected. By doing this assumption the density and viscosity can be seen as constant due to conditions where the velocity is below Mach number 0.3 (Ma = 0.3 ≅ 100 m/s) and the temperature is relatively low during the simulation of the flow field. [49]

Reynolds Number: The Reynolds number is defined as [66]

$$R_{eL} = \frac{\rho V_{tr} H_t}{\mu} \tag{3.1}$$

Where: - ρ is the air density, V_{tr} is the train velocity, H_t is the tunnel height, μ is the dynamic viscosity.

For external flows; $R_{eL} \geq 500{,}000$, along the surface, and $R_{eL} \geq 500{,}000$, around the obstacle. The flow is turbulent. [61][70] The Reynolds number calculated at maximum train velocity with train velocity (V_{tr} = 33.33 m/s), air density of (ρ = 1.177 kg/m^3 at temperature value of 30°c), dynamic viscosity (μ = 1.846e-05 kg/ (m-s) at temperature value of 303 K (30°c) of temperature value), tunnel height of H_{tu} = 7.406m.

$$R_{eL} = \frac{\rho V_{tr} H_t}{\mu}$$

$$R_{eL} = \frac{1.117 * 33.33 * 7.406}{1.846 * 10^{-5}}$$

$$= 14936212.98$$

$$\cong 14.94 * 10^6$$

At this value of Reynolds numbers for air/train velocity of 120 km/h (33.33 m/s), indicates occurrence of turbulent flow of air over a rigid body. Therefore to simulate external aerodynamics at this much amount of Reynolds number, it is important to consider turbulence flow of the fluid.

Regarding the compressibility effect, this concept has been investigated by the expression employed by (*Ricco et al*). (2007) [35], where it is shown that one must operate in the framework of incompressible flows when $M_a^2 \frac{L_{tu}}{L_{tr}}$ <<1, (3.2)

Where: - M is the Mach number based on train velocity ($M_a = \frac{V_{tr}}{a}$), a is the speed of sound which is 349.3 m/s at temperature of 30^{o}c and V_{tr} is velocity of train of 33.33m/s.

The Mach number $M_a = \frac{V_{tr}}{a}$ (3.3)

$$= \frac{33.33 m/s}{349.3\ m/s} \cong 0.095$$

For train length, L_{tr} = 70 m, and tunnel length, L_{tu} = 179, the expression in equation (3.3) gives

$$M_a^2 \frac{L_{tu}}{L_{tr}} = \frac{(0.093)^2 * 179m}{70m} \cong 0.23$$

Therefore; in this case, for all simulation the expression M_a^2 is less than 0.3 and $M_a^2 \frac{L_{tu}}{L_{tr}}$ <<1, is less than 1. Therefore, the air flows is considered as an incompressible fluid. This is justified as velocities of trains in an underground railway are relatively low (average of 33.33 m/s) and thus compressible effects are moderate, given that the flow Mach number is small and with assumption of there is an absence of tunnel features which may create compressible effects. [66] For the unsteady, incompressible fluid flow in an underground railway, the Reynolds-averaged Navier Stokes equations are solved using Fluent.

I. Reynolds Average Never Stocks (RANS)

After finding of Reynolds number and Mach number, the assumption on the numerical method approximation which will be discussed next is become meaningful. As fluid dynamics is the study of fluids in motion, such as airflow around a vehicle, and the physics can be described by the conservation laws of mass, momentum and energy. [61]

The CFD approach uses the finite-volume method to solve the governing Navier-Stokes equations for a fluid which are derived from the conservation mass equation, the conservation of momentum and the conservation of energy [61].

- **Conservation of mass** – Conservation of mass is expressed by the continuity equation, which states that the amount of mass flow that enters a control volume must be equal to the amount leaving it.

Continuity equation: this equation takes the form:

$$\frac{\partial u}{\partial x} + \frac{\partial v}{\partial y} + \frac{\partial w}{\partial z} = 0 \tag{3.4}$$

- **Conservation of linear momentum** (Newton's 2nd law of motion) – relation between pressure, momentum and viscous force. This set of formulas are referred as the incompressible *Navier–Stokes equations*, which are non-linear differential equations.

Momentum equation: this equation takes the form:

$$\rho g_x - \frac{\partial p}{\partial x} + \mu\left(\frac{\partial^2 u}{\partial x^2} + \frac{\partial^2 u}{\partial y^2} + \frac{\partial^2 u}{\partial z^2}\right) = \rho \frac{du}{dt} \tag{3.5}$$

$$\rho g_y - \frac{\partial p}{\partial y} + \mu\left(\frac{\partial^2 v}{\partial x^2} + \frac{\partial^2 v}{\partial y^2} + \frac{\partial^2 v}{\partial z^2}\right) = \rho \frac{dv}{dt} \tag{3.6}$$

$$\rho g_z - \frac{\partial p}{\partial z} + \mu\left(\frac{\partial^2 w}{\partial x^2} + \frac{\partial^2 w}{\partial y^2} + \frac{\partial^2 w}{\partial z^2}\right) = \rho \frac{dw}{dt} \tag{3.7}$$

Together with the Navier-Stokes equation the Continuity equation gives four unknowns, *u, v, w & p*, which will be solved with differential equations.

- **Conservation of Energy** (1st law of thermodynamics) – the total amount of energy within the system stay constant.

Energy equation: this equation takes the form:

$$\rho C_p \frac{dT}{dt} = K\nabla^2 T + \phi \tag{3.8}$$

Where: - ρ = density, t= time, p= pressure, μ= static viscosity, g= gravity constant, C_p= specific heat capacity, T= temperature, K= coefficient of thermal conductivity, ϕ = viscous dissipation function.

Navier-Stokes equations are derived from Newtons second law and can be seen as a force equilibrium for an infinitesimal small volume element. In order to convert the stresses to velocity components the Navier - Stokes equations are usually expressed for an incompressible Newtonian fluid with constant viscosity. An incompressible fluid is a fluid where the divergence of the velocity is zero, and a Newtonian fluid is a fluid which stress versus strain rate curve is linear. The Navier-Stokes equations can then be expressed as in Eq (3.5), (3.6), (3.7) above, three partial non-linear differential equations, one for each velocity vector. [51]

As mentioned above, the governing equations become very complex. In order to numerically solve them, the differential equations are discretized into large system of algebraic equations in order to solve them. The general approach is to assume incompressible and isothermal flow where the Mach number under 0.3 (for this case Ma = 0.095) and a constant temperature since vehicles travel at a relatively low speed. The governing equations are therefore simplified and the energy equation can be neglected.

Furthermore, since stochastic, three-dimensional and time dependent, fluid flows are almost always turbulent and will experience fluctuations and therefore Reynolds decomposition method is used. In order to solve these equation and analyze the flow the simplest approach is the Reynolds decomposition, also called *Reynolds Average Navier Stokes* (RANS). In the RANS approach the instantaneous velocity and pressure is split into two parts, an average part and a fluctuating part, Eq. (3.9) and Eq. (3.10). Which is the basis of the Reynolds decomposition Flow variables can be expressed as

$$U = \frac{1}{T}\int_0^T U\,dT \qquad (3.9)$$

$$U = \bar{u} + u',\ P = \bar{p} + p', T = \bar{\bar{\bar{T}}} + T' \qquad (3.10)$$

In many cases it is easier to analyze the time-averaged quantities. Thus the Reynolds decomposition is applied into the governing equations to obtain what is called the Reynolds Averaged Navier Stokes (RANS) equations. Inserting *Reynolds decomposition* into Navier-Stokes equation (x-direction) and in the continuity equation will results in new fluctuating terms.

$$\frac{\partial \bar{u}}{\partial x} + \frac{\partial \bar{v}}{\partial y} + \frac{\partial \bar{w}}{\partial z} = 0 \qquad (3.11)$$

$$\rho g_x - \frac{\partial \bar{p}}{\partial x} + \frac{\partial}{\partial x}\left(\mu \frac{\partial \bar{u}}{\partial x} - \rho \overline{u'^2}\right) + \frac{\partial}{\partial x}\left(\mu \frac{\partial \bar{u}}{\partial y} - \rho \overline{u'v'}\right) + \frac{\partial}{\partial z}\left(\mu \frac{\partial \bar{u}}{\partial z} - \rho \overline{u'w'}\right) = \rho \frac{d\bar{u}}{dt} \quad (3.12)$$

Eq. (3.12) now consists of new unknown terms like $\rho\overline{u'v'}$, also called for *Reynolds stresses.* Since the number of unknowns are greater than the number of equations a so called *closure problem* is generated, the extra stress terms has to be modeled to get a closed equation system. This is done by using turbulence models. [6]

Fluent obtains a solution such that the mass, momentum, energy and other quantities are conserved for each cell. The code of the CFD software solves directly the values of the flow variables at the cell centers and the values at other locations are appropriately interpolated. In other cases, where there is no complicated geometry, but rather there is more flow gradients occurring around a certain area, the user can apply a bias.

II. Turbulence flow and Turbulence modeling

The largest difficulty with CFD simulations is to calculate the turbulent flow. A turbulent flow is irregular and varies randomly in time and space. By using so called turbulence models the flow field can be calculated with less computer capacity. Such a model will modify the equations and only consider the average effects of the turbulence. The flow will then be divided into an average term and a fluctuation term, this can be done using *Reynolds Average Navier Stokes* (RANS). A turbulence model can never give an exact solution, but a better choice will give a more accurate solution. The choice of model is a matter of computer capacity and required level of accuracy. [47]

The fidelity of CFD predictions for turbulent flow is highly dependent upon the quality of the turbulence modeling. Based on experience, Fluent recommends two types of turbulence models for external aerodynamic studies. The k -ε - model and The Reynolds stress model (*RSM*). The k - ε - model is the most commonly used turbulence model in the industry, this due to the robustness of the model which gives safe convergence. A good overview of the flow field is achieved with the model, but in areas with high velocity and pressure gradients the accuracy is not that high. The $k-\varepsilon$ model is an *Eddy Viscosity model,* which means that the turbulence is modeled by adding the turbulence viscosity(μ_t). This model is a semi-empirical method based on how the kinetic energy, k, is transported and its dissipation rate ε.

$$k = \frac{1}{2}\left(\overline{u'^2} + \overline{v'^2} + \overline{w'^2}\right) \tag{3.13}$$

$$\varepsilon = u[(\frac{\partial u'}{\partial x})^2 + (\frac{\partial u'}{\partial y})^2 + (\frac{\partial u'}{\partial z})^2 + (\frac{\partial v'}{\partial x})^2 + (\frac{\partial v'}{\partial y})^2 + (\frac{\partial v'}{\partial z})^2 + (\frac{\partial w'}{\partial x})^2 + (\frac{\partial w'}{\partial y})^2 + (\frac{\partial w'}{\partial z})^2$$

The transport equation for k is derived exact while the transport equation for ε is derived from physical reasoning. [46]

This paper had no intention to compare different turbulence models and there are turbulence models that are more advanced than the *realizable k-ε turbulence* model, but this means that they are more complex to use and more time consuming. Although the results could probably be improved, the *realizable k-ε turbulence* model can be considered sufficient for this project. The numerical simulation model used in this paper is the *realizable k-ε turbulence* model together with non-equilibrium wall-functions for solving the *RANS*-equations in fluent.

Once the test object has been drawn and meshed in Workbench or imported from other software package (CatiaV5 for this paper case), FLUENT then allows the user to analyze it in different flow parameters. Another modeling capability FLUENT is capable of using is enhanced wall treatment. When the user chooses to use enhanced wall treatment, they can use this especially for turbulent cases using the k-epsilon model because it analyzes the object closer near the wall region.

3.3 Numerical Simulation Methods

Numerical simulations have been performed on the train 3D CATIA models using the CFD techniques. The software used for the numerical analysis was ANSYS FLUENT®. Trains traveling in the tunnels are tested by using CFD. Numerical simulation were conducted to estimate the aerodynamic loads around a passenger train operating in confined spaces, starting from the open air. Further the effect of blockage ratio with a particular emphasis on the influence of the aerodynamic drag and peak-pressures acting on the train body are investigated.

In this paper the governing equations of unsteady incompressible flow are mass conservation equation and Reynolds-averaged-Navier–Stokes equations are solved using ANSYS-Fluent code.

Another well documented practice within CFD-simulations is the use of the *realizable k-ε turbulence* model together with non-equilibrium wall-functions when solving the *RANS*-equations in fluent. The simulation of train in tunnels using *RANS* in fluent, with the *realizable k-ε turbulence* model is utilized in this work is due to it's suitable on the investigation of train induced flows, in which it was found to perform well in many related literatures. [61][43][45] [6]

A computational analysis of the passenger train traveling at 120km/hr in the present tunnel (Addi-onfito) system was performed to estimate the aerodynamic loads when the train is travelling in tunnel. The effects of the size of the confined space (tunnel cross-sectional area) were investigated by analyzing the aerodynamic drag forces, pressure and the flow field around the train. The tunnel chosen as a base model of the simulation does not include any features such as shafts or passages to allow the investigation of the train induced flows without interference from other factors. As described in the theoretical chapter, the blockage ratio has been known to be one of the most important parameters influencing the aerodynamics of train/tunnel systems.

From equation of blockage ratio; the β of the train operating in the tunnel is:

$$\beta_1 = \frac{A_{tr}}{A_{tu}}$$

Where A_{tr} = 13.764 m^2 is the cross sectional area of the train front head (from result of ANSYS) and

A_{tu} =31.61m^2 is the cross sectional area of the tunnel.

$$\beta_1 = \frac{13.764\ m^2}{31.61 m^2} = 0.4355 = 43.55\ \%$$

Therefore; when the blockage ratio of the base model is calculated with the cross-sectional areas of the mentioned train and Addi-onfito tunnel, the blockage ratio is approximately 0.4355. Configurations and conditions for the simulation cases are summarized in Table 3.5.

Table 3.5: Train tunnel configuration for simulation of train in tunnel

	Aspect	**Parameter**
Train	Type	Passenger Train
	Length	70m
	Velocity	120km/h (33.33m/s)
	Cross-sectional area	13.764 m^2
Addi-onfito Tunnel	Type	Rectangular cross-section
	Length	179m
	Cross-sectional area	31.61m^2
	Blockage ratio (B_1)	43.55%

The aerodynamic effects generated by a train moving through a tunnel; is due to the train is confined by the tunnel walls, a pressure gradient is generated along the train and air is pushed ahead of the train and sucked from behind, thus generating an air flow. Researchers suggest that the entity of the aerodynamic drag of train operating in tunnel depends on several parameters such as the blockage ratio (ratio of a vehicle to free tunnel cross-sectional area), tunnel network geometry and surface, number of pressure relief ducts, train type and train speed, and the presence of other trains, however the blockage ratio has been known to be one of the most important parameters influencing the aerodynamics of train/tunnel systems. [10][11] [69]

This paper also investigate the effect of the blockage ratio (ratio of train cross-sectional area to tunnel) on the influence of the aerodynamic drag and pressure developments on the passenger train. To evaluate the effect of the cross-sectional area of the tunnel, tests are carried out by changing dimensions of the original train-tunnel gaps. The new dimensions calculated by increasing the original Addi-onfito tunnel gaps Y_a and Z_a by 20% to reach up with blockage ratio of 0.3824. This is to arrive to a tunnel model with certain parameters similar to a current underground railway operating at 0.4 blockage ratio in Basle-Zurich Swiss-metro tunnel. [69]

Due to the change in the train-tunnel gaps, new geometric dimensionless variable is defined: The blockage ratio (β_2), which is the cross-sectional area of the train divided by the cross-sectional area of the tunnel.

The blockage ratio $\beta_2 = \frac{A_{tr}}{A_{tu2}}$

$$= \frac{13.764\ m^2}{35.99\ m^2}$$

$$= 0.3824$$

$$= 38.24\%$$

The blockage ratio of 0.3824 is similar to the blockage ratio of the (*Basle-Zurich Swiss-metro tunnel*), the Swiss-metro consists in a high-speed underground transport network which would be composed by blockage ratio tunnels about 0.4 and 89.1 km length. [69] Configurations and conditions for the test cases are summarized in Table 3.6.

Table 3.6: Summary of tunnel geometries

Tunnels	**Train-Tunnel cross-sections (m)**						
	Y_a	Z_a	Y_{tr}	Z_{tr}	Y_{tu}	Z_{tu}	$A_{tu}\ (m^2)$
Tunnel 1 (β_1 = 0.4355)	2.973	0.5812	4.433	3.105	7.406	4.268	31.61
Tunnel 2 (β_2 = 0.3824)	3.568	0.6975	4.433	3.105	8.001	4.499	35.99

The aerodynamic drag of the train in the tunnel varies depending on the cross-sectional area of the tunnel. Therefore, tests are performed to reach upon the relationship between the blockage ratio and the aerodynamic loads the train traveling at 120 km/h. Development of computational model, grid generation, boundary conditions, cell zone conditions and solver setup are carried out in the same way as the first train-tunnel simulation (β_1 = 0.4355) for the second train-tunnel simulation with different blockage ratio (β_2 = 0.3824).

3.3.1 ANSYS Fluent Setup

A computational analysis of the present train-tunnel system was performed to estimate the aerodynamic loads. In order to provide initial estimates of the magnitude of the aerodynamic forces and pressure propagation on the train body; a series of numerical simulation were undertaken on 6 different scenarios based on the train position relative to the tunnel.

The train will be positioned statically at different locations of the tunnel in each area of study.

- ✓ 1 The train is moving in open field (far away from the tunnel)
- ✓ 2 The train is approaching the tunnel entrance
- ✓ 3 The train head just enters the tunnel entrance
- ✓ 4 Half of the train body has entered the tunnel
- ✓ 5 The train is inside the tunnel
- ✓ 6 The train is about to exit the tunnel

After the basic shape of the train and tunnel has been imported to ANSYS, a parallelepiped computational domain is created. Rectangular domain is the most used for automotive and railway industries for the study of aerodynamics as it better simulates the air flow from inlet to outlet. Domain is a requirement for external flows analysis, it is a box filled with fluid and has boundaries. The passenger train simulated consists of one passenger car and two locomotives which are assumed to be fully loaded with length of 25m and 22.5m respectively, resulting in total length of 70 m (Figure. 3.7) moving at a speed of 33.33 m/s (120 km/h), [Appendix1]

The computational domain is extended by two lengths of train both upstream and downstream of the train. The total length of the computational domain is around 3 times the length of the train. The computational domain is also extended in the transverse directions by 0.5 times the length of the model each on either side of the train. The height of the computational domain is also extended by about 0.5 times the length of the model. A small gap of 0.25m is modeled between the train body and the ground to account for the wheel/rail height. [26].

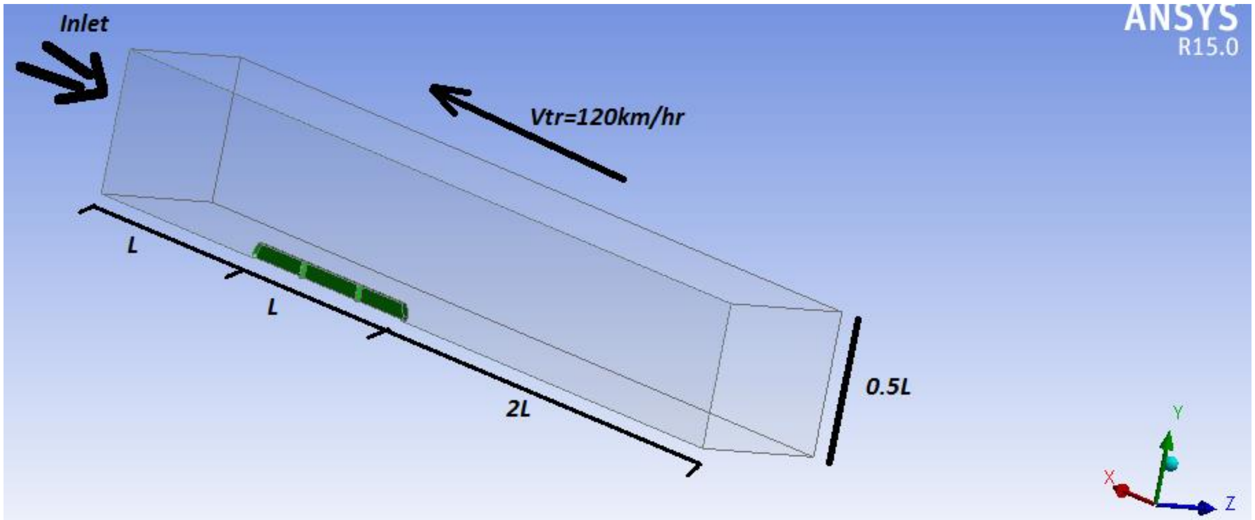

Figure 3-7: Computational domain boundaries for train operating in open field (No tunnel)

The computational domain consists of 4 boundaries Velocity inlet, Pressure outlet and three wall surfaces (Road, Train and tunnel). By increasing the size of the domain box the distance between nose of vehicle and the inlet boundary is sufficient to ensure that the velocity and pressure fields are uniform at the inlet and to allow the flow to develop by the time it reaches the train. The model is also sufficiently far from the top and side walls to minimize near wall effects. The aim of the simulation is to analyze actual trains and tunnel so the full dimensions on all the parameters are used, however, any effect from rails and sleepers is neglected and is not going to be meshed.

1. **The train is moving in open field (far away from the tunnel)**

First numerical simulation for the passenger train traveling in open field, far away from the tunnel entrance were conducted to see the aerodynamic effect on the movement of the train.

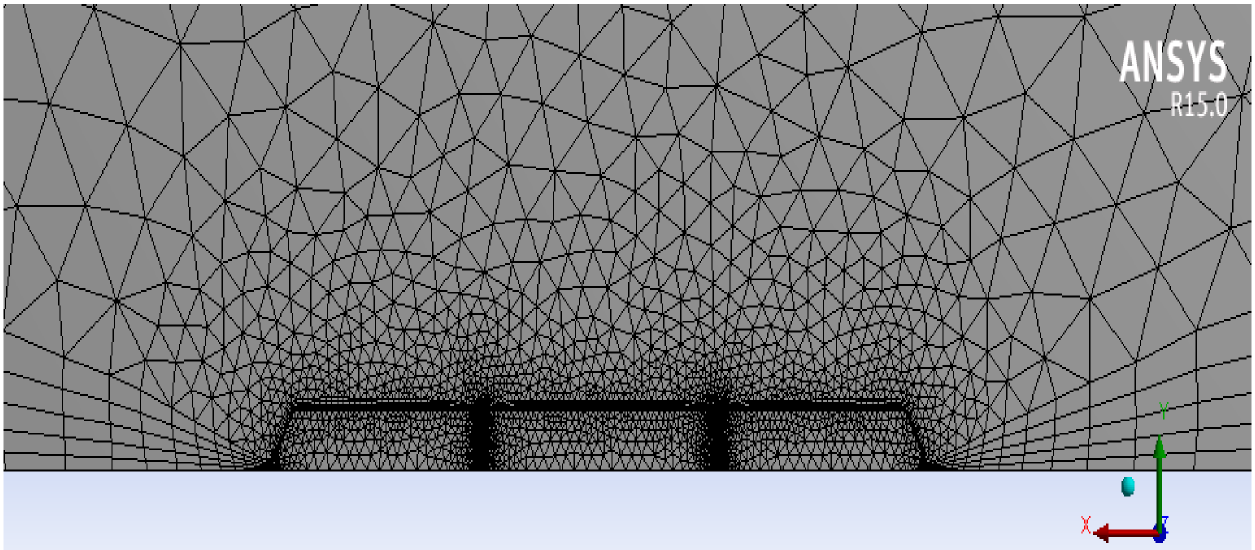

Figure 3-8: Computational mesh for train operating in open field (No tunnel)

All 6 surfaces of the virtual wind tunnel (air-box) have been named so the numerical solver of ANSYS FLUENT® would recognize them and apply the appropriate boundary conditions automatically.

Table 3.7: Boundary conditions and zone names for computational domain of train in open field simulation

Zones name	Boundary conditions
Inlet	Velocity-inlet
Outlet	Pressure-outlet
Train	Wall
Ground	Wall
Symmetry side	Symmetry
Symmetry side1	Symmetry

2. The Train is approaching the tunnel entrance

The domain features (tunnel and train) correspond nearly the same to the shapes and size of real objects. The tunnel portal is modelled as vertical flat wall rectangular to the train motion direction. For the modeling of the train approaching the tunnel entrance, the train is initially positioned with the front head of the train 2 m from the tunnel entrance portal, while the whole train body is placed in open field. This distance gap is enough to show the aerodynamic loads on the train as the train approaches the confined space. [66]. In figure 3.9; the computational domain and mesh topology for the train approaching the tunnel entrance can be seen.

Table 3.8: Setup for train approaching the tunnel entrance

Parameters	**Values**
Train length [m]	70m
Blockage ratio [-]	43.55 % and 38.24%
Tunnel length [m]	179m
Distance between the entrance portal and the monitoring point in tunnel [m]	2m

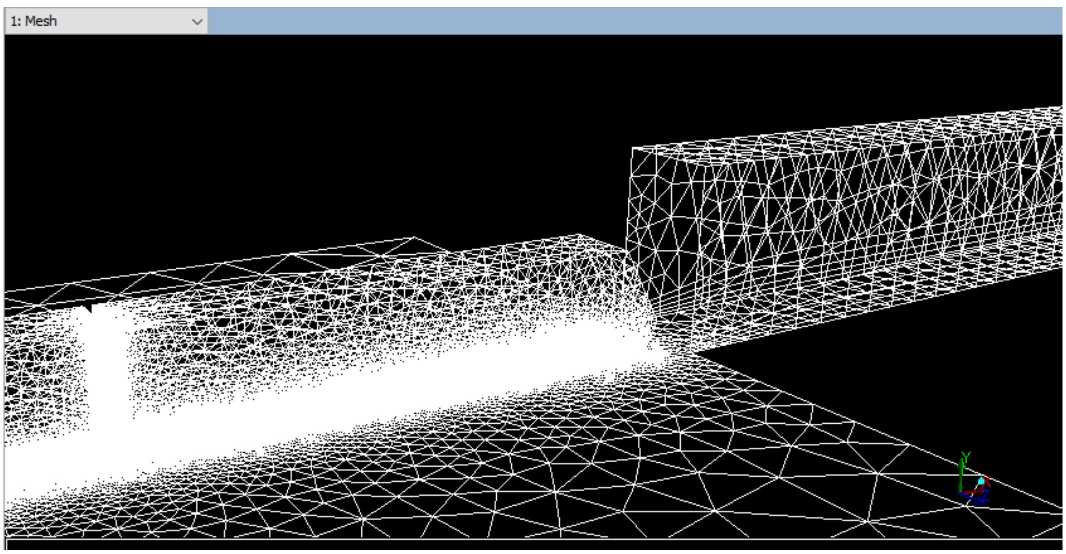

Figure 3-9: Computational domain and Mesh topology for train approaching the tunnel entrance

The computational domain consists of 4 boundaries: velocity inlet, pressure outlet, wall surfaces and symmetry. Boundary conditions for train approaching the tunnel the computational domain including the train and the tunnel have the following named zones (Table 3.9)

Table 3.9: Computational settings and zone names for train approaching the tunnel entrance

Zones name	Type
Inlet	Velocity-inlet
Tunnel side	Wall
Tunnel side1	Wall
Tunnel top	Wall
Outlet	Pressure-outlet
Train	Wall
Passing Symmetry	Wall
Ground	Wall
Symmetry side	Symmetry
Symmetry side 1	Symmetry

3. The train just enters the tunnel entrance

For the train just enters the tunnel entrance, numerical simulation carried out to study the aerodynamic drag and pressure waves generated by a train after the train front head reaches 5 meters inside from the tunnel entrance. In figure 3.10 the computational domain and mesh topology for the train entering the tunnel can be seen.

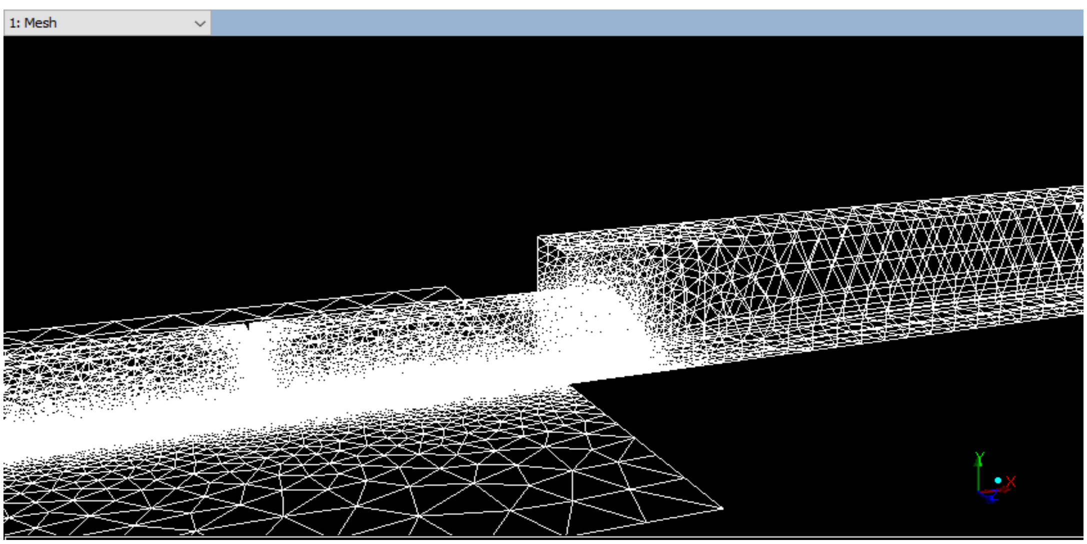

Figure 3-10: Computational domain and Mesh topology for train entering in the tunnel

At the tunnel entrance an inlet boundary condition is defined as a uniform velocity inlet at the extended tunnel exit and a pressure outlet boundary condition is defined at the atmosphere behind the train tail. A symmetry boundary condition (i.e. zero normal velocity and gradients) is assigned to the side and top of the open field zone, while zero static (gauge) pressure is imposed at the end fields behind the tail of the train. A velocity inlet boundary condition is assigned from the extended tunnel exit zone.

4. Half of the train has entered the tunnel

The pressure and aerodynamic flow also studied when the half of the train body entered in tunnel. The basic computational geometry and mesh topology can be seen in Figure 3.11.

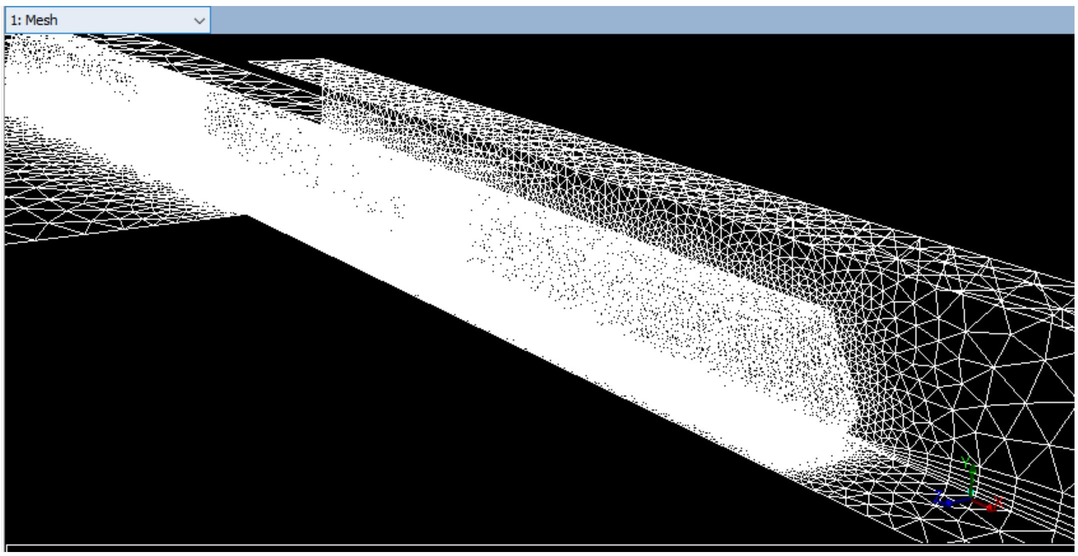

Figure 3-11: Computational domain and Mesh topology when half of the train body has entered the tunnel

At the computational domain boundary following conditions have been set. On boundaries limiting the open spaces ahead and behind the tunnel, the velocity inlet (33.33m/s) and pressure outlet boundary condition (Pstp = 0Pa) respectively has been applied, while the ground, tunnel and train set surfaces were defined as a solid wall.

5. The train is passing through the tunnel

The scenario when the train is traveling inside the tunnel, the whole train body remained within the confines of the tunnel for the entire period of travel. The air-zone length in front of and behind the train is equal to the tunnel length of 179 m, to take into account the pressure gradients created by the train traveling inside the tunnel. The set-up consisted of a tunnel, both ends open to the atmosphere, in which a model train was passed. Here we refer to the tunnel entrance as the portal which the train is travelling away from and the tunnel exit as the portal the train is travelling towards.

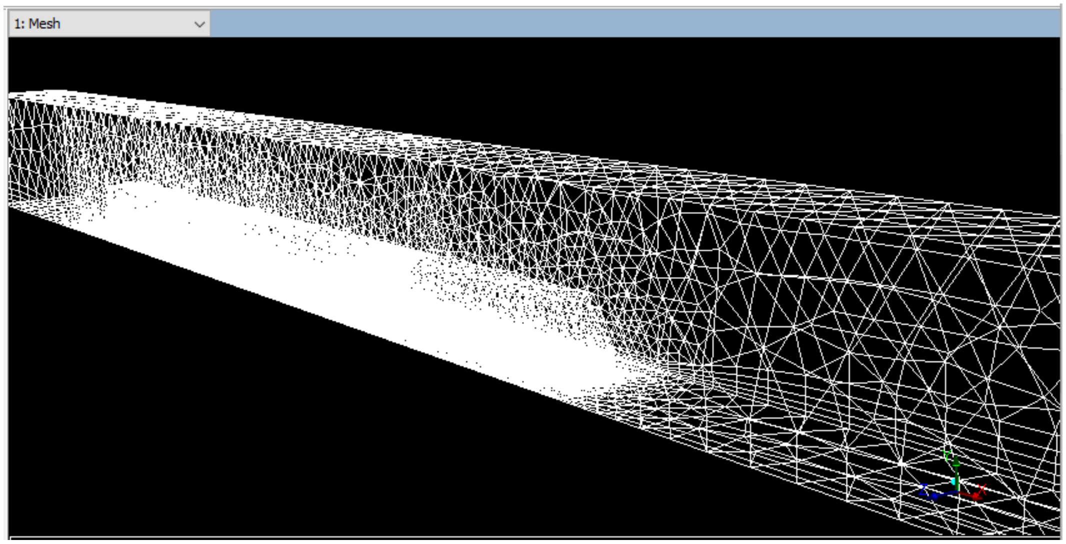

Figure 3-12: Computational domain and Mesh topology for train traveling inside the tunnel

6. The train is exiting the tunnel

For the train just exiting from the tunnel exit portal, numerical simulation carried out to study the aerodynamic drag and pressure loads generated by a train after the train front head exits 5 meters from the tunnel exit portal. In figure 3.13 the computational domain and mesh topology for the train coming out of the tunnel can be seen.

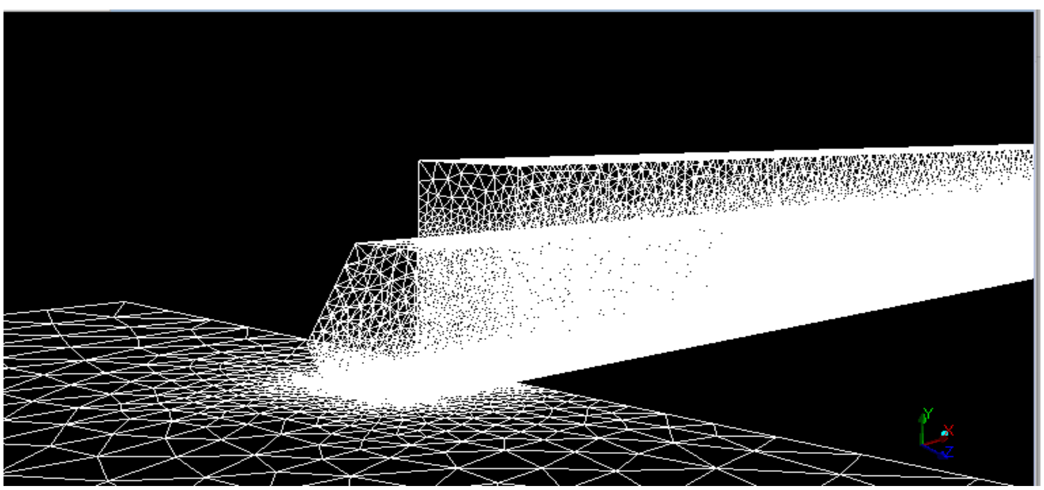

Figure 3-13: Computational domain and Mesh topology for train exiting the tunnel

The computational domain boundary conditions have been set an inlet boundary condition of air (33.33m/s) and at the tunnel entry portal, an outlet boundary condition of 0 Pa was applied.

Mesh sizing

Mesh generation constitutes one of the most important steps during the preprocess stage after the definition of the domain geometry. General proportions of the 3D computational domain takes into account both volumetric needs of the problem (resulting from the tunnel and train proportions prescribed as well as from the mesh method applied for the train movement simulation) and computational power available on the other hand.

CFD requires the subdivision of the domain into a number of smaller, non-overlapping subdomains in order to solve the flow physics within the domain geometry that has been created; this results in the generation of a mesh (or grid) of cells (elements or control volumes) overlaying the whole domain geometry. With the global mesh sizing settings, ANSYS Meshing® recognized that there were some curvatures around the vehicle body. But the meshing was very coarse and it was only the initial guess by the software.

The accuracy of a CFD solution is governed by the number of cells in the mesh within the computational domain. In general, the provision of a large number of cells leads to the attainment of an accurate solution. However, the accuracy of a solution is strongly dependent on the imposed limitations dominated by the computational costs and calculation turnover times. In order to capture more accurate data through solver we needed to improve the mesh. The first thing to do was changing the mesh sizing parameters. Note that the grid is chosen based on grid-sensitivity analysis with three grid configurations shown in Figure 3.14.

i. Course Meshing

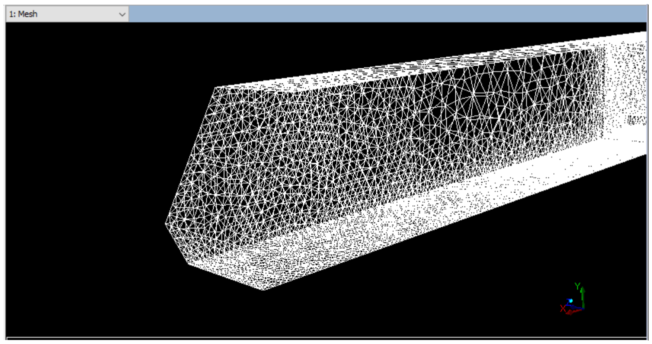

Statistics	
Nodes	209563
Elements	569359
Mesh Metric	Skewness
Min	6.35289207738143E-04
Max	0.881139588129516
Average	0.254701684766765
Standard Deviation	0.132410623356032

ii. Medium Meshing

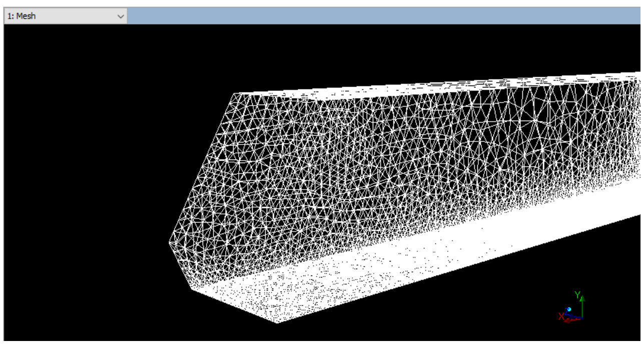

Statistics	
Nodes	483162
Elements	1238026
Mesh Metric	Skewness
Min	1.07558991171874E-04
Max	0.897809275949934
Average	0.242245136863746
Standard Deviation	0.12910425736133

iii. Fine Meshing

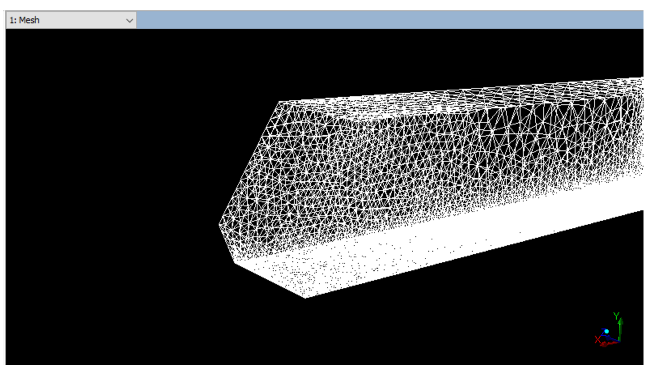

Statistics	
Nodes	482722
Elements	1239762
Mesh Metric	Skewness
Min	3.4306847798049E-04
Max	0.897809380080899
Average	0.242018285236878
Standard Deviation	0.1287434283953

Figure 3-14: Overview of three grids for grid-sensitivity analysis.

The aerodynamic drag coefficient are computed for the three grids (Fig. 3.15). Results of the middle and fine grids correspond well to each other, while the coarse grid provides markedly different aerodynamic drag coefficient when the train is travelling in the tunnel.

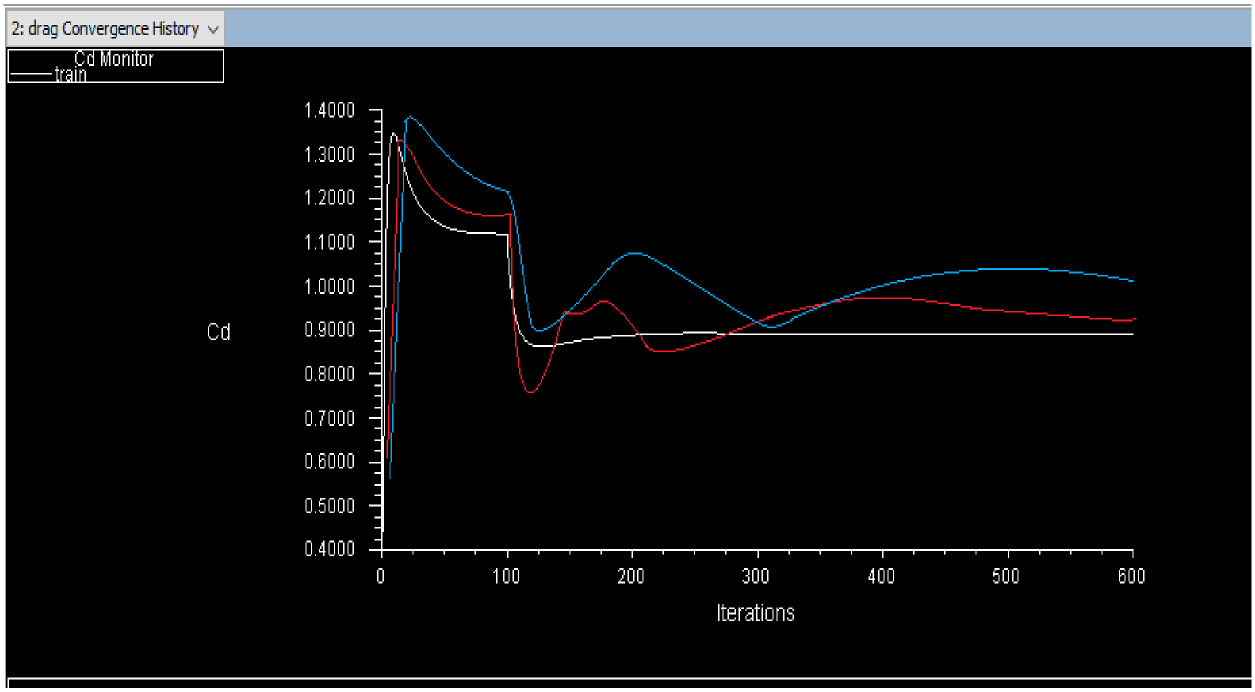

Figure 3-15: Coefficients of drag convergence history obtained by CFD simulations with the three different grids; Colored with 'Blue' for coarse, 'Red' for Medium and 'White' for Fine grids.

The convergence plots indicates of satisfying results is: as the residuals of all equations of drag and lift convergence history solved dropped below the 10^{-3} ratio and the fine grid shows enough for proper convergence history compared with the others grids. Therefore, the fine grid is used in the simulation study. For this grid, the number of cells along the computational domain is 1239762 number of cells.

3.3.2 Fluent Solver settings

The problem of vehicle external flow numerical analysis required the solver settings to be completed before starting the simulations. The solver setting includes type of solver (3D or 2D), the viscous model, boundary conditions and solution controls. For the present work the solver used was Fluent 15. In this section a short descriptions of the boundary conditions are presented in order to give an overview of the driving conditions during the simulation, see Table 3-10. The established wind speed or driving speed of the passenger train used in current Ethiopian railway system is 120 Km/hr (33.33m/s) and this speed is used in this investigation. At this velocity the density can be assumed to be constant and the governing equations are then pressure based and the flow is incompressible [66]. The governing equations of unsteady incompressible flow are mass conservation equation and Reynolds-averaged-Navier–Stokes equations are solved using ANSYS-Fluent code. Another well documented practice within CFD-simulations is the use of the *realizable k-ε turbulence* model together with non-equilibrium wall-functions when solving the RANS-equations in fluent, which will also be used during this project. The solver settings, boundary condition and solver settings for all the cases are shown in the tables below (Table 3.10, Table 3.11 and Table 3.12).

Table 3.10: Summary of solver settings

Solver	Fluent 15.0
CFD Simulation	3D Pb (3-D Pressure Based)
Solution Procedure	Coupled
Processing (Run Precision)	Single
Time	Steady state
Velocity formulation	Absolute
Gradient Option	Cell-Based
Fluid Flow	Incompressible (viscous) Flow

Following are the steps taken for setting up the solving techniques in solver for 3D, steady state, incompressible flow using single precision and serial processing technique.

- Imports the meshed model created in Workbench and check the mesh.
- Scale the mesh as per the dimensions specified with appropriate scaling factor.
- The solver specifications such as pressure based, absolute velocity formulation and steady state are set.
- Defining models such as viscous model (Realizable k-ε model) is done. A Non-equilibrium wall function is opted for near-wall treatment.

The inlet of the computational domain was indicated by the term “velocity-inlet” Air coming through the inlet was given a velocity of 120 km/h which approximated to 33.33 m/s, while the outlet of the computational domain was termed as “pressure-outlet”. The rail road, the train body were and the tunnel made walls. The surrounding enclosure surfaces, being imaginary surfaces, were all named symmetry planes having a “no slip‟ condition.

Table 3.11: Summary of boundary conditions settings

Boundary Conditions		
Turbulence Model	*realizable k-ε turbulence* Model	
Velocity Inlet	Magnitude (normal to boundary)	33.33m/s
	Turbulence Specification Method	Intensity and Viscosity Ratio
	Turbulence Intensity	1%
	Turbulence Viscosity Ratio	10%
Pressure Outlet	Gauge pressure magnitude	0 Pascal
	Gauge pressure direction	Normal to boundary
	Turbulence Specification Method	Intensity and Viscosity Ratio
	Back flow turbulence Intensity	5%
	Turbulence Viscosity Ratio	10%
Wall Zones	Wall	Stationary wall (No-slip condition)
	Symmetry	Wall (with specified shear stress=0)
Fluid Properties	Fluid Type	Air
	Density	ρ = 1.117 kg/m^3 (at 303K)
	Kinematic Viscosity	V = 1.568 * 10^{-5} m^2/s (at 303K)

For numerical simulation of the train in open field, the final solution was obtained by performing the iterations in two stages. With each progressive stage, the solver accuracy was raised by employing higher order equations. In the first stage, first order equations were used to prevent the solution from the possibility of divergence. Once sufficient convergence was achieved, the equation order was raised to second order equations. For the numerical simulation of the train operating in the tunnel, the first order equations were used. Iterations were carried up to the point where the change in the value of drag coefficient was found negligible.

Solution Accuracy

Good engineering practice suggests that prior to using an analysis technique on a new configuration, one should benchmark the technique against a known (respected) initial case or test case similar to the new configuration. The validation assessments of a CFD simulation that have been used in this thesis by examine iterative convergence. Validation assessment requires that a simulation demonstrate iterative convergence. During the numerical simulation carried for all cases in this paper, the solution monitors results showed iterative convergence. The mesh metrics-skewness results for all simulations are less than 0.95, therefore the meshing is good enough to show the accurate simulation results. The minimum volume of the meshed domain for simulations is positive, which is the recommended value when doing external aerodynamics. [46]

Table 3.12: Summary of Solution controls settings

Equations	**Flow and Turbulence**	
	For Train in Open field	**For Train in Tunnel**
Discretization	Pressure: Standard	Pressure: Standard
	Momentum: 2^{nd} Order Upwind	Momentum: 1^{nd} Order Upwind
	Turbulence Kinetic Energy: 2^{nd} Order Upwind	Turbulence Kinetic Energy: 1^{nd} Order Upwind
Monitor	Residuals, Drag and Lift Coefficient	Residuals, Drag and Lift Coefficient
Convergence Criterion	Continuity=0.001 X-Velocity=0.001 Y-Velocity=0.001 Z-Velocity=0.001 *k*- = 0.001 ε =0.001	Continuity=0.001 X-Velocity=0.001 Y-Velocity=0.001 Z-Velocity=0.001 *k*- = 0.001 ε =0.001

CHAPTER 4:- RESULT AND DISCUSSIONS

4.1 Results

A 3D steady state, incompressible solution of the Reynolds Average Navier-Stokes equations was performed using ANSYS FLUENT®. Turbulence modeling was done with the realizable k-ε model using non- equilibrium wall functions. The computational results of aerodynamic drag, contour of static pressure and air flow velocity vector for the following cases are presented and discussed.

1. Train moving in open field (far away from the tunnel)
2. Train moving in Addi-onfito tunnel (β_1 = 0.4355)
3. Train moving in tunnel (with smaller blockage ratio), β_2= 0.3824

According to the events mentioned in the numerical sections above, the main part of computed results deals with position-variations of the train aerodynamic drag, static pressure values and component of velocity vectors on the train body along different train positions of train with respect to the tunnel.

4.1.1 Aerodynamic drag

Numerical simulations carried out at the exact same train speed of 120Km/hr and same tunnel length of 179 m, in order to investigate the relationship among the coefficient of aerodynamic drag acting on the passenger train operating in open field and as it travels in the tunnel, with having two different blockage ratios (β_1 = 0.4355 and β_2=0.3824),

By running the simulation for 600 iterations shown to be an adequate in order to achieve low residuals values. The first 100 iterations is done by calculating the RANS equations in first order and the next 500 iterations is done by solving the second order of the numerical mesh. The indicator of satisfying results is: the residuals of all equations of drag and lift convergence history solved dropped below the 10^{-3} ratio by far the simulation of train operating in open field, therefore the 600 iterations appeared to be enough for proper convergence. Simulated results obtained in terms of coefficients of drag, lift and moment for a train moving in open field, at corresponding velocity of air 120km/hr, as shown in Fig 4-1 and Fig 4-2.

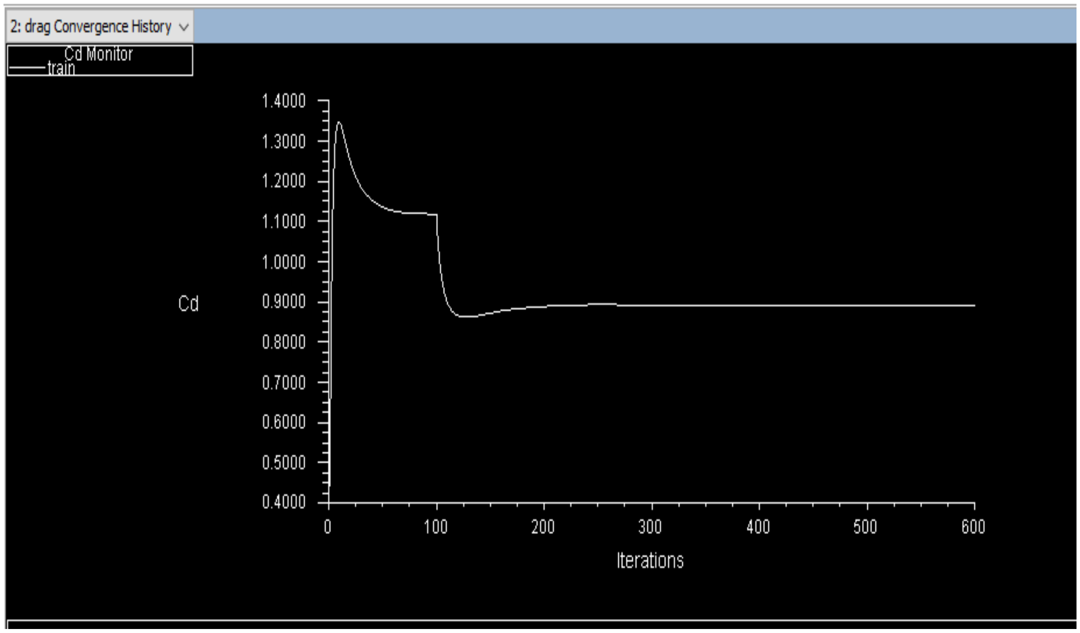

Figure 4-1: Coefficients of drag force convergence history of train moving in open field

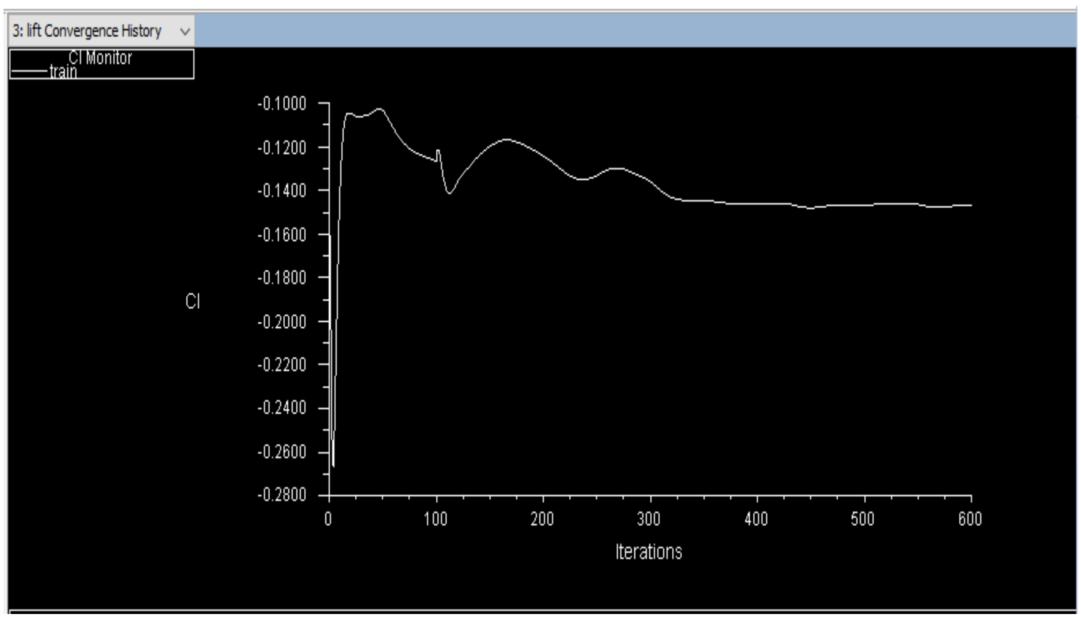

Figure 4-2: Coefficients of lift force convergence history of train moving in open field

The solution is converged at 600'siteration; by calculating the mean value of the last 50 iterations the drag coefficient is 0.89198, and the lift coefficient is -0.14674. From the result the value of drag coefficient (C_D =0.89), with train speed of 120Km/hr and train frontal area A_{tr} of 13.76 m^2 is almost similar with the result of the previous study done on the aerodynamic drag of the train traveling in open filed by (*Mamo Nigussie,2014* [57]), which used same train speed and model.

The present paper is more concerned on the aerodynamic loads effect on the train as it travels in the tunnel, since the effect of train speed and front head shape of the train on the aerodynamic loads of train traveling in tunnel is not as much as the effect of blockage ratio: the effect of train speed and frontal area is not considered.

All the results for two different train-tunnel (β_1 andβ_2) configuration were obtained with the same meshing resolution, the same $k-\varepsilon$ turbulence model, and also the same boundary conditions. The free stream velocity was set to be 120Km/hr (~33.33m/s, which is the speed design in Ethiopia railway line). For the first 100 iterations, a first order upwind discretization has been applied and iterations have continued until it reached to the convergence criteria. the residuals of all equations of drag and lift convergence history solved dropped below the 10^{-3} ratio by far the simulation of train operating in tunnel, therefore the 100 iterations appeared to be enough for proper convergence. The plots of coefficients of drag for a train moving in the tunnel for 2 different blockage ratios (β_1 andβ_2) are shown in Figure 4-3 and figure 4-4.

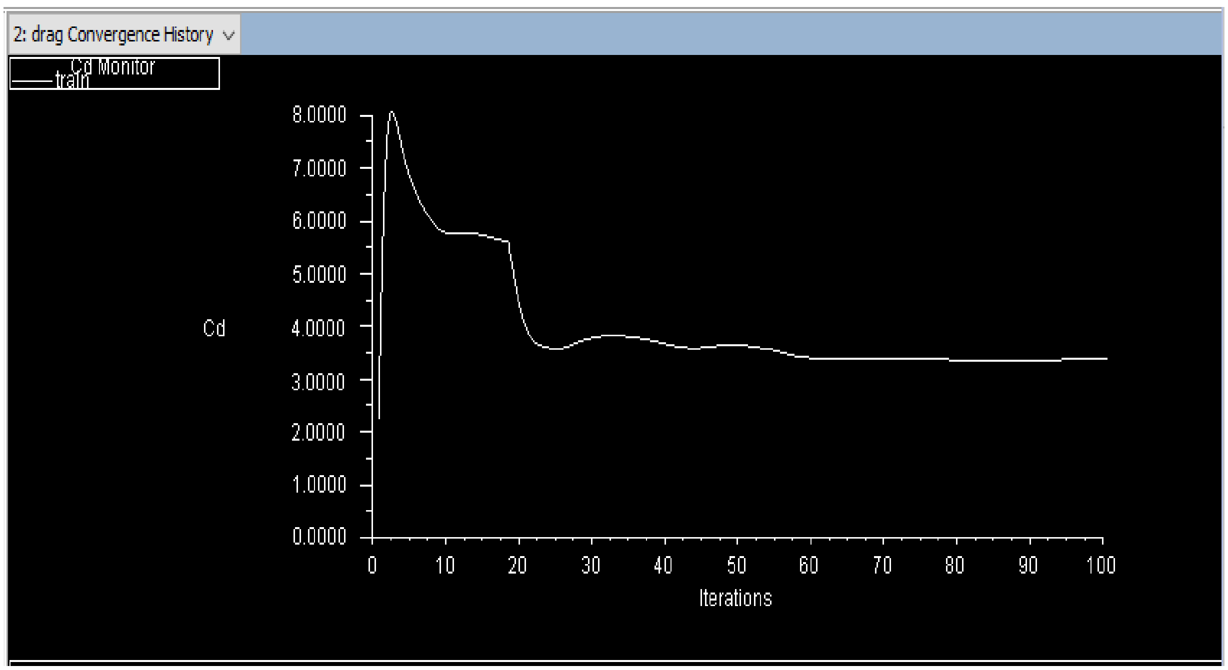

Figure 4-3: Coefficient of drag for train entering the Addi-onfito tunnel entrance (β_1=0.4355)

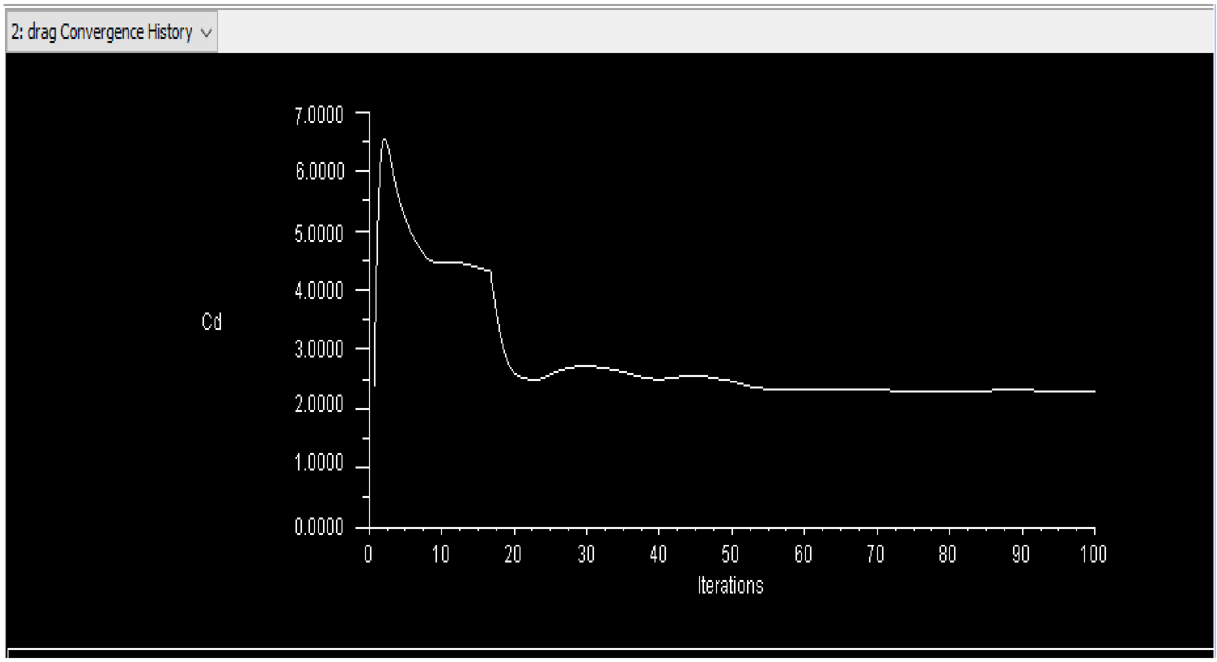

Figure 4-4: Coefficient of drag for train entering the tunnel entrance for blockage ratio (β_2=0.3824)

From the simulation results of the drag coefficient convergence plot above; the aerodynamic drag forces increased; as the train travels in the tunnel. In order to maintain the desired speed the train as it travels in tunnel, it is necessary that the electric motor power increases or the aerodynamic drag reduces. The above figures of coefficient of drag convergence history for both train-tunnel configurations, shows that; the coefficient of drag for the train traveling in smaller blockage ratio, tunnel **(β_2 = 0.3824)**, ($C_{D2} = 2.302$) is visibly smaller than coefficient of drag force of the train travelling in Add-onfito tunnel **(β_1 = 0.4355)**, ($C_{D1} = 3.261$). This will afford the stability and reduction on the aerodynamic power consumption in the modified train-tunnel configurations **(β_2=0.3824)**.

In the open air traveling, the aerodynamic drag on train can be divided into two contributions; one is dependent on train length and the other is independent of it. The drag independent of the train length is the pressure drag caused by the fore- and after-bodies of train, which is the force caused by the pressure distributed on the train along the reverse running direction. Friction drag of the train is the sum of shear stress (viscous), which is the reverse direction of train running direction.

The friction drag on the train body should involve all kinds of the drags occurring in the connecting parts between trains, photographs, the structures under the train, etc.

The Drag Force, F_D, acts in the direction of the free stream while the Lift Force, F_L, is normal to the free stream. Typically, the lift and drag are given in terms of the Coefficient of Lift (C_l) and the Coefficient of Drag (C_D) which are dimensionless forms of the Lift and Drag forces. The formula for the relationship of required variables given optionally as follows [61].

The friction coefficient, C_F, $$C_F = \frac{\tau}{{}^1\!/_2 * \rho * {V_{tr}}^2} \quad (4.1)$$

The pressure coefficient, C_P, $$C_P = \frac{P}{{}^1\!/_2 * \rho * {V_{tr}}^2} \quad (4.2)$$

The drag coefficient, C_D , $$C_D = \frac{F_D}{{}^1\!/_2 * \rho * {V_{tr}}^2\ A} \quad (4.3)$$

The lift coefficient, C_L , $$C_L = \frac{F_L}{{}^1\!/_2 * \rho * {V_{tr}}^2\ A} \quad (4.4)$$

Where: - A is the frontal cross sectional area of the train in the traveling direction, F_D is the drag force in opposite to the travelling direction, V_t is the train speed (V_{tr} = 33.33 m/s), ρ is the density of air (ρ = 1.177 kg/m^3 at temperature value of 30°c).

As aerodynamic drag is composed of the pressure drag and friction drag, the drag force on a rigid body surface could be divided into two components, namely frictional drag (viscous drag) and pressure drag (form drag). The aerodynamic forces on a body come primarily from differences in pressure and viscous shearing stresses. The net drag force could be decomposed as follows:

$$C_D = \left(\frac{2\,F_D}{\rho\,V^2 A}\right) = C_P + C_F \quad (4.5)$$

$$= \left(\frac{1}{\rho\,V^2 A}\right) \oint_s \ dA(p - p_o)(\hat{n}.\hat{\imath}) + \left(\frac{1}{\rho\,V^2 A}\right) \oint_s \ dA(\hat{t}.\hat{\imath})\,\tau_w \quad (4.6)$$

Where: C_P = the pressure drag coefficient, C_L = the friction drag coefficient, $\hat{t}$ = Tangential direction to the surface with area dA, $\hat{n}$ = Normal direction to the surface with area dA, τ_w = the shear Stress acting on the surface dA, p_o = the pressure far away from the surface dA, p = pressure at surface dA, $\hat{\imath}$ = the unit vector in direction normal to the surface dA, forming a unit vector dA.

Thus, on the above equations, the total aerodynamic drag is the sum of friction and pressure drag components. Trade-off relationship between pressure drag and friction drag means the total drag increase while either of the drag components are fluctuating.

$$C_D = \frac{F_D}{1/_2\ \rho V_t^2 A} = C_F + C_P = \frac{\tau}{1/_2 * \rho * V_{tr}{}^2} + \frac{P}{1/_2 * \rho * V_{tr}{}^2}$$

The above formula shows the direct relationship between the coefficient of drag and shear stress and pressure. This shows for any place where maximum velocity being higher will lead to higher shear stress and will be cause for coefficient of drag becoming higher. But as discussed above at appoint where shear stress (friction) being higher leads to the reduction of pressure part of the drag. It means, there is tendency of compromising between the shear and the pressure part of the total drag force (total coefficient of drag).

In the case of train travels in open field, the aerodynamic drag expressed previously in Equation (2.5)

$$D = \frac{1}{2}\ \rho A_{tr} V^2 (C_{dp} + \frac{\lambda'}{d'} l)$$

Where V is the train speed, ρ the density of air, A_{tr} the cross-sectional area of train, C_{dp} the coefficient of the pressure drag caused by the fore- and after-bodies of train, d' the hydraulic diameter of train, l the train length, and λ' the hydraulic friction coefficient caused by the connecting parts between trains, photographs, the structures under the train, etc.

A pantograph system may produce the aerodynamic drag corresponding to that caused by one train. In particular, the structures underneath the train may produce more drag, so the aerodynamic drag caused by pantograph system is relatively small and not considered in this case.

Compared with the open air traveling, the aerodynamic drag is considerably increase as the train passes through a tunnel. This is because the train induced flows do work to increase the pressure by interacting with the tunnel walls.

The aerodynamic drag on the train traveling in the tunnel is given by in equation Eq (2.16)

$$\frac{D}{A_{tr}} = \frac{1}{2}\rho \begin{Bmatrix}\beta \\ o\end{Bmatrix} (u' - V)^2 + \frac{1}{2}\rho C_{dp} \begin{Bmatrix}(u' - V)^2 \\ u^2\end{Bmatrix}$$
$$+ \frac{1}{2}\rho \frac{\lambda'}{d'} \left\{ \int_{in} (V - u') \parallel V - u \parallel dx + V^2 \int_{out} dx \right\} + \Delta p'$$

Where D is the aerodynamic drag and A_{tr} the cross sectional area of train. β and 0 in the first term on the right side are, respectively, taken for the fore-body of train to be inside and outside tunnel. In similarly $(u' - V)^2$ and u^2 in the second term are selected for the after-body of train to be inside and outside tunnel, respectively. The integral of the third term is performed along train length, and the subscripts in and out indicate the inside and outside tunnel, respectively. The last term p' on the right side is the pressure difference between the fore- and after-bodies of train. In the case where the train is fully outside tunnel, Eq. (2.16) reduces to Eq. (2.5) mentioned previously.

The coefficient of aerodynamic drag and lift values for the train moving in open field and while as it travels along in tunnel at different position of train relative to a tunnel, of two different blockage ratios (β_1 $and\beta_2$) are summarized in Table 4.1.

Table 4.1: Summary of aerodynamic drag and lift forces values

	For Blockage ratio 1(β_1 = 0.4355)				**For Blockage ratio 2 (β_2=0.3824)**			
Cases	C_D	F_D(N)	C_L	F_L(N)	C_D	F_D(N)	C_L	F_L(N)
Open field	0.892	8358.94	-0.147	-1375.	0.892	8358.94	-0.147	-1375.
Approaching tunnel	2.03724	19093.9	-1.454	-1362	1.769	16523.7	-0.408	-1825
Entering tunnel	2.68714	31762.8	-0.525	-2925	2.186	21386.3	-0.148	-2394
Entering tunnel (half body)	3.2612	36221.3	-0.295	-2772	2.302	25912.7	-0.285	-2678
In the tunnel	1.8580	17412.0	-0.163	-1532	1.8068	16932.2	-0.141	-1317
Exiting tunnel	1.51270	14175.94	-0.328	-3080	1.5088	14140.1	-0.285	-2677

The largest aerodynamic drag is obtained, when the train heads entered in the tunnel (F_D = 36221.3 N) as the train travels in Addi-onfito tunnel compared with the train operating in open field; however, the aerodynamic drag in the smaller blockage ratio (β_2=0.3824) configuration shows a less drag increment at each positions of the train relative to the Addi-onfito tunnel configuration **(**β_1 = 0.4355**)**.

4.1.2 Pressure contours

A series of numerical simulation were undertaken on the train traveling in Addi-onfito tunnel, the simulated results; contours of pressure on the train body due to the train movement through the tunnel has been studied for six different scenarios based on the position of the train relative to tunnel. In order to investigate the relationship among the peak values of aerodynamic pressure acting on the passenger train operating in Addi-onfito tunnel (β_1 = 0.4355) and other tunnel with smaller blockage ratio (β_2=0.3824), numerical simulations carried out at the exact same train speed of 120km/hr and same tunnel length of 179 m.

1. Train moving in open field

The illustration below depicts the contour plots of the static pressure acting on the surface of the front head of train body moving in open field is shown in figure 4-5 and figure 4-6.

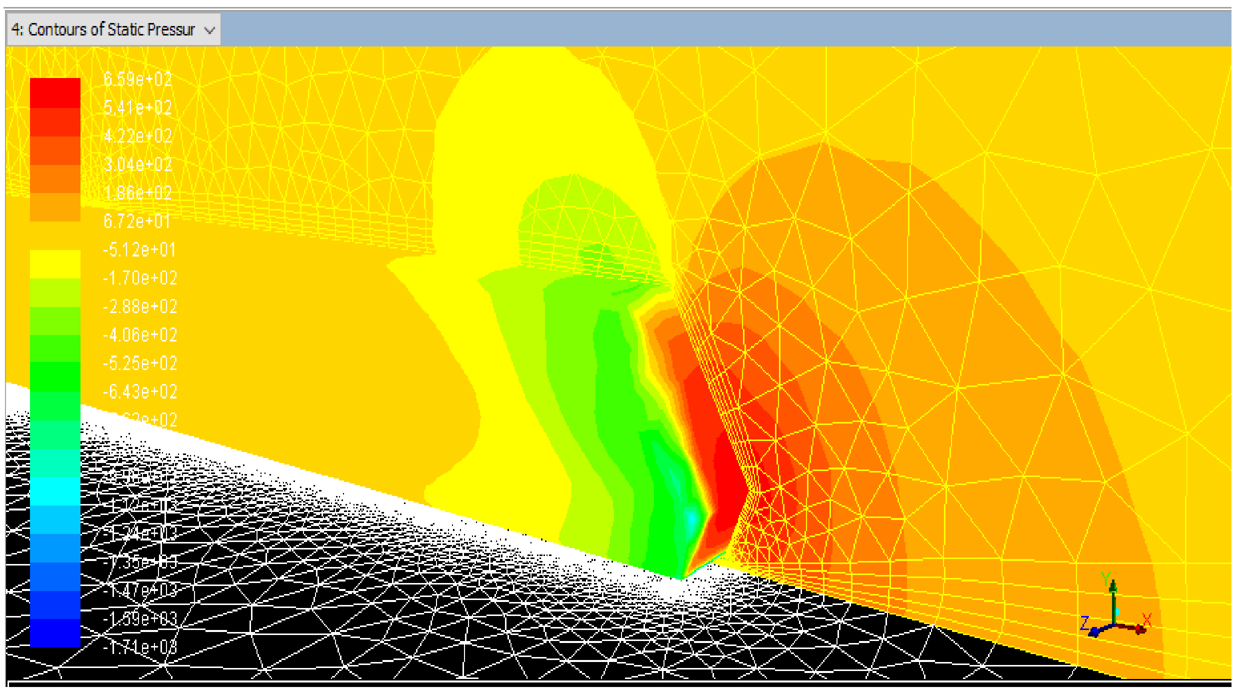

Figure 4-5: The contours of static pressure on the front head of the train moving in open field

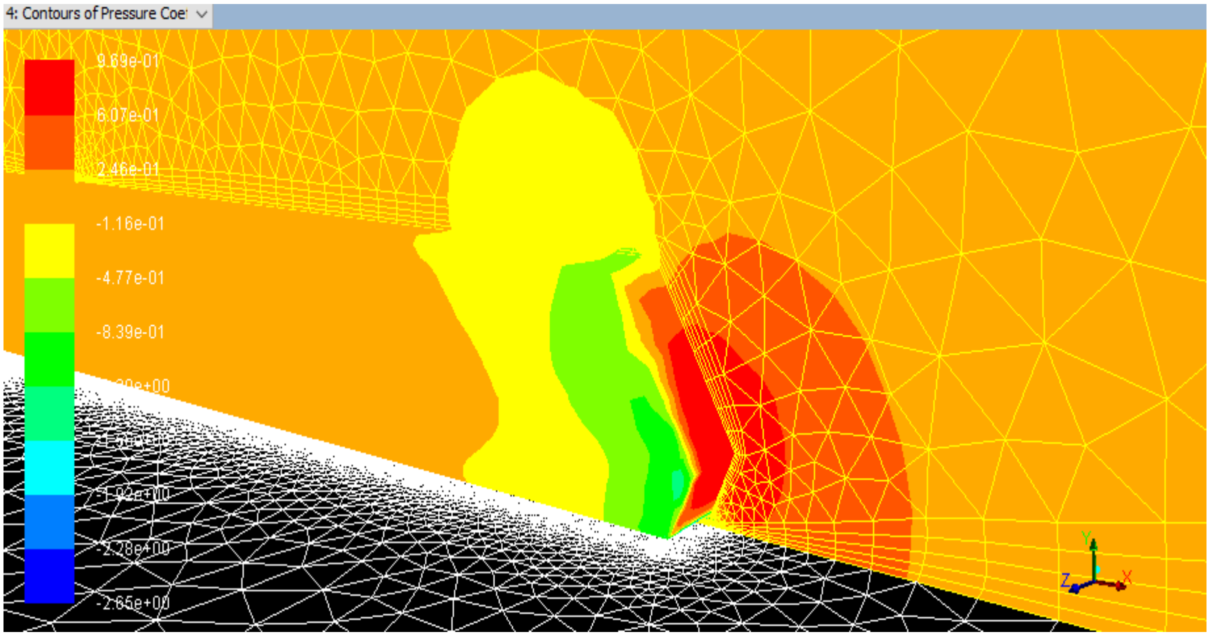

Figure 4-6: The contours of pressure coefficients on the front head of the train moving in open field

As seen in above figure, the present simulation for train moving in open field at speed of 33.33 m/s; the air pushed ahead of the train causes a significant pressure increase in front of the train nose and creates a pressure decrease in the wake behind the tail. Resulting maximum C_p on the front head of 0.96 value, and static pressure reaches P_{st} of 659.07Pa.

2. Train approaching the tunnel entrance

The illustration below depicts the contour plots of the pressure acting on the surface of the train body, when the train approaching the tunnel entrance at the position when the train front head reaches 2 meters from the tunnel entrance portal. The contour plots of the static pressure acting on the surface of the front head of train body approaching the tunnel entrance is shown below in figure 4-7 and figure 4-8.

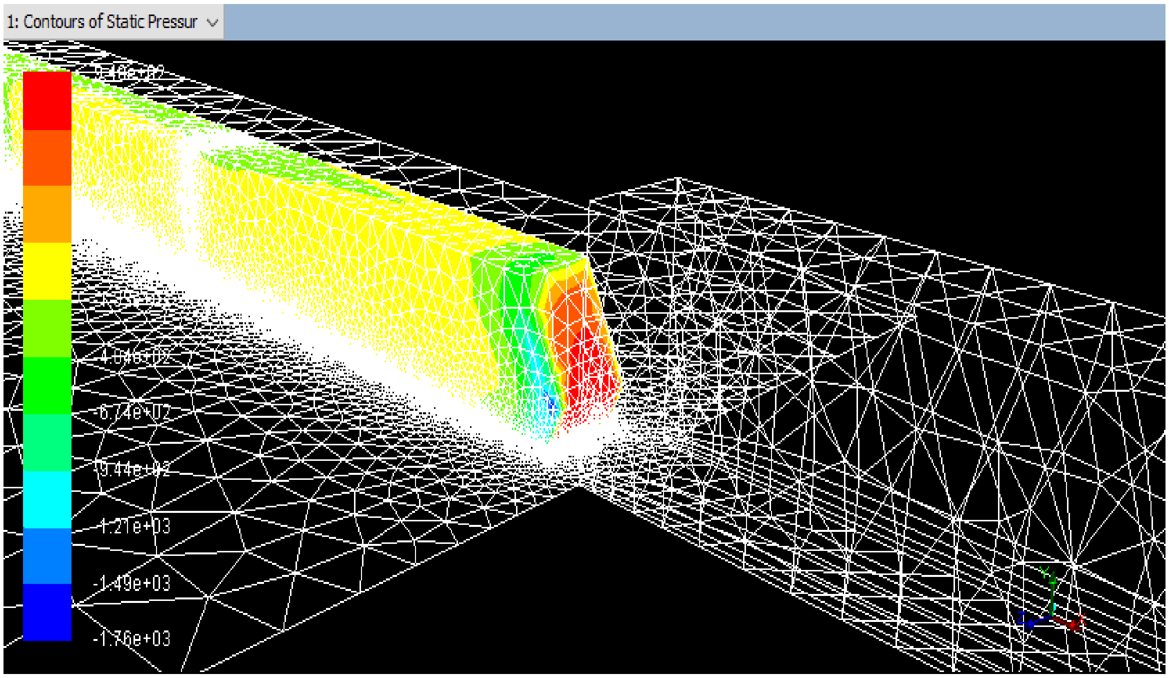

Figure 4-7: The static pressure on the front head of the train at x= 2 m from the entrance portal of Addi-onfito tunnel for configuration (β_1=0.4355)

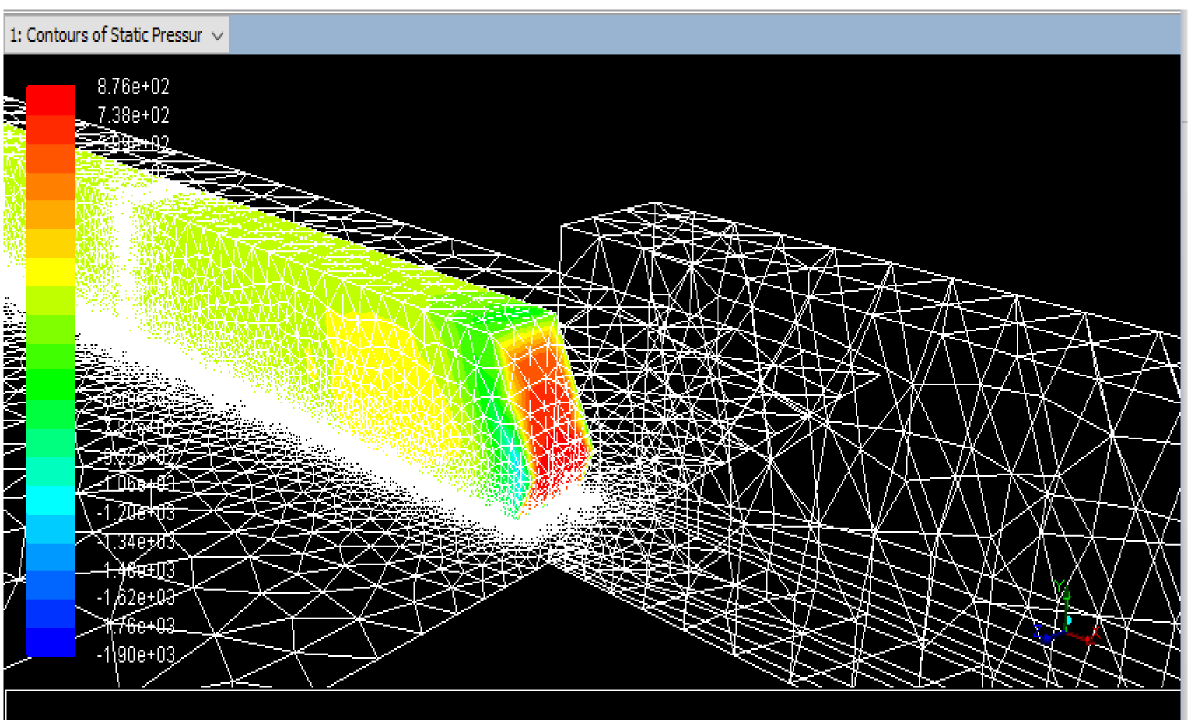

Figure 4-8: The static pressure on the front head of the train at x= 2 m from the entrance portal of the tunnel for configuration (β_2=0.3824)

3. Train entering the tunnel

Simulation results of the contour of static pressure generated on the train body after the train front head reaches 5 meters inside the tunnel entrance for both different blockage ratios (β_1 *and* β_2) is presented.

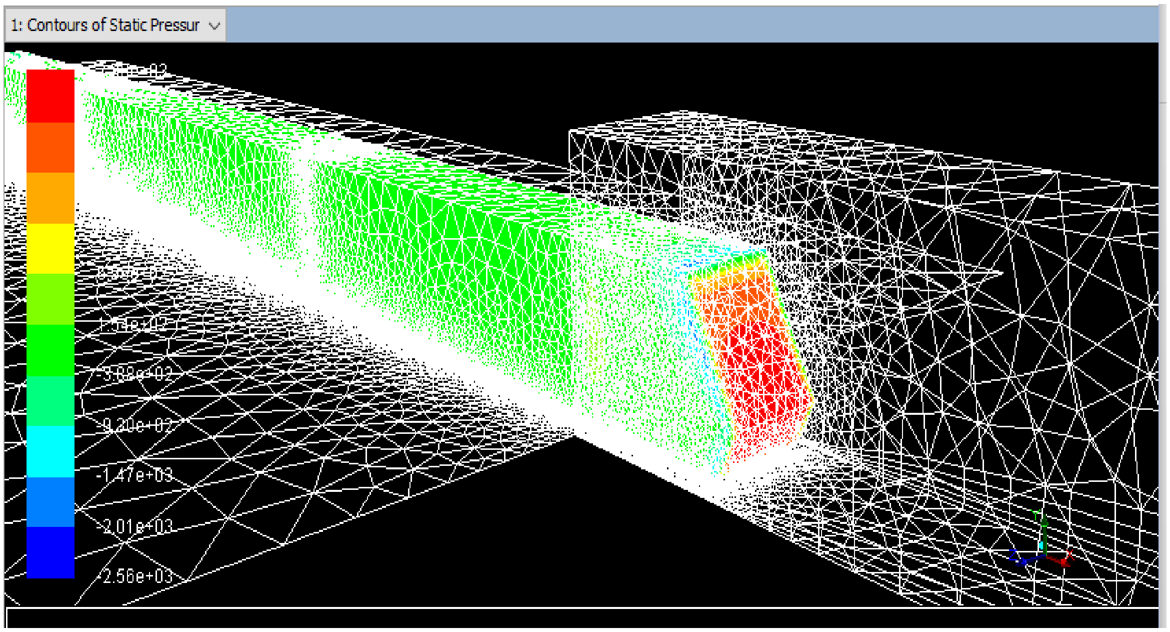

Figure 4-9: Counter of Static pressure on train body due to the train head entrance of 5 meters inside the Addi-onfito tunnel configuration (β_1=0.4355)

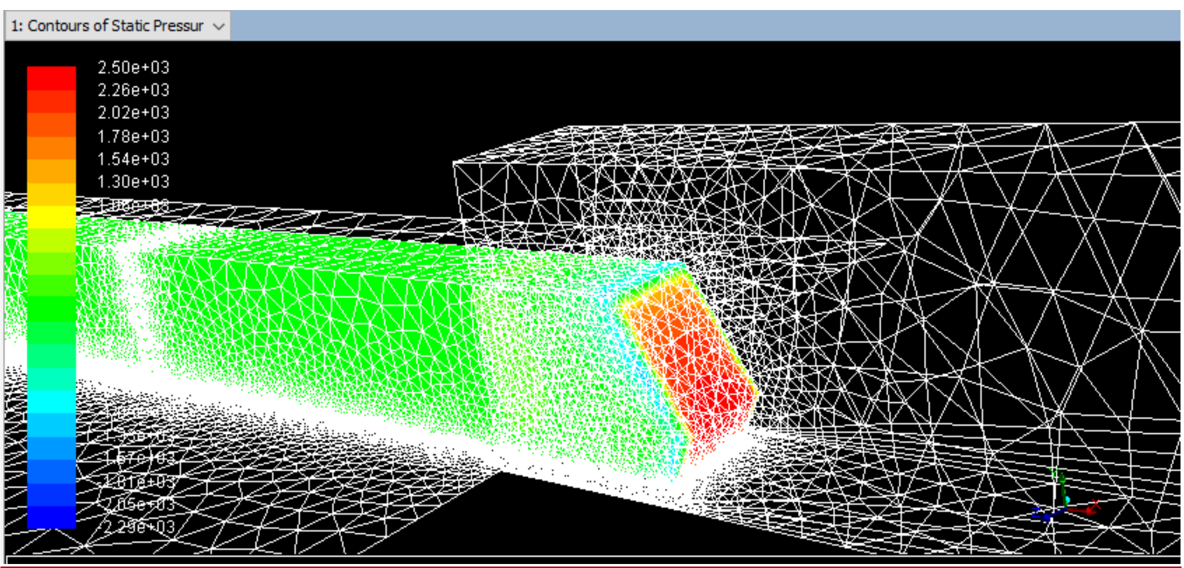

Figure 4-10: Counter of Static pressure on train body due to the train head entrance of 5 meters inside the tunnel for (β_2=0.3824)

4. Half of train body entered the tunnel

The simulation results of static pressure on the front head of the train after the half of the body entered in the tunnel is shown in Figure 4-11 and Figure 4-12, for two blockage ratios (β_1 andβ_2)

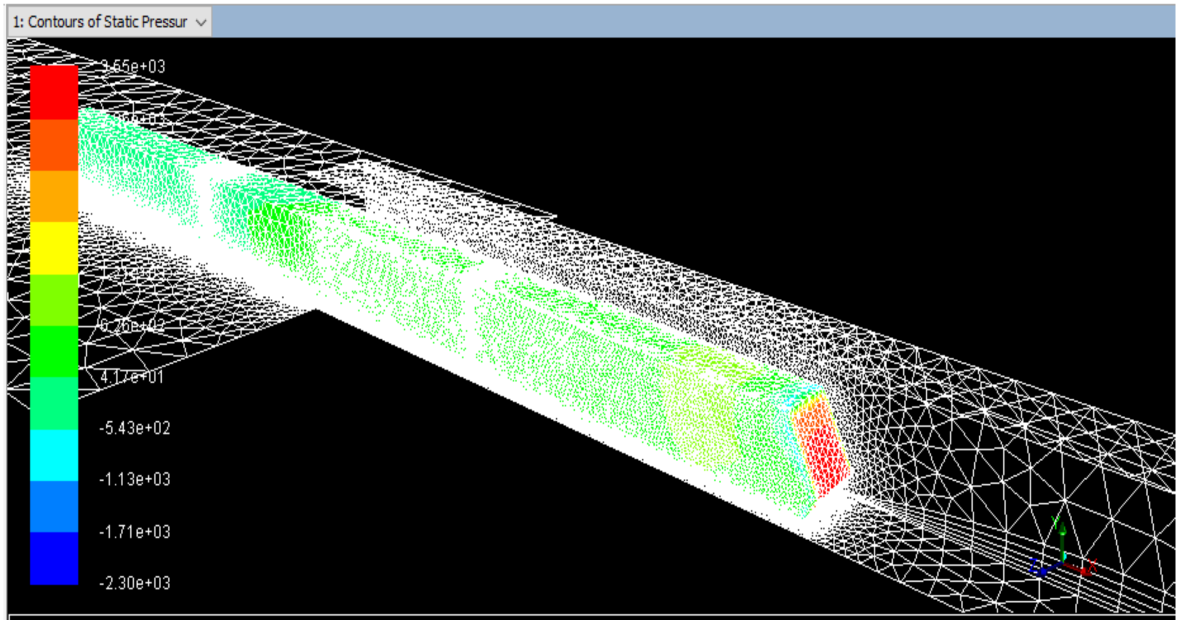

Figure 4-11: Counter of Static pressure on train body when half of the train body entered the Addi-onfito tunnel (β_1=0.4355)

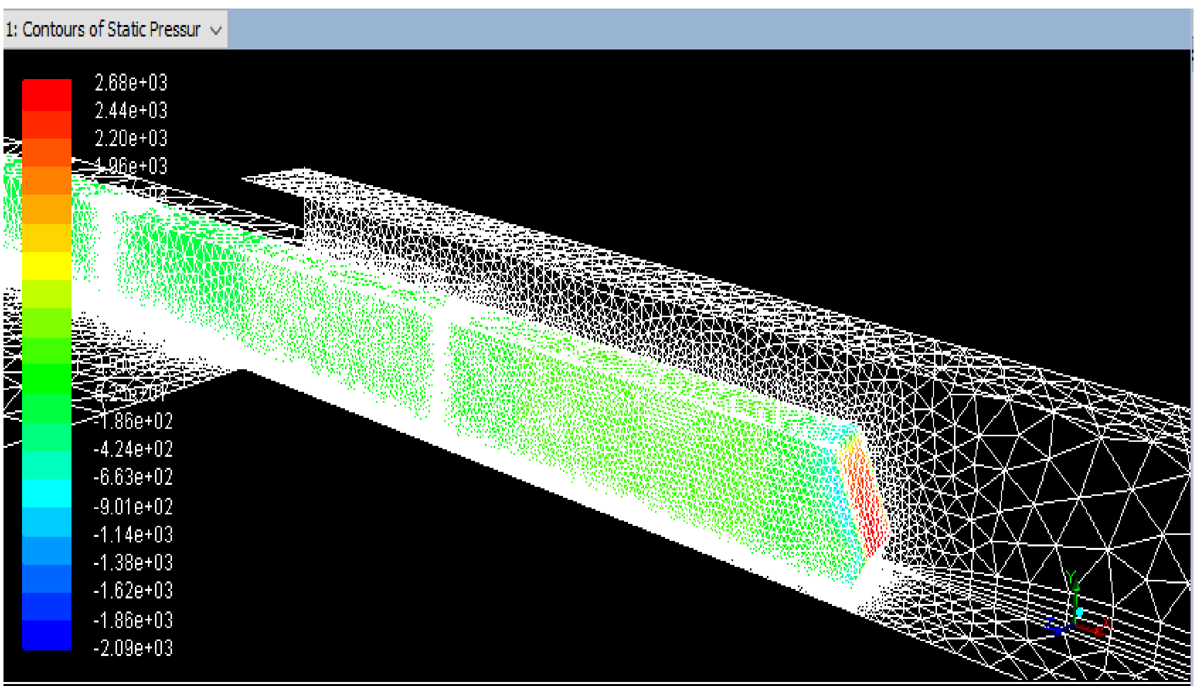

Figure 4-12: Counter of Static pressure on train body when half of the train body entered the tunnel for blockage ratio (β_2=0.3824).

5. Train inside the tunnel

The scenario when the train is traveling inside the tunnel, the whole train body remained within the confines of the tunnel for the entire period of travel. Figure 4-13 and Figure 4-14 shows the contour of static pressure on the front head of the train due the train traveling inside the tunnel.

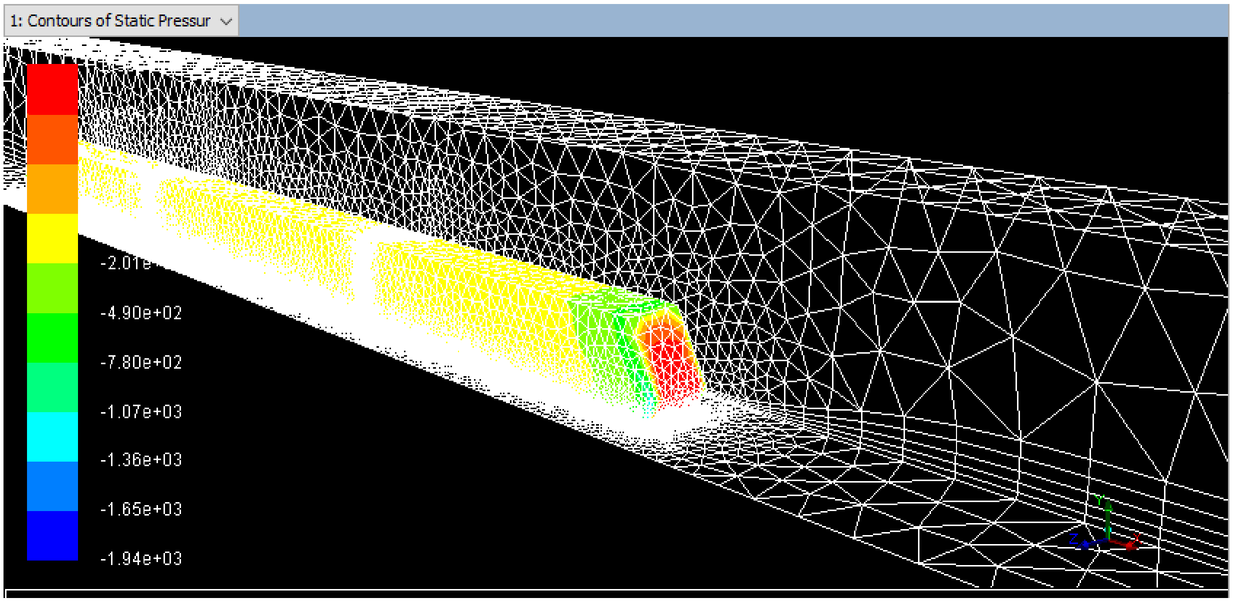

Figure 4-13: Counter of Static pressure on train body when the train passing inside the Addi-onfito tunnel for (β_1=0.4355)

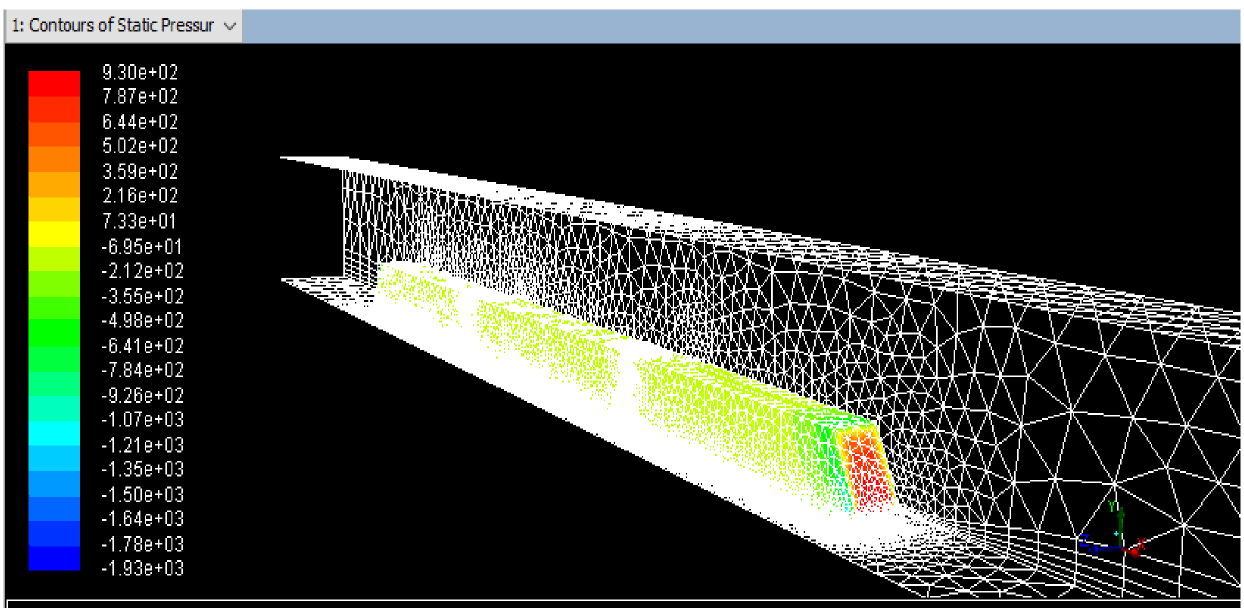

Figure 4-14: Counter of Static pressure on train body when the train passing inside the tunnel for blockage ratio (β_2=0.3824).

From above figures, When the train tail passed the entrance of the tunnel by S-50 m, a noticeable decrease in positive pressure peak was noted for β_1=0.4355 which is 958.73 Pa. Similarly for the smaller blockage β_2 =0.3824 a similar event was observed, a decrease of the maximum static pressure on the front head of the train approximately to 930.04 Pa.

6. Train exiting the tunnel

The simulated contour of static pressure when the train head exits at x= 5 m from the tunnel exit portal is shown in Fig. 4-15 and Fig.4-16.

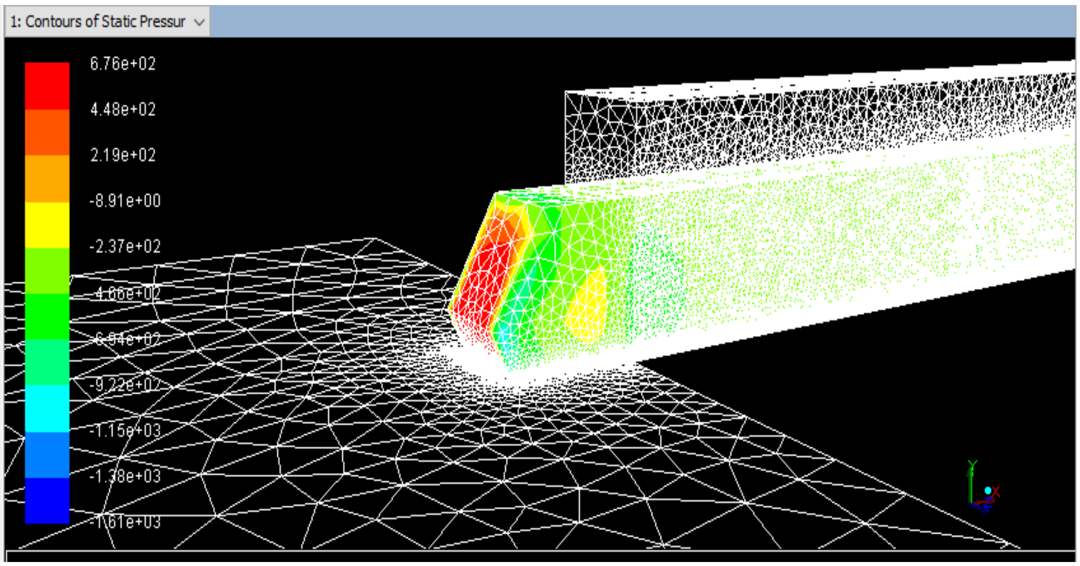

Figure 4-15: Counter of Static pressure on train body when the train exiting the Addi-onfito tunnel (β_1=0.4355)

According to Fig. 4-15, when the nose of the train exiting the tunnel, the peak static pressure gradually fall to 676.18 Pa for the first blockage ratio β_1=0.4355. Similarly at the blockage ratio β_2=0.3824. In Fig.4-16, a gradual fall of peak-static pressure was observed resulting to value of 670 Pa, when the nose of the train exiting the tunnel.

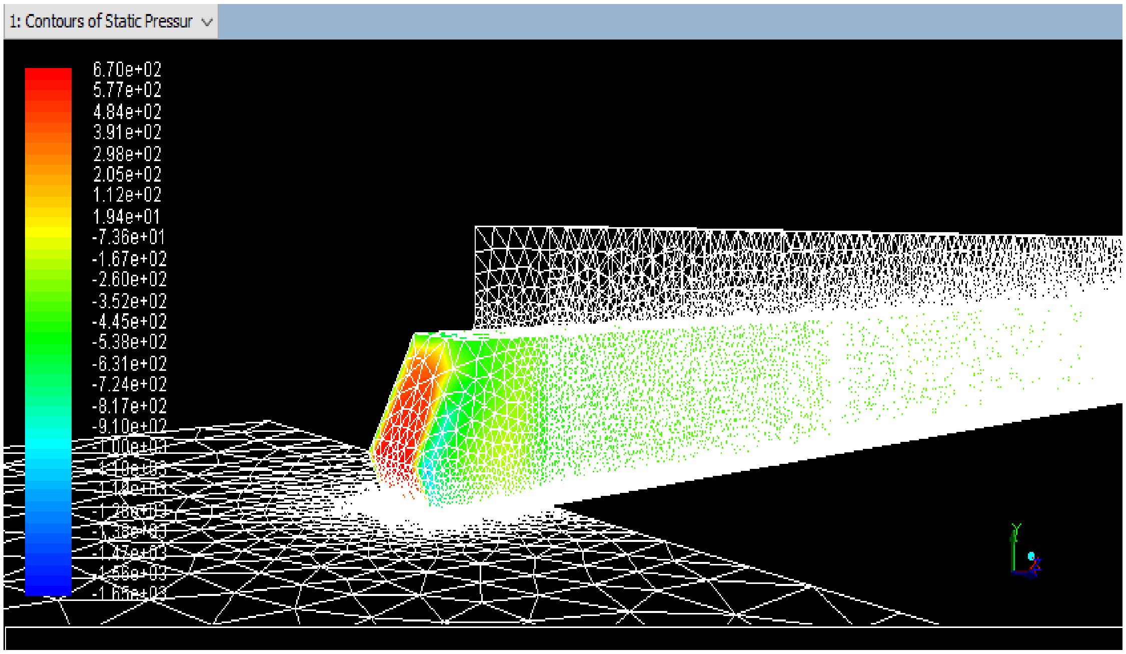

Figure 4-16: Counter of Static pressure on train body when the train exiting the tunnel for blockage ratio (β_2=0.3824)

From the simulated results obtained above; there is a pressure rise on the train body starting at the train position approaching the tunnel entrance, and further magnified when it enters into tunnel. A train entering into the tunnel compresses the atmospheric air ahead of the train and the resulting compression waves will propagate nearly at the speed of sound towards the exit of the tunnel.

Meanwhile, the air displaced by the train entering into the tunnel will discharge back from the entrance of tunnel. In this case, the air flow should overcome the frictional drag on the train body and tunnel walls, resulting in a pressure gradient. Due to this fact, the pressure on the train body will increase as the train proceeds into the tunnel, as schematically shown in above figures.

From the above results; it is shown that the pressure acting on the train body experienced very small changes as the train travels through the tunnel, whereas the nose of the train will first experience a sharp rise in pressure as the train is moving into the tunnel, then a gradual fall as it travels through the tunnel and eventually exit the tunnel. This phenomenon is because the train is traveling through a confined volume of air, thus the pressure will hence experience great appreciation and depreciation.

The pressure experienced at the train nose in each case shows that the presence of pressure waves in a confined volume can greatly affect the pressure force acting on the body. The contour of static pressures acting at the train front, train back, train body and the coefficient of pressures in each cases are tabulated for easy comparison in Table 4-2 and Table 4-3.

Table 4-2: Values of contour of static pressure acting on the train body moving in Addi-onfito tunnel (β_1=0.4355.)

	Static pressure (P_{sta}) for Addi-onfito tunnel (β_1=0.4355.)			
Case	At train head	At train back	At train body	Pressure Coefficient(C_p)
No Tunnel	659.07 Pa	-125.18 Pa	22.45 Pa	0.96
Approaching tunnel	948.32 Pa	-742.37 Pa	-95.65 Pa	1.39
Entering tunnel	2864.63 Pa	-618.64 Pa	-112.85 Pa	4.20
Half of train body entered	3546.76 Pa	-821.13 Pa	176.57 Pa	5.21
In the tunnel	958.73 Pa	-514.36 Pa	-241.35 Pa	1.40
Exiting tunnel	676.18 Pa	-251.01 Pa	-158.24 Pa	0.99

Table 4-3: Values of contour of static pressure variation acting on the train body moving in tunnel (β_2=0.3824)

	Static Pressure(P_{sta}) For Blockage ratio 2 (β_2=0.3824)			
Case	At train head	At train back	At train body	Pressure Coefficient(C_p)
No Tunnel	659.07 Pa	-125.18 Pa	22.45 Pa	0.96
Approaching tunnel	876.29 Pa	-452.35 Pa	-116.27 Pa	1.29
Entering tunnel	2502.34 Pa	-245.63 Pa	-54.68 Pa	3.67
Half of train body entered	2675.49 Pa	-524.92 Pa	221.45 Pa	3.94
In the tunnel	930.04 Pa	-418.79 Pa	-93.52 Pa	1.37
Exiting tunnel	670.10 Pa	-208.54 Pa	-211.23 Pa	0.98

4.1.3 Velocity vectors

The behavior of the aerodynamic parameters, velocity around the train body were studied for both train moving in open field and in tunnels with two different blockage ratios. The velocity ranges from 0 m/s to approximately 78 m/s. the direction of travel in this contour plot will be from left to right.

1. **Train moving in open field**

The contour plots of the velocity of the airflow around the train and velocity magnitude when the train is moving in open field are shown in Figure 4-17 and Figure 4-18.

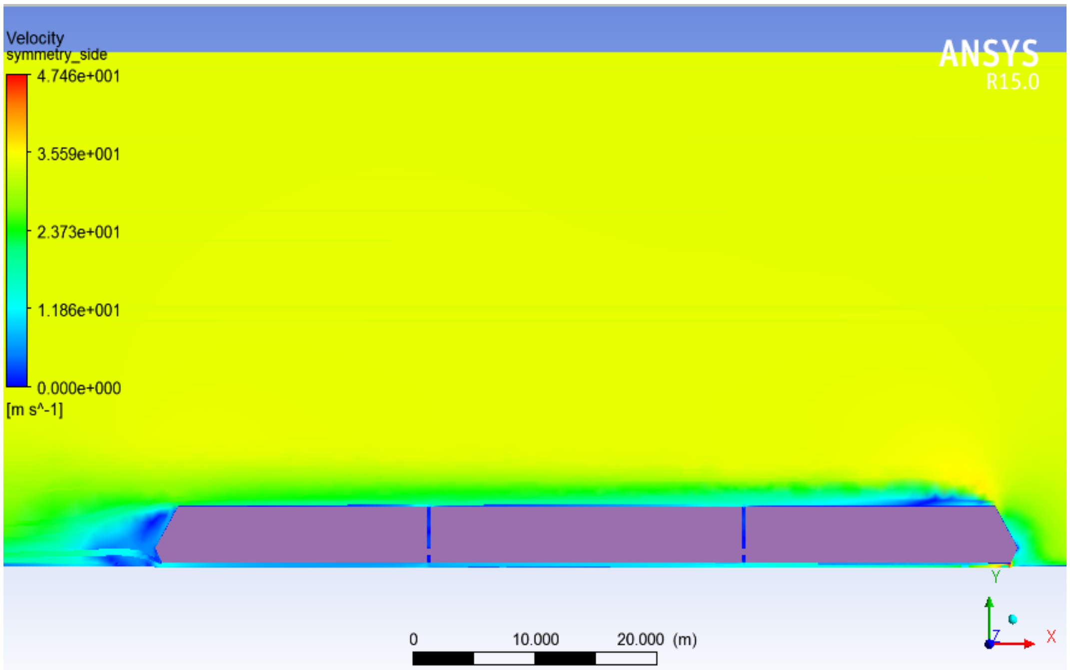

Figure 4-17: Contours Velocity around the train body moving in open field

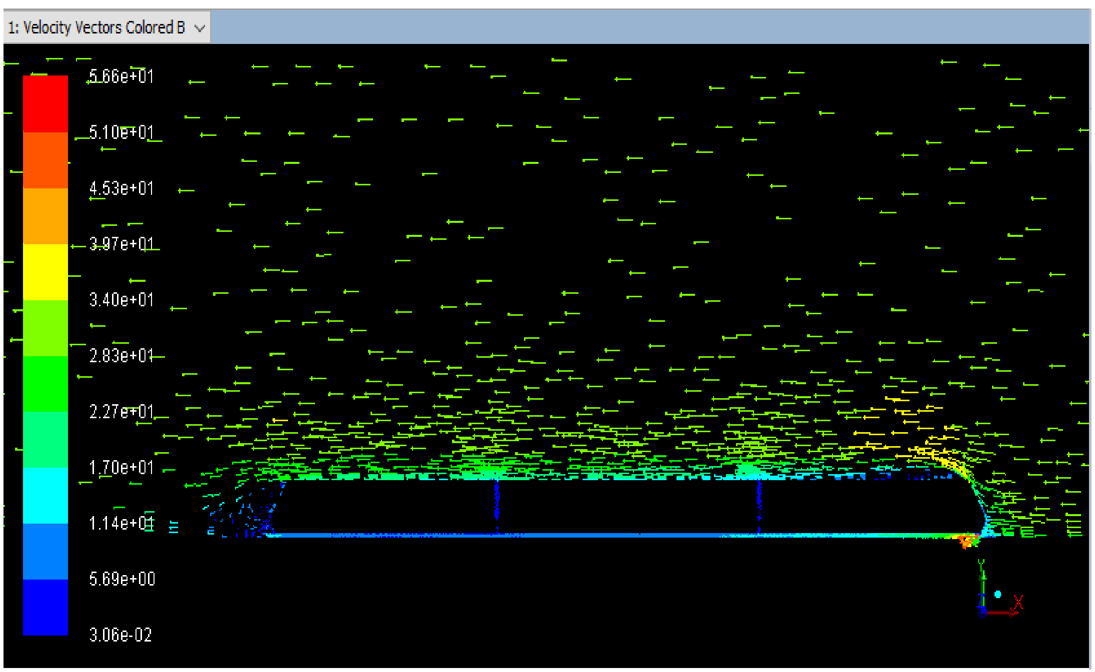

Figure 4-18: Velocity vectors for train moving in open field

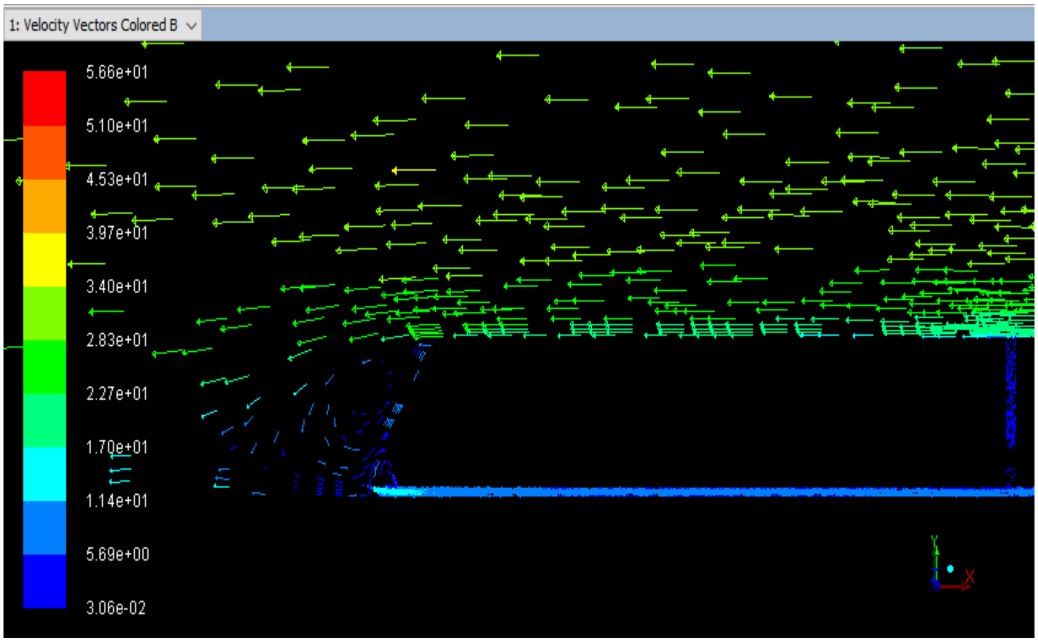

Figure 4-19: Velocity magnitude at train wake region

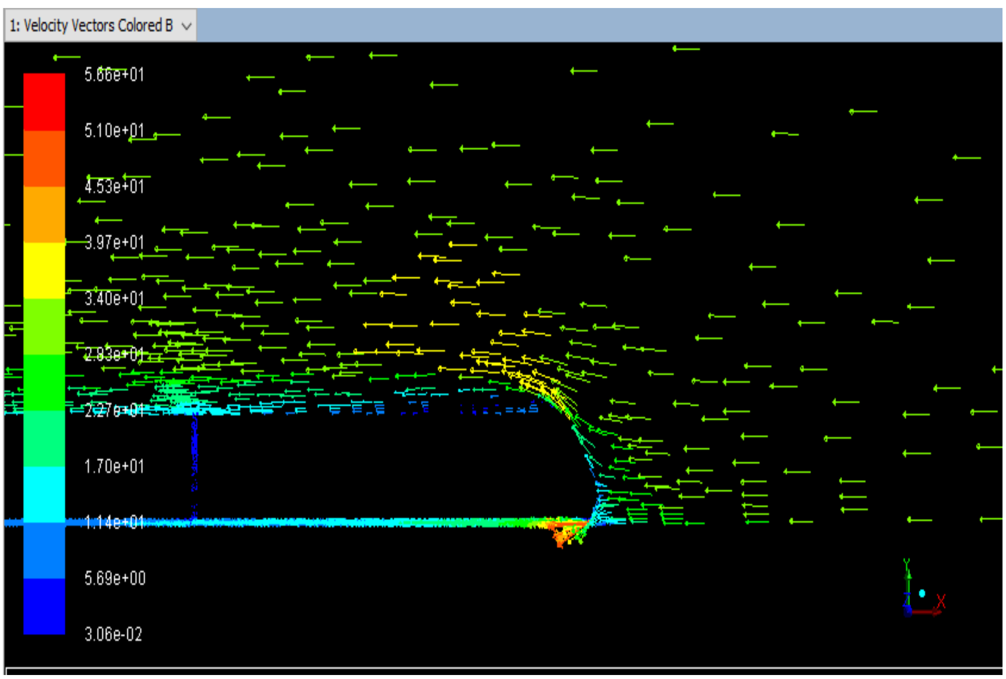

Figure 4-20: Velocity magnitude at train nose region

The passenger train have higher range of maximum velocity magnitude at the sharp corners at the front top and bottom of the train body, low velocity zone is obtained right in front of the train air where the air is stagnated and while a reduced portion of the air flows around the wake region of the train.

2. Train moving in tunnel

The contour plots of the velocity of the airflow around the train as it travels through the tunnel are presented below for both different blockage ratios (β_1 and β_2)

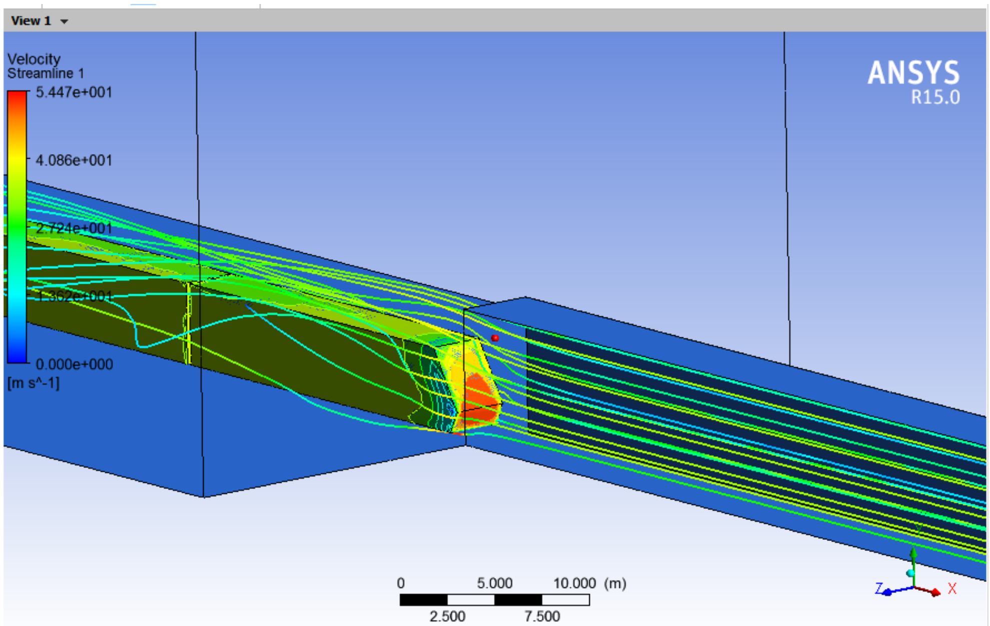

Figure 4-21: The contour plots of the velocity of the airflow streamlines around the train approaching the tunnel entrance at position of 2 meters from the Addin onfito tunnel entrance portal (β_1=0.4355)

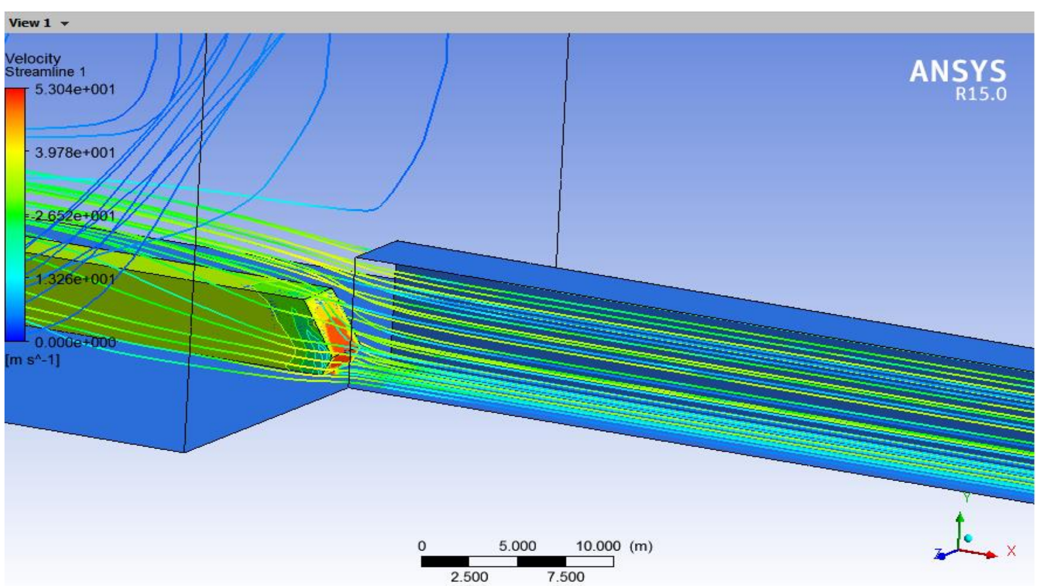

Figure 4-22: The contour plots of the velocity of the airflow around the train approaching the tunnel entrance at position of 2 meters from the entrance portal for blockage ratio of (β_2=0.3824)

The contour plots of the velocity of the airflow around the train as it travels through the tunnel are presented at five several positions of the train with respect to the tunnel, the direction of travel in this contour plot will be from right to left.

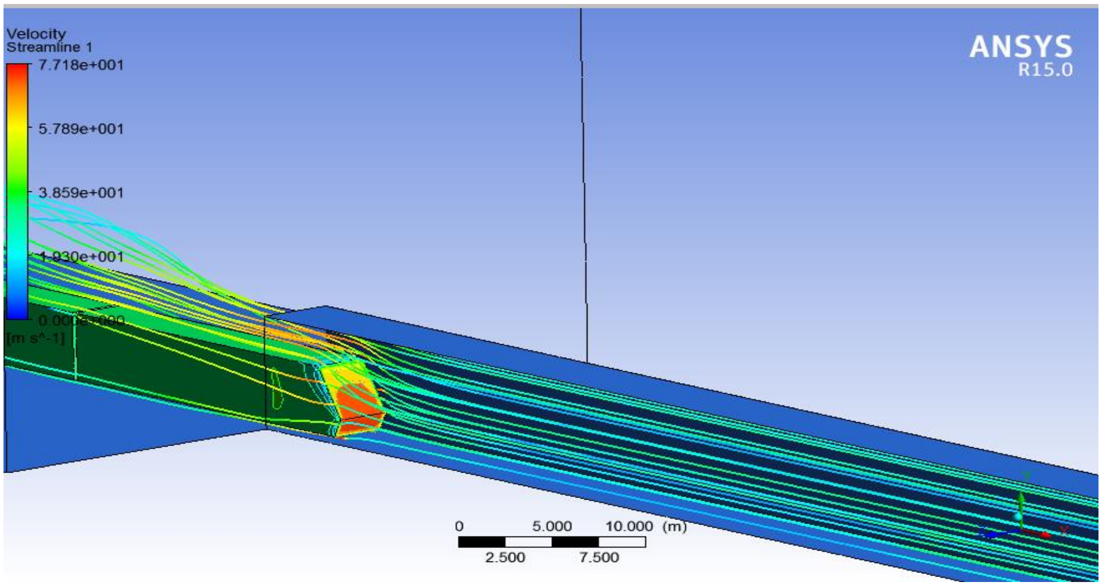

Figure 4-23: The contour plots of the velocity of the airflow around the train due to the train head entrance 5 meters inside the Addi-onfito tunnel (β_1=0.4355)

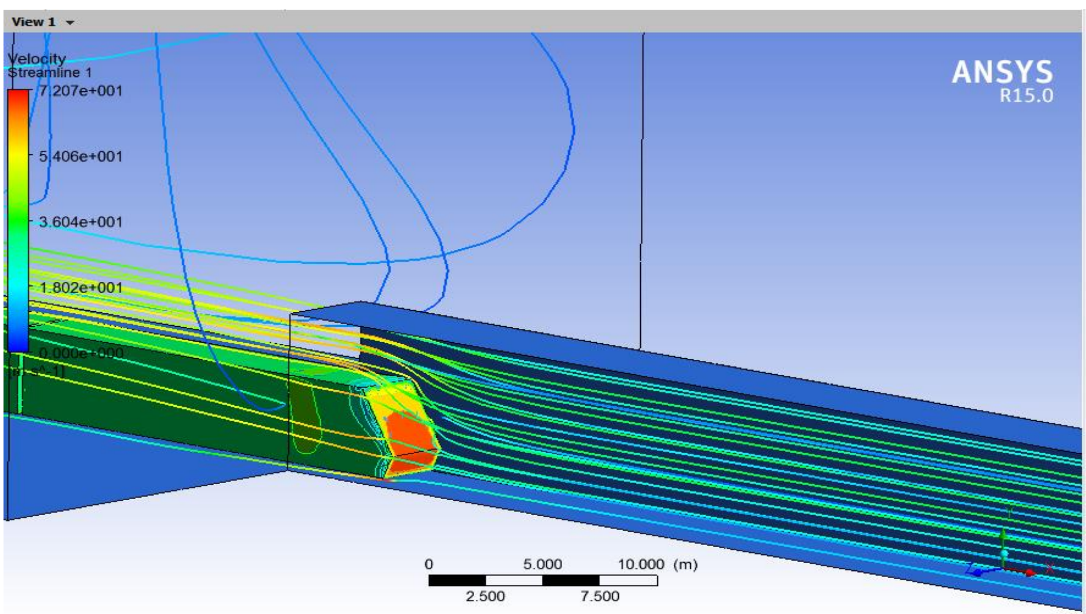

Figure 4-24: The contour plots of the velocity of the airflow around the train due to the train head entrance 5 meters inside the tunnel with blockage ratio of (β_2=0.3824).

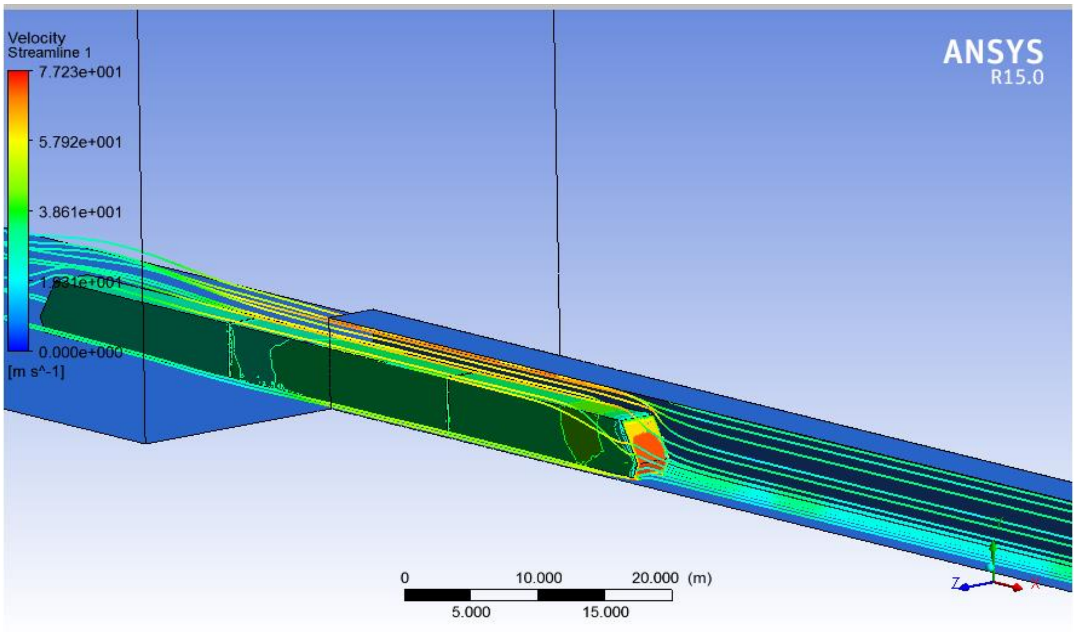

Figure 4-25: The contour plots of the velocity of the airflow around the train when half of the train body entered in the Addi-onfito tunnel (β_ 1 =0.4355).

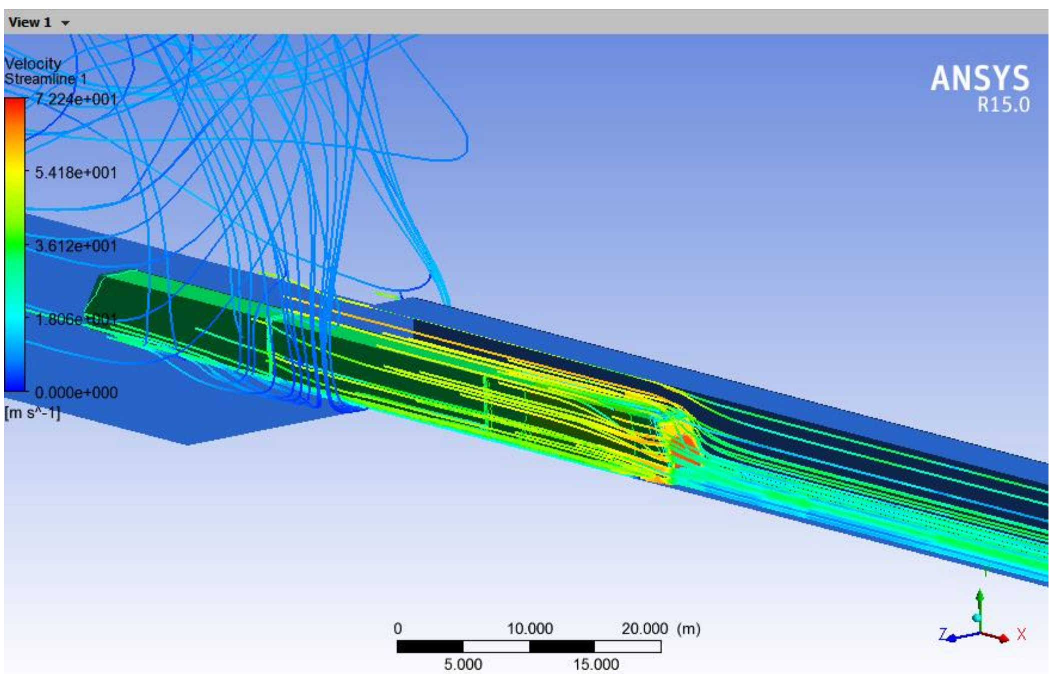

Figure 4-26: The contour plots of the velocity of the airflow around the train when half of the train body entered in the tunnel with blockage ratio (β_2=0.3824).

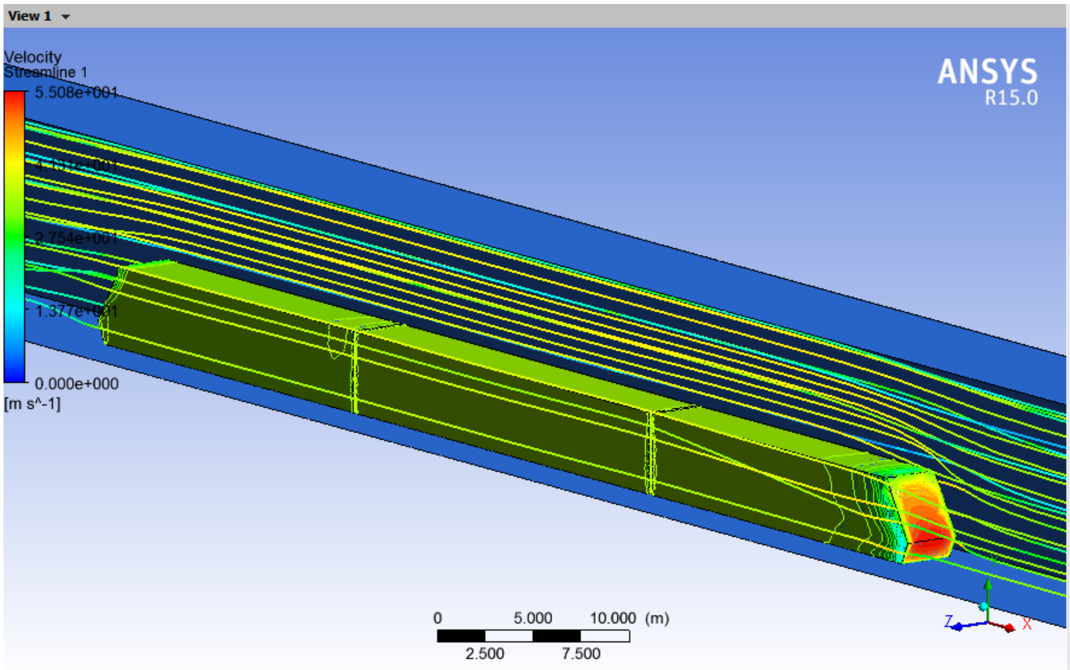

Figure 4-27: The contour plots of the velocity of the airflow around the train traveling inside the Addi-onfito tunnel (β_1=0.4355)

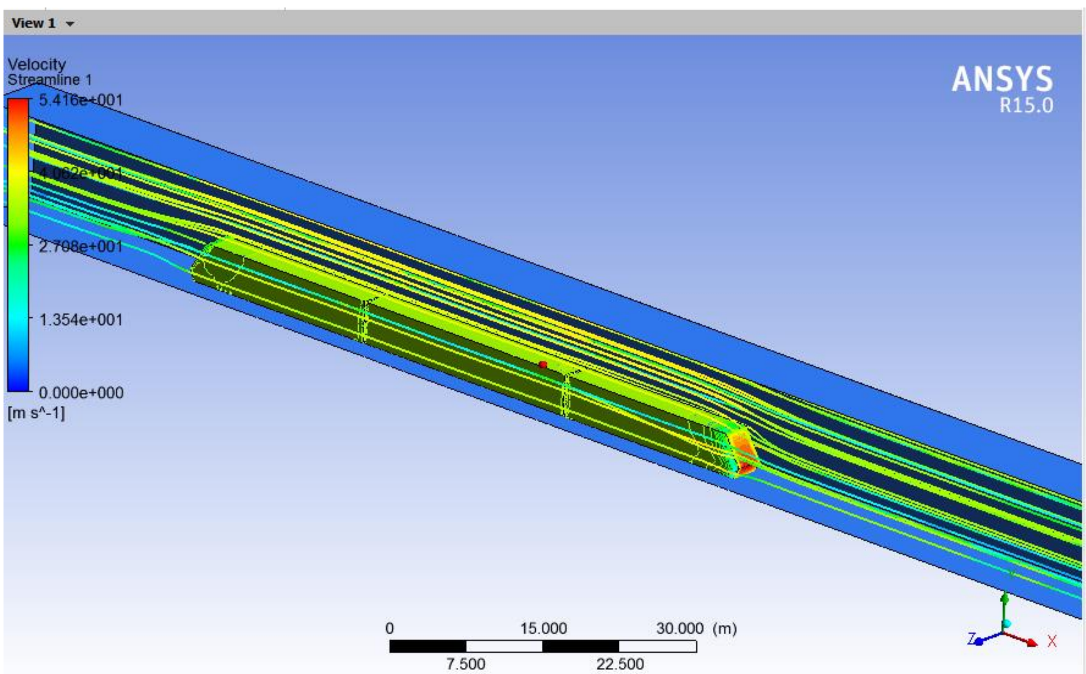

Figure 4-28: The contour plots of the velocity of the airflow around the train traveling inside the tunnel with blockage ratio of (β_2=0.3824).

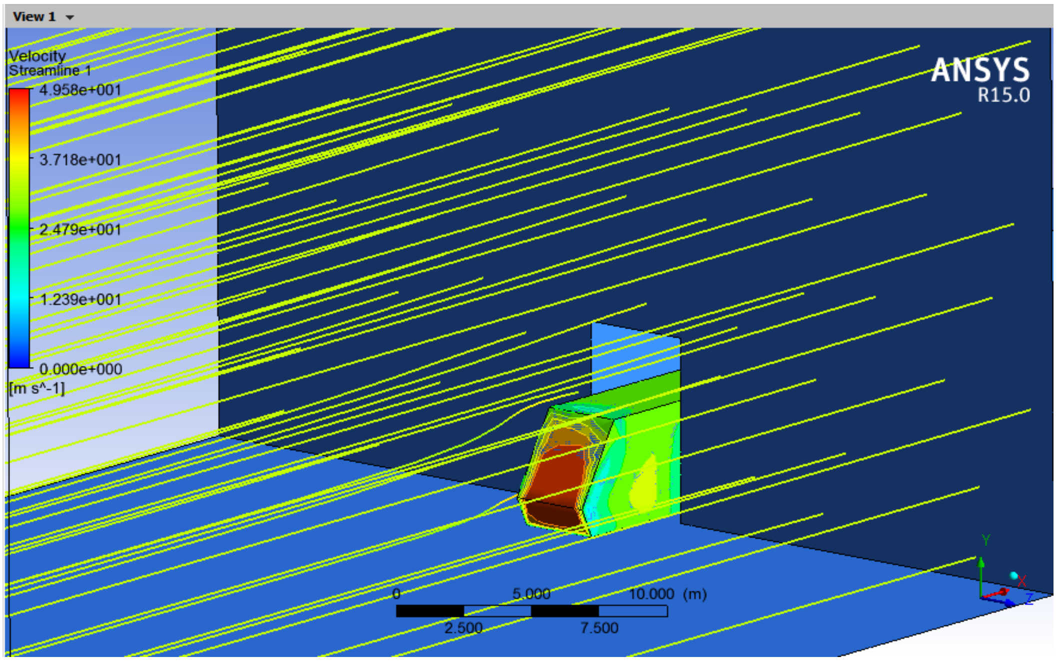

Figure 4-29: The contour plots of the velocity of the airflow around the train exiting from the Addi-onfito tunnel (β_1=0.4355).

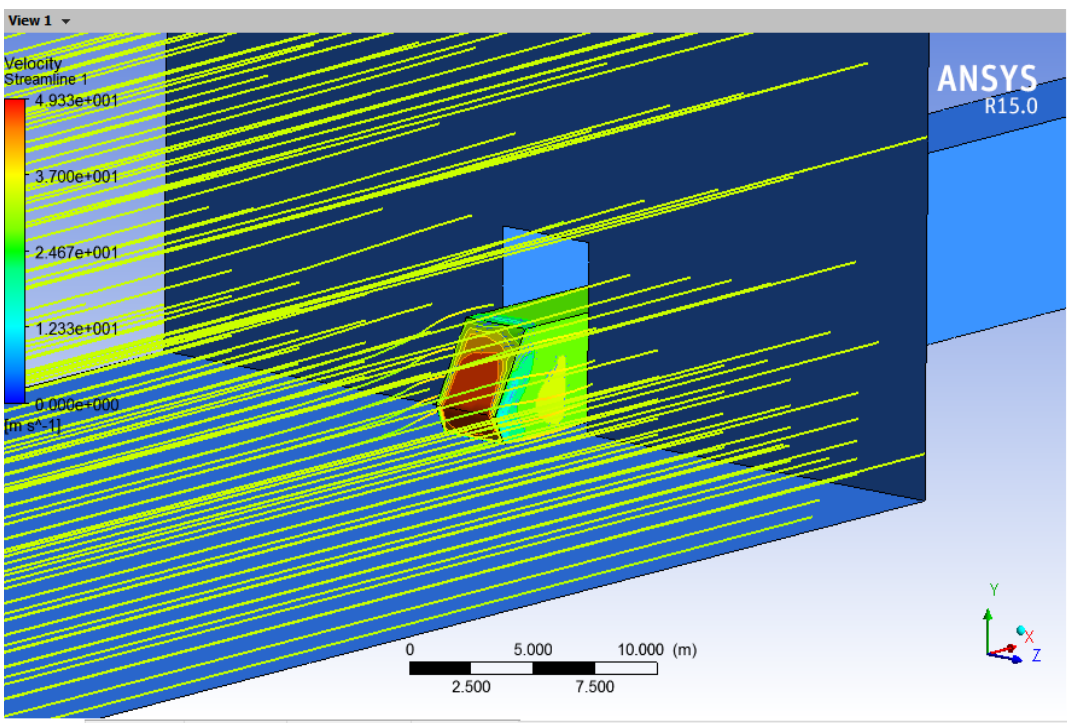

Figure 4-30: The contour plots of the velocity of the airflow around the train exiting from the tunnel of blockage ratio (β_2=0.3824).

From the above results the contour of the velocity of the air flow around the train moving in open field and in tunnels, the magnitude of the air velocity at the front head of the train increases as the train approaches the tunnel entrance, and further magnified when the train head entered the tunnel entrance.

The propagating pressure waves induce a flow in a tunnel. The head wave of the train causes a flow in the direction of train motion between the front of the wave and the train head. In the gap between the tunnel wall and the train wall there is a flow to the entrance portal during the entrance phase of the train. Due to the reflections of the pressure waves a very complex flow field in space, especially if the track is not in the center of the tunnel cross section. The induced flow velocity depends on the train speed V_{tr}, the blockage ratio β, the length of the train L_{tr} and of the tunnel L_{tu} respectively, the roughness of the train and the tunnel wall respectively and on the initial air speed in the tunnel. The highest value of the flow speed is normally caused by the wake of the train after the main end has passed. [6]

In the Table 4-4, the maximum velocity of the air at the front head of the train is tabulated for the train moving in open field and while as it travels in tunnels of two different blockage ratios (β_1 $and \beta_2$).

Table 4-4: Summary of the maximum contour of air flow velocity around the train.

	The contour plots of the velocity of the airflow around the train (m/s)	
Case	**For Blockage ratio 1 ($\beta_1 = 0.4355$)**	**For Blockage ratio 2 ($\beta_2 = 0.3824$)**
Open field (No Tunnel)	47.46	
Approaching tunnel	54.47	53.04
Entering tunnel	**77**.18	72.07
Entering tunnel (Mid way)	77.23	72.24
In the tunnel	55.08	54.16
Exiting tunnel	49.58	49.33

4.2 Discussions

Aerodynamic loads of aerodynamic drag, peak-pressure acting on train body and velocity of the airflow around the passenger train body moving in open filed, and as it travels in the tunnel were examined with two different blockage ratios.

4.2.1 Discussion of CFD method and results

The difference of aerodynamic loads between the train traveling in open field and while inside the tunnel is large. It is also interesting to study the effect of blockage ratio on the aerodynamic loads of the passenger train traveling inside the tunnel. Different scenarios of train positions with respect to the tunnel are simulated to study what consequences they have on the aerodynamic loads.

The validation of the accuracy of the numerical model is performed through the comparison between numerical results by this numerical model and with the previous study done on the aerodynamic drag of the train traveling in open filed by (*Mamo Nigussie,2014* [57]), which used the same train shape, length and speed as of the present paper. Even though the numerical simulations were made with an entirely different meshing with the afro mentioned study (*Mamo Nigussie,2014* [57]), the behavior and magnitudes of the drag and lift forces acting on the train ($C_D$value of 0.93) [Appendix II], are almost similar to one of the results presented in this paper (simulation result of coefficient of drag of the train operating in open field, $C_D$value of 0.892). Which indicate acceptable result for the methodology used in this paper. However there is slight difference in the value of the drag coefficient, which is due to the probability of different meshing arrangements or other extrude parts on the whole train body which are not include or considered under this computation.

The result of behavior of: the pressure and velocity variations along the different positon of the train relative to the tunnel, presented in this paper also showed a similar phenomenon with previous studies (*Lun and Wang*, [43]). The pressure acting on the train body experienced huge fluctuations as the train moved along the train, a similar trend in the pressure variation along the different positions of train body is observed. However there is a big difference on the magnitude of the pressure values and air flow velocity, [Appendix III], which is due to the different train model, speed, tunnel length and type of turbulence method used in the simulation.

4.2.2 Aerodynamic drag

From the results of the simulation shown previously, as the train travels in the tunnel the train exposed to piston effect; the air pushed ahead of the train causes a significant pressure increase in front of the train nose and creates a pressure decrease behind the tail, which results in increments of aerodynamic drag.

To compare the aerodynamic drag of the train traveling between open field and in tunnels, variation of the drag coefficient for train in open field and in tunnel is presented for case of Addi-onfito tunnel with blockage ratio ($\beta_1 = 0.4355$) and train speed ($V_t = 33.33 m/s$) is presented in Fig.4-31.

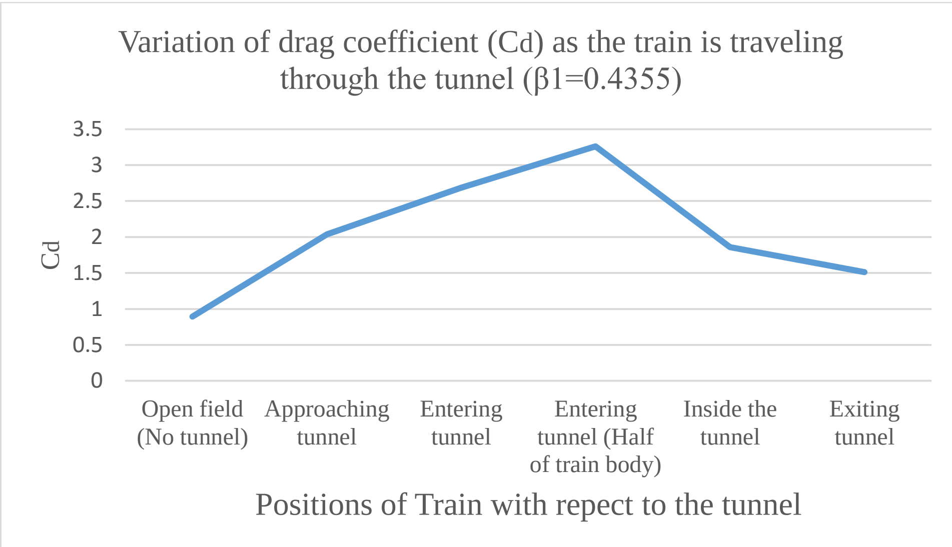

Figure 4-31: Variation of drag coefficient when the train travels in open field and in tunnel (β_1=0.4355).

Compared with the open air traveling, the aerodynamic drag can considerably increase as the train passes through in Add-onfito tunnel. This is because the train induced flows do work to increase the pressure by interacting with the tunnel walls.

At the moment of train entry into the tunnel the drag coefficient increases dramatically to the amount of about 3.26, which is the maximum drag occurred compared to the other train positions relative to the tunnel. The obtained maximum drag is generally due to the compression pressure wave generated by the entry of the train nose, and due to the maximum pressure difference between the front head pressure and train back, this abrupt increase in pressure difference makes the drag significantly increased. The drag coefficient increment due to train entry into the tunnel is compared with the C_D of the train operating open field, which results; the C_{D1} due to train entry in the first blockage ratio (β_1) is 3.65 time greater than that of free flow field irrespective of the train shape and length.

Relationship between blockage ratio and aerodynamic drag

The effect of blockage ratio on the aerodynamic drag due to a passage of train in tunnel is provided by the simulation results of both; Aerodynamic drag force, F_D and the dimensionless form of the aerodynamic drag, called aerodynamic drag coefficients C_D.

The variation of drag coefficient, C_D for two different blockage ratios have been compared in the figure 4-32 below, along the different position of the train as it travels in the tunnel. The maximum drag coefficient for both blockage ratios results when the half of train body entered in the tunnel, and with decrease in the blockage ratio (β_2), the drag coefficient decreases.

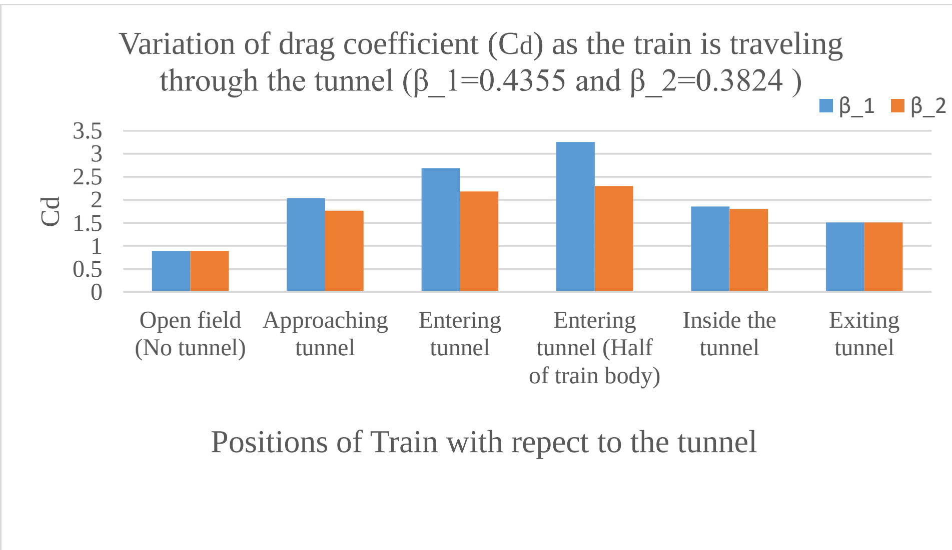

Figure 4-32: Variation of drag coefficient (Cd) as the train is traveling through the tunnel

Thus the higher blockage ratio leads to a more pronounced piston effect resulting in greater value of aerodynamic drag. A drag at the train position when the half the train body entered in the tunnel is compared for both blockage ratios in order to analyze the tendency of the drag reduction in detail.

The percentage reduction of the drag due to entry of the train in the smaller blockage ratio (β_2), calculated as $\%\Delta C_{D-max}$ where, C_{D1-max}= 3.261 and C_{D2-max} = 2.302 are the maximum drag coefficients for the first blockage ratio (β_1) and smaller blockage ratio (β_2) respectively.

$$\%\Delta C_{D-max} = \frac{C_{D1-max} - C_{D2-max}}{C_{D1-max}} \times 100\%$$

$$= \frac{3.261 - 2.302}{3.261} \times 100\%$$

$$\cong 29.38\ \%$$

Therefore, the drag coefficient (C_{D1-max}) due to train entry is reduced by 29.38% in the smaller blockage ratio ($\beta_2 = 0.3824$) than that of the first blockage ratio ($\beta_1 = 0.4355$).

The trends of the coefficient of drag history and drag forces in both cases (blockage ratios) are similar, although the slope and the value are different. The total drag is significantly reduced linearly while the blockage ratio is decreased from 0.4355 to 0.3824. The change in maximum aerodynamic drag force of the two blockage ratios in percentage is calculated as $\%\Delta F_{D-max}$ where, F_{D1-max} = 36221.29 N and F_{D2-max} = 25912.72 N are the maximum drag forces for the first blockage ratio (β_1) and smaller blockage ratio (β_2) respectively.

$$\%\Delta F_{D-max} = \frac{F_{D1-max} - F_{D2-max}}{F_{D1-max}} \times 100\%$$

$$= \frac{36221.29\,N - 25912.72\,N}{36221.29\,N} \times 100\%$$

$$\cong 28.46\ \%$$

Therefore, the total drag of the train speed of 120Km/hr traveling in tunnel with blockage ratio of ($\beta_2 = 0.3824$) reduced up to a 28.46 % than that of the first blockage ratio ($\beta_1 = 0.4355$).

4.2.3 Pressure acting on the train

The factors which effect the drag and tunnel airflows are the pressure difference between the train front and back and the air flow in the annular region. The pressure distribution on the train body moving along the Addi-onfito tunnel with different train positions relative to tunnel is shown in Fig. 4-33., where the points indicate the positon of train relative to tunnel; 1) Train operating in open field (far away from the tunnel), 2) train approaching the tunnel entrance, 3) train head entered in the tunnel, 4) half of the train entered in the tunnel, 5) train inside the tunnel and 6) train exiting the tunnel.

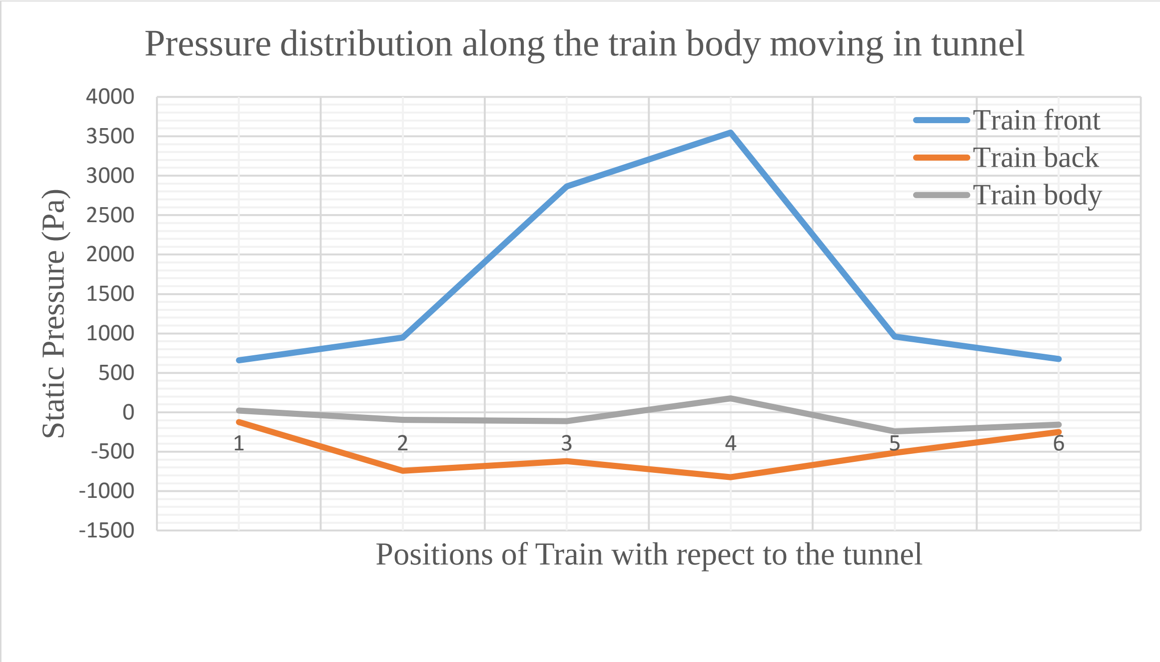

Figure 4-33: Pressure distribution along the train body moving in Addi-onfito tunnel

Due to the piston effect, the pressure increment is observed starting at the position when the train approaches the tunnel entrance, reaching its maximum value of 3546.76 Pa at the position when half the train body entered in the tunnel.

The maximum pressure difference (ΔP_{max}) between the front and back of the train occurred at entry of half of the train body in the tunnel with a value of ΔP_{max} = 4.36 kPa. This changes in pressure throughout the train motion in Addi-onfito tunnel ($\beta_1 = 0.4355$) exceeds the safe level of pressure change given by the (*International Union of Railways (2005))* as 4 kPa. [66][71][72][4]

Although the pressure acting along the train body is relatively constant, the maximum differential pressure acting on the train body was the largest when the train is moving inside the tunnel. The pressure distribution on the train body moving along the Addi-onfito tunnel is presented in the figure 4-34 below. As seen in the figure of the pressure distribution (figure 4-34), the train body will experience approximately to a 241.35 Pa of pressure on the train surface while moving in the tunnel. Over a long period of time, this may cause critical damage to the train structure on actual case.

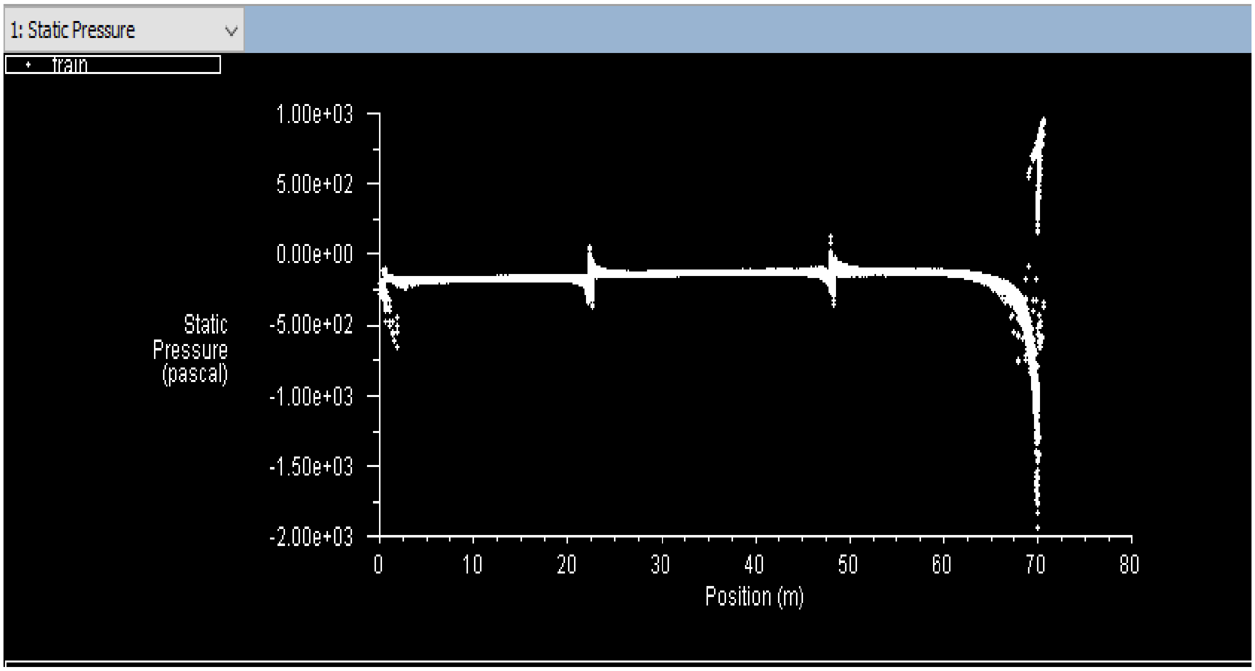

Figure 4-34: Static pressure graph on the train body moving along the Addi-onfito tunnel.

Relationship between Blockage ratio and Pressure difference

The effect of blockage ratios on the contour of static pressure and pressure coefficient is studied by comparing the results of six different positions of the train as it travels through the tunnel. The variation of pressure coefficient for two different blockage ratios, at the moment of train entry into the tunnels have been compared. With decrease in the blockage ratio (β_2), the pressure coefficient decreases. The percentage reduction of the coefficient of pressure due to entry of the train in the tunnel calculated as ($\%\Delta C_{P-max}$) where, C_{P1-max} and C_{P2-max} are the maximum pressure coefficients for the first blockage ratio (β_1) and second blockage ratio (β_2) respectively.

$$\%\Delta C_{P-max} = \frac{C_{P1-max} - C_{P2-max}}{C_{P1-max}} \times 100\%$$

$$= \frac{5.21 - 3.93}{5.21} \times 100\%$$

$$\cong 24.56\ \%$$

Therefore, the maximum pressure coefficient (C_{P-max}) due to train entry is reduced by 24.56% in the smaller blockage ratio ($\beta_2 = 0.3824$) than that of the first blockage ratio ($\beta_1 = 0.4355$).

The variation on magnitude of maximum and minimum static pressures developed at the body of the train, as it travels through the tunnel with two different blockage ratios is shown in Figure 4-35.

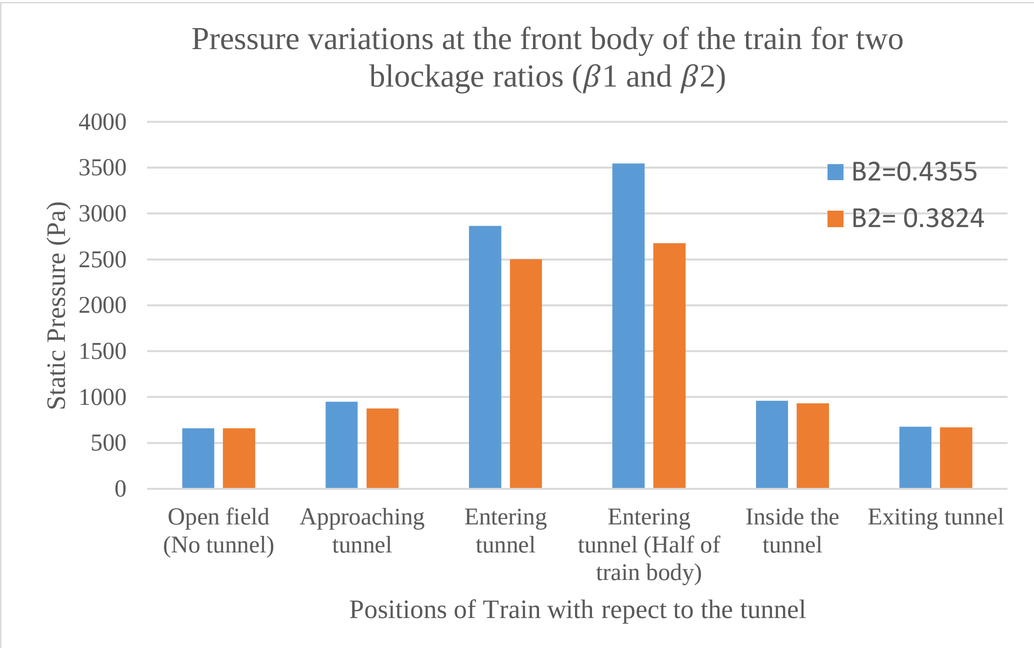

Figure 4-35: Pressure variation at the front body of train for β_1=0.4355 and β_2=0.3824.

Note that for both blockage ratios, the maximum static pressure on the train body develop at the position when half of the train body entered in the tunnel. This abrupt increase in pressure of nose region makes the drag significantly increased. The largest deviation in pressure was noticed when the train is entering along the Addi-onfito tunnel ($\beta_1 = 0.4355$). This phenomenon can be due to the compression waves generated as the tunnel is moving into the confined volume of air within the tunnel and the effect of the free train-tunnel space.

As seen in Figure (4-35), with decrease in the blockage ratio (β_2), the maximum static pressure decreases. The percentage reduction of the maximum static pressure due to entry of the train in the smaller blockage ratio (β_2), calculated as $\%\Delta P_{sta-max}$ where, $P_{sta1-max}$ and $P_{sta2-max}$ are the maximum static pressure for the first blockage ratio (β_1) and smaller blockage ratio (β_2) respectively.

$$\%\Delta P_{sta-max} = \frac{P_{sta1-max} - P_{sta2-max}}{P_{sta1-max}} \times 100\%$$

$$= \frac{3546.79\ Pa - 2675.49\ Pa}{3546.79\ Pa} \times 100\%$$

$$= 24.56\ \%$$

Therefore for decrease in blockage ratio of $\Delta\beta$ by 12.19%, the maximum pressure rise due to the entry of the train is decreased by 24.56%.

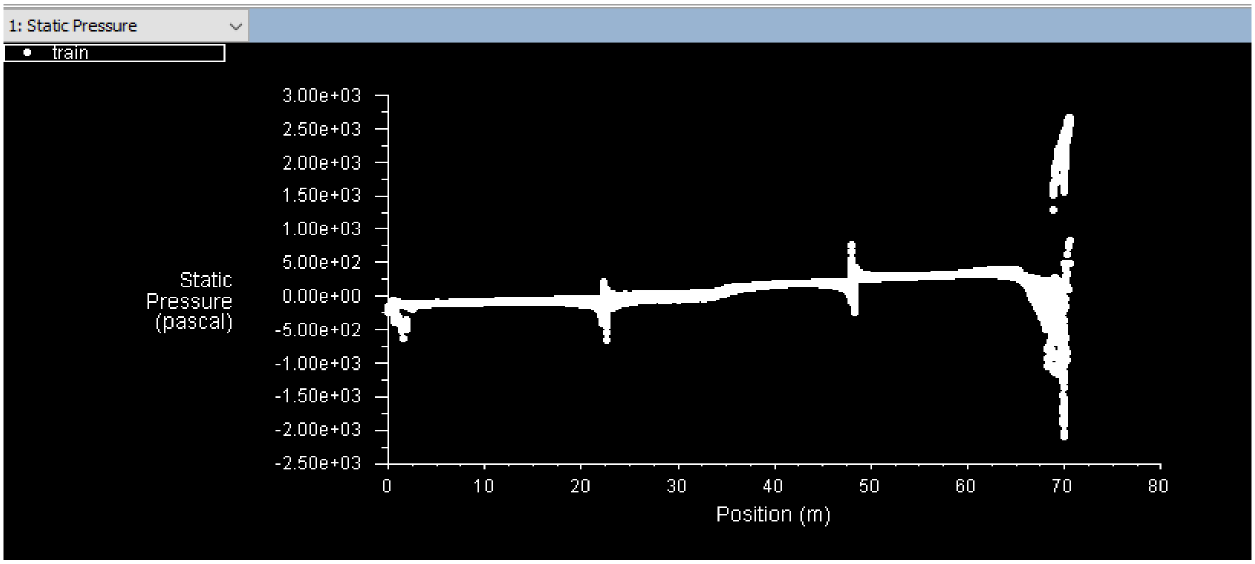

Figure 4-36: Static pressure graph on the train body entering the smaller blockage ratio tunnel (β_2=0.3824)

The factors which effect the drag and tunnel airflows are the pressure difference between the train front and back and the air flow in the annular region. The pressure difference between the front and back of the train is shown for the smaller blockage ratio ($\beta_2 = 0.3824$) in Fig. 4-36. Although the pressure along the train body can be deemed to be constant, the change in pressure between the train front head and back ΔP_{max} was reduced to value of a 3.20 kPa compared to the value of the pressure difference of the first blockage ratio (ΔP_{max}= 4.36 kPa). This value of maximum changes in pressure (ΔP_{max}= 3.20 kPa) throughout the train motion unlike the first blockage ratio configuration, is below of the maximum level of pressure change 4 kPa given by the standard of (*International Union of Railways (2005)).* [66][71] [4]

4.2.4 Velocity of air flows around the train

When the velocity vector magnitude on the front head of train are compared for all different locations of train respect to the tunnel, the change in the magnitude of the velocity of air around the train is almost the same for the two different blockage ratios. When it comes in term of the velocity, the effect of blockage ratio on the velocity of air films which are in contact with the train as it travels in the tunnel is small, however small reduction in the velocity showed for the smaller blockage ratio (β_2) when compared with (β_1).

The variation of the velocity vectors acting on the train is presented for the train moving in open field and in tunnels (with two different blockage ratios) is shown in Figure 4-37, the velocity vector of the train operating in open field compared with that of traveling in the tunnel at constant train speed.

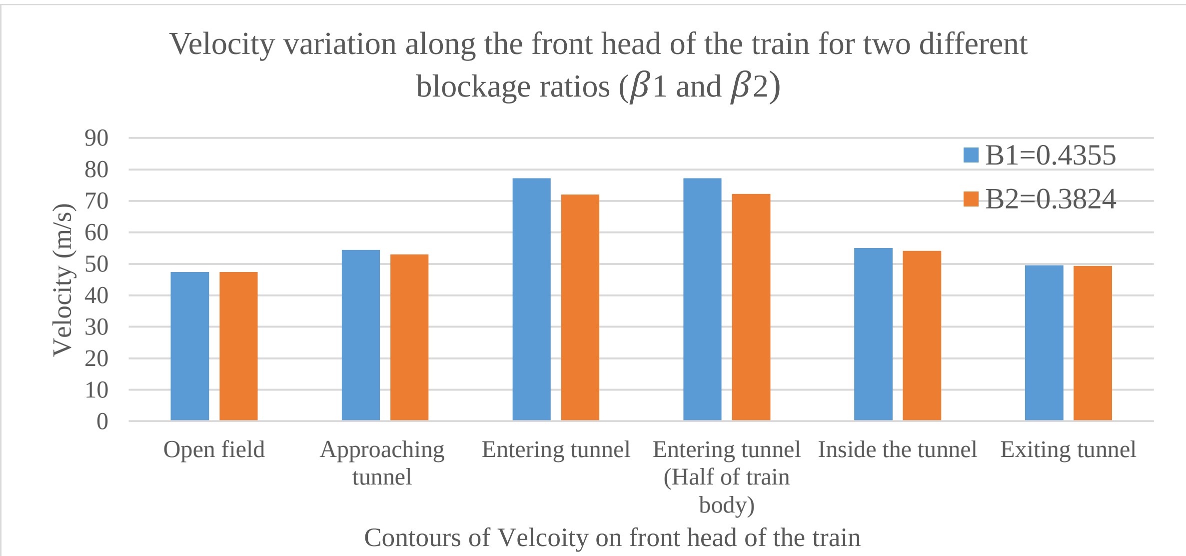

Figure 4-37: Velocity Variation along the front head of the train traveling in the tunnel for the two different blockage ratios ($\beta 1$ and $\beta 2$)

The velocity of the air at the front of the train magnified to approximately 34.97% faster when the train is entering in the first blockage ratio ($\beta_1 = 0.4355$), and approximately 28.61% in the smaller blockage ratio ($\beta_2 = 0.3824$). The velocity increment is also observed approximately 12.39% when it is moving inside the tunnel, for the first train-tunnel configuration ($\beta_1 = 0.4355$), and approximately 5.1% in the second train-tunnel configuration ($\beta_2 = 0.3824$). On the other hand, when the train approaching and leaving the tunnel the velocity magnitude change is small for both blockage ratios.

4.2.5 Relationship between Aerodynamic drag and Power consumption

From the results the aerodynamic drag acting on the train increase due to the confinement of the surrounding space. The aerodynamic drag is important because the portion of the aerodynamic drag on a train traveling in a tunnel can exceed 90% of the total drag [67] [60]. The results of numerical simulation in this paper shows that the entity of the aerodynamic drag greatly depends on blockage ratio.

The relationship between aerodynamic drag resistance and the traction power is complex. The assumptions will also get numerous such as mass of train, traction power etc., and because of these parameters other parameters which come next to them will also be a set of guess. Thus the approximate relationship of these two parameters will be discussed using their empirical formula as shown below as also used on Orellano A. (Dr.) [64][61]

$$\text{Power} = \text{Force} * \text{Velocity} \tag{4.7}$$

To get more exact value using the relationship between drag and that of traction power the use of Davis experience formula discussed in literature part considering that methods is essential. But for prediction purpose, basic formulas may be used as written above. Thus, from the above formula; where; P is traction power consumed by the aerodynamic drag, V is the speed of the train and F is the aerodynamic drag resistance force.

With the values obtained from the simulation it is possible to calculate the traction power using the drag force for each blockage ratios or by using only the change in drag force. First the traction power used by aerodynamics drag resistance force of the passenger train traveling in the Addi-onfito tunnel ($\beta_1 = 0.4355$), is calculated.

$$P_{D1} = F_{D1-max} * V_{tr}$$

$$= 36221.29\ N * 33.33\ m/s$$

$$= 1207{,}255.59\ W$$

$$\approx 1207.26\ kW$$

The traction power used by aerodynamics drag resistance force of the passenger train traveling in the smaller blockage ratio ($\beta_2 = 0.3824$) will be computed in similar way.

$$P_{D2} = F_{D2-max} \times V_{tr}$$

$$= 25912.72\ N \times 33.33\ m/s$$

$$= 863{,}670.96\ W$$

$$\cong 863.67\ kW$$

The percentage reduction of the power due to traveling of the passenger train in the smaller blockage ratio (β_2), calculated as $\%\Delta P_D$ where, P_{D1-max} and P_{D2-max} are the maximum traction power used to overcome the aerodynamic resistance force of the passenger train traveling in the first blockage ratio (β_1) and smaller blockage ratio (β_2) respectively.

$$\%\Delta P_D = \frac{P_{D1} - P_{D2}}{P_{D1}} \times 100\%$$

$$= \frac{1207.67 - 863.67}{1207.67} \times 100\%$$

$$\cong 28.48\ \%$$

Therefore for decrease in blockage ratio of $\Delta\beta$ by 12.19%, the traction power requirement for the aerodynamic drag resistance as the train travels in the tunnel is decreased by 28.48%. The amount of reduction in power usage can also be calculated as

$$\Delta P = P_{D1} - P_{D2}$$

$$= 1207.67\ kW - 863.67\ kW$$

$$\cong 344\ kW$$

These results indicate that without affecting the shape and speed of the train with little modification of the blockage ratio one can save a 344 kW of energy by reducing drag force, which is directly related to energy efficiency.

CHAPTER 5: - CONCLUSIONS, RECOMMENDATIONS AND FUTURE WORKS

5.1 Conclusions

This paper analyze the aerodynamics behavior of the pressure and drag forces when the train is traveling through the tunnel by using CFD approach. In addition, a series of numerical simulations were performed to study the effects of the blockage ratio (β) on the pressure and drag force coefficients with constant train speed of 120Km/hr and tunnel length of 179m. The simulations were done with the train positioned at different locations with respect to the tunnel.

From the present numerical simulations, it is concluded that as the train travels in the existing high blockage ratio underground railway (Addi-onfito tunnel$\beta_1 = 0.4355$), the pressure on the train body is significantly increased due to the piston-like action starting at the position of train approaching the tunnel entrance this makes the drag rapidly increased. The peak-pressures experienced are greater at the all train position of the train as the train travels in the tunnel compared to the train operating in open field. The pressure acting on the train body experienced huge fluctuations as the train moved along the Addi-onfito tunnel. The maximum pressure difference and drag forces are showed at the position when half of the train body is entered in the tunnel and this pressure difference (ΔP_{max}= 4.36 kPa) between the front and back of the train exceeds the maximum admissible limits of a peak to peak pressure change on train body of 4 kPa. These big deviations in pressure acting on the train body can be damaging to the structural integrity of the train body and create discomfort to the passenger, should there be any air leakage. This pressure difference leads to a value of increment of the aerodynamic drag approaches the value of about four times to the values drag of train operating outside of tunnel (open field).

In order to investigate the effect of blockage ratio on the drag, velocity and pressure fields around the train, new blockage ratios was set by increasing the present Addi-onfito train-tunnel gaps Y_a and Z_a by 20%, to reach up with blockage ratio of 0.3824. This is to arrive to a tunnel model with certain parameters similar to a current underground railway operating at 0.4 blockage ratio in Basle-Zurich Swiss-metro tunnel. This little modification of blockage ratio resulting in reduction of the original Addi-onfito blockage ratio approximately by 12.19%.

Further the simulation results shows that due to reduction of the blockage ratio of train in tunnel (β_2), the big pressure deviations developed on the train body are reduced in the smaller blockage ratio. The magnitude the maximum pressure difference between the front and back of train greatly reduced to a value of (ΔP_{max}= 3.2 kPa); which satisfy the safe limit of the maximum admissible pressure change. The reduction in blockage ratio also results in decrement of the aerodynamic drag coefficient (C_{d-max}) by 29.38 % to the value of 2.302 and the total aerodynamic drag force is also decreased by 28.46 % to the value of 25.91 kN at constant train speed and tunnel length. These results of reduction of the aerodynamic drag indicate that without affecting the shape and speed of the train we can save 28.48% of aerodynamic power requirements by little modification of the blockage ratio.

These all results presented in this study leads to conclude that the aerodynamic drag and peak pressure deviation developed on the train considerably increases when the train operates in the underground tunnel, and these aerodynamic loads on trains traveling through the tunnel are greatly affected by the blockage ratio of train in the tunnel. Notice that as proven in this paper, the maximum pressure and force coefficients are functions of the blockage ratio; at constant length of tunnel, train speed and length. Therefore the highest pressure and drag was greatly reduced by the reducing the blockage ratio. Hence, the drag and peak pressure coefficients shown in the paper only applied to the described setting. However, the present numerical model could be applied to simulate and estimate the aerodynamic forces and pressure under similar scenarios. These paper indicate that without affecting the shape and speed of the train, with little modification of the blockage ratio we can safe lots of aerodynamic power demand of trains as the train travels in tunnel by reducing drag force, which is directly related to energy efficiency.

5.2 Recommendations

The results of this study indicate that the estimation of pressure and drag forces for the passenger train traveling underground railway lines is an important requirement for the design of the new tunnel system. Although the Ethiopian National Train is not as fast as high-speed train, the total drag considerably increases in the underground tunnel.

The pressure acting on the train body and in the tunnel experienced huge fluctuations as the train moved along the current Addi-onfito tunnel. These big deviations in pressure can be damaging to the structural integrity of the train body in the practical case and will lead to create discomfort to the passenger, if there is any air leakage. This occurrence was caused by the propagation of strong pressure waves (compression and expansion waves) due to the restriction of the confined space (tunnel) and due to the size of free train-tunnel cross-sections. To reduce the total aerodynamic drag and big pressure deviation developed, countermeasures can be done by reducing the blockage ratio, with little modification on train tunnel gaps. As proven in this paper, the highest pressure change was greatly reduced by reducing blockage ratio. Such design also benefited operational efficiency. Therefore by doing this we can safe lots of aerodynamic power demand of trains as the train travels in tunnel by reducing drag force, which is directly related to energy efficiency. However strengthening the facilities on the train body to resistance pressure change maybe still is necessary under the improved design.

5.3 Future Works

The results in this thesis are based on the steady RANS using the realizable k-ε model. The results of RANS simulations provided a good appreciation of the aerodynamic patterns around and on the train, focused on the; aerodynamic drag and, and contour plots of pressure and velocity as the train travels through the tunnel.

The study of passenger trains in tunnels should be including the following points in addition to the points covered under this steady, other factors such as

- Speed and frontal shape of train.
- Configurations of the tunnel network geometry and tunnel length,
- Occurrence of multiple trains, air shafts and shape of entrance and exit portals of tunnel are can be further studied.

In general it is recommended that, further work can be done to give more conclusive results of the numerical simulation method, such as:

- Experimental wind tunnel testing can be done to validate the numerical results using a scaled-down model of the train and tunnel.
- Refine the geometry model of the train and tunnel. This includes adding wheels, gearbox assembly, additional train cabins and train track etc. into the geometry model.
- Numerical runs can be done using the sliding mesh method. The computational domain will be divided into two subdomains: the stationary subdomain will consist of the tunnel,

while the moving subdomain includes the moving train and a volume of air around it. This method of dynamically (instead of static conditions) modeling the train could better show the pressure variations as the train moves through a tunnel.

- More accurate CFD technique such as Large Eddy Simulation (LES) can be used.

REFERENCES

[1] Ethiopia Railway Corporation, Weldia- Mekelle Railway line design program draft.

[2] Florian Guillou, 'CFD Study of the Flow around a High-Speed Train'. Kungliga Tekniska Hogskolan, Stockholm, 2007

[3] European Standard EN 14067-3, "Railway application – Aerodynamics – Part3: Aerodynamics in tunnels", Comité Européen de Normalisation (CEN), Brussels, (2003).

[4] European Standard Draft prEN 14067-5, "Railway application – Aerodynamics – Part5: Requirements and test procedures for aerodynamics in tunnels", Comité Européen de Normalisation, Brussels (CEN), (2003).

[5] R. Raghunathan, H. Kim and T. Setoguchi, "Aerodynamics of highspeed railway train", Progress in Aerospace Sciences, vol. 38, no. 6-7, pp. 469-514, 2002

[6] J. Novák (2006), Single train passing through a tunnel, Proceedings of European Conference on Computational Fluid Dynamics ECCOMAS CFD 06, Egmond aan Zee, 2006, pp. 263.

[7] 'Aerodynamics in a contrained cross-section of a train tunnel system layout'' Kuo-Lun Hwang

[8] European Standard EN 14067-2, "Railway application – Aerodynamics – Part2: Aerodynamics on open track", Comité Européen de Normalisation (CEN), Brussels, (2003).

[9] Kim HD. Aerodynamic analysis of a train running in a tunnel(1). Korean Soc Mech Eng (KSME), 1997;21(8):963–72.

[10] Vardy AE. Aerodynamic drag on trains in tunnels. 1.Synthesis and definitions. Proc World Congr Inst Mech Eng 1996;210:29–38.

[11] Vardy AE. Aerodynamic drag on trains in tunnels. 2. Prediction and validation. Proc World Congr Inst Mech Eng 1996;210:39–49.

[12] de Wolf WB, Emmenie EAFA. A new test facility for the study of interacting pressure waves and their reduction in tunnels for high-speed trains. In: Proceedings of the InternationalSymposium on the Aerodynamics and Ventilation of Tunnels, 9th, Aosta Valley, Italy, London, 1997.

[13] Gr! egoire R, R! ety JM, Masbernat F, Morin" ere V, Bellenoue M, Kageyama T. Experimental study (scale 1/70th) and numerical simulations of the generation of pressure waves and mirco-pressure waves due to high speed train-tunnel entry. In: Proceedings of the International Symposium on the Aerodynamics and Ventilation of Vehicle Tunnels, 9th, Aosta Valley, Italy, 1997.

[14] Howe MS. Review of the theory of the compression wave generated when a high-speed train enters a tunnel. Proc World Congr Inst Mech Eng 1999;213F:89–104.

[15] Mancini G, Violi AG. Pressure wave effects of high speed trains running parallel on large and medium sized tunnels of Italian high speed lines. Proc World Congr Railw Res, Tokyo: Railr Tech Res Inst, 1999.

[16] Schulte-Werning B, Matschke G, Gregoire R, Johnson T.RAPIDE: a project of joint aerodynamics research of the European high-speed railoperators. Proc World Congr Railw Res, Tokyo: Railr Tech Res Inst, 1999.

[17] Yamamoto A. Aerodynamics of train and tunnel. RTRI JNR 1983:1230 (in Japanese)

[18] SockelH. The aerodynamics of trains. In: Schetz JA, Fuhs AE, editors. Handbook of fluid dynamics and fluid machinery. New York: Wiley, 1996. p. 1721–41.

[19] Matsuo K, Aoki T, Mashimo S, Nakatsu E. Entry compression wave generated by a high-speed train entering a tunnel. In: Proceedings of the International Symposium on the Aerodynamics and Ventilation of Vehicle Tunnels, 9th, Aosta Valley, Italy. 1997.

[20] Ozawa S. Numerical simulation of aerodynamic problems in train/tunnel systems. RTRI Rep 1990; 4–8 (in Japanese).

[21] Ogawa T, Fujii K. Numerical simulation of compressible flows induced by a train moving into a tunnel. J Comp Fuilds Dyn 1994;3(1).

[22] Ogawa T, Fujii K. Aerodynamics on train/tunnel systems. JSME 1994;970–940 (in Japanese).

[23] Yamamoto A. Pressure variations, aerodynamic drag, and tunnel ventilation in shin-kan-sen type tunnel. RTRI Rep 1973;871 (in Japanese).

[24] Iida M, Maeda T. Numerical calculation of pressure transients in railway tunnels. RTRI Rep 1990;4(7) (in Japanese).

[25] Schultz M, Sockel H. Pressure transients in railway tunnels. In: Schneider W, Troger H, Ziegler F, editors. Trends in applications of mathematics to mechanics. BHRA Fluid Engineering, Harlow, UK, 1989. p. 33–9.

[26] Komatsu N, Yamada F. The reduction of the train draft pressure in passing by each other. Proc World Congr Railw Res, Tokyo: Railr Tech Res Inst, 1999.

[27] Gawthorpe RG. Pressure comfort criteria for railtunnels operations. In: Haerter A, editor. Aerodynamics and ventilation of vehicle tunnels. New York: Elsevier, 1991. p. 173–88.

[28] Sato K, Ikada M, Nakagawa M. Effects of pressure changes on pain sensation of human ears. RTRI JNR 1989;3(3) (in Japanese).

[29] Zenda Y. Study on the ventilating system of Shinkansen vehicle by simulating the internal pressure. RTRI JNR 1988;2(12) (in Japanese).

[30] Kobayashi M, Suzuki Y, Akutsu K. Alleviating ear pains by controlling air pressure in ventilating system of Shinkansen car. RTRI JNR 1990;4(7) (in Japanese)

[31] Baker C., (2010b), 'Train aerodynamic problems and solutions', Railway Strategies, April-May,2010,Available,.at:
http://www.railwaystrategies.co.uk/articlepage.php?contentid=10286&issueid=317

[32] Ko Y., Chen C., Hoe I., and Wang S., (2012), 'Field measurement of aerodynamic pressures in tunnels induced by high speed trains'. Journal of wind engineering and industrial aerodynamics. Vol. 100, issue 1, pp. 19-29.

[33] Suzuki M., Ido A., Sakuma Y., and Kajiyama H., (2008), 'Full-scale measurement and numerical simulation of flow around high-speed train in tunnel'. Journal of mechanical systems for transportation and logistics, Volume 1 number 3.

[34] Krylove V., (2001), 'Noise and vibrations from high-speed train'. Thomas Telford publishing, Thomas Telford Ltd. First published 2001.

[35] Ricco, P., Baron, A., Molteni, P., 2007. Nature of pressure waves induced by a high speed train travelling through a tunnel. Journal of Wind Engineering and Industrial Aerodynamics 95, 781–808

http://www.sciencedirect.com/science/article/pii/S0167610507000189

[36] Gilbert, T., Baker, C., Quinn, A., and Sterling, M., 2012. Aerodynamics of high-speed trains in confined spaces. Proceedings of the 7th International Colloquium on Bluff Body Aerodynamics and Applications, pp.10. Shanghai, China, 2-6 September 2012.

[37] Samane Faramehr, "Aerodynamic of the Trains in Tunnels" MRes in Railway Systems Engineering and Integration College of Engineering, School of Civil Engineeringm university of Beringham, 2014

[38]Baker, C., (2014), 'A review of train aerodynamics, part 1—fundamentals' The Aeronautical Journal, vol 118, no. 1201.

[39] Howe, M.S., 1999. Review of the theory of the compression wave generated when a high-speed train enters a tunnel. Proceedings of the Institution of Mechanical Engineers Part F: Journal of Rail and Rapid Transit 213, 89–104

[40] Howe M. S., Iida M., Fukuda T., and Maeda T., (2000), 'Theoritical and experimental investigation of the compression wave generated by a train entering a tunnel with a flared portal'. Journal of fluid mechanics, vol. 425, pp. 111–132.

[41] Howe M. S., Iida M., Fukuda T., and Maeda T., (2003), 'Influence of an unvented tunnel entrance hood on the compression wave generated by a high-speed train'. Journal of fluids and structures 17 (2003) 833-853

[42] Khayrullina, B. Blocken, W. Janssen and J. Straathof, "CFD simulation of train aerodynamics: Train-induced wind conditions at an underground railroad passenger platform", Journal of Wind Engineering and Industrial Aerodynamics, vol. 139, pp. 100-110, 2015.

[43] Yeo Zhuan Lun, Peng Cheng Wang, "Numerical Simulation of Train Aerodynamics" Singapore Institute of Technology – University of Glasgow Singapore

[44] Erik Bjerklund Mikael Ohman, 2009, " Stability of High Speed Train under Aerodynamic Excitations" Department of Applied Mechanics Division of Dynamics and Division of Fluid Mechanics CHALMERS UNIVERSITY OF TECHNOLOGY

[45] Abel Demisse MSc, 2015 "Stability of trains under aerodynamic excitation for AALR" Addis Ababa University Technology Faculty School of Mechanical and Industrial Engineering. Addis Ababa Ethiopia.

[46] ANSYS. Fluent 6.3 User's Guide. Fluent Inc., 2009

[47] L. Davidsson. "An Introduction to Turbulence Models". Department of Thermo and Fluid Dynamics. Chalmers University of Technology, 2003

[48] W. Malalasekera H. K, Versteeg. "An introduction to Computational Fluid Dynamics the Finite Volume Method". Pearson Education Limited, 2007

[49] Jesper Marklund. "Minimize vortex drag of a passenger car". 2010

[50] C.D. Scott-Pomerantz. "The K-Epislon Model in the Theory of Turbulance". Doctoral Thesis, 2004.

[51] Frank M.White. "Fluid mechanics sixth Edition". McGraw-Hill International Edition, 2008.

[52] ANETTE WALL, "Simulating the Volvo Car Aerodynamic Wind Tunnel with CFD". , Master's Thesis in the Automotive Engineering Master's Programme, Department of Applied Mechanics, Division of Vehicle Engineering & Autonomous Systems, Chalmers University of Technology

[53] The Numerical Computation of Turbulent Flows – Launder, B.E. And Spalding - 1974

[54] Jiyuan Tu, Guan Heng Yeoh and Chaoqun Liu, "Computational Fluid Dynamics: A Practical Approach", Butterworth-Heinemann; 1St edition, Burlington, MA, November 2007

[55]. Oleg Zikanov, "Essential Computational Fluid Dynamics", John Wiley & Sons, Inc. Hoboken, New Jersey, March 2010

[56]. European Standard Draft prEN 14067-5, "Railway application – Aerodynamics – Part5: Requirements and test procedures for aerodynamics in tunnels", Comité Européen de Normalisation, Brussels (CEN), (2003).

[57] "Aerodynamic Characteristics and Aerodynamic Shape Optimization Of Ethiopian National Train, Case Study On Addis Ababa Dire Dawa Passenger Train" By Mamo Nigusie, 2014, Addis Ababa, Ethiopia.

[58] *"K-epsilon models -- CFD-Wiki, the free CFD reference", Cfdonline.com, 2011. [Online]. Available: http://www.cfdonline.com/Wiki/K-epsilon_models. [Accessed: 16- Mar- 2016].*

[59] Baker, C., (2014), 'A review of train aerodynamics, part 1—fundamentals' The Aeronautical Journal, vol 118, no. 1201.

[60] Baron, A., Mossi, M., Sibilla, S., 2001. The alleviation of the aerodynamic drag and wave effects of high-speed trains in very long tunnels. J. Wind Eng. Ind. Aerodyn. 89, 365–401

[61] Solomon Asmamaw, 2016. Effect of aerodynamic drag on performance of high speed train. Addis Ababa University Technology Faculty School of Mechanical and Industrial Engineering. Addis Ababa Ethiopia.

[62] Kwon, H.B., Nam, S.W., Kwak, J.H., 2009. Assessment of the pressure trainsient inside the passenger cabin of high-speed train using computational fluid dynamic. Conf. Korean Soc. Railway 12, 65–71

[63]. Tian H.Q. "Formation mechanism of aerodynamic drag of high-speed train and some reduction measures." J. Cent. South Univ. Technol. (2009) 16: 0166−0171, DOI: 10.1007/s11771−009−0028−0.

[64]. Orellano A. (Dr.) "Aerodynamics of high speed trains." Stockholm, KTH, 2010, Germany.

[65] Ethiopian Railways Corporation, Operations and Services Division, Equipment Supply and Technical Services Department, "Operations and Services Division Equipment Supply and Technical Services Department Rolling Stocks Specifications''

[66]Cross, D., Hughes, B., Ingham, D., Ma, L., 2015. A validated numerical investigation of the effects of high blockage ratio and train and tunnel length upon underground railway aerodynamics. J. Wind Eng. Ind. Aerodynam. 146, 195–206.

http://dx.doi.org/10.1016/j.jweia.2015.09.004

http://www.sciencedirect.com/science/ article/pii/S0167610515002202

[67] Choi, J.K., Kim, K.H., 2014. Effects of nose shape and tunnel cross-sectional area on aerodynamic drag of train traveling in tunnels. Tunnell. Undergr. Space Technol. 41, 62–73.

http://dx.doi.org/10.1016/j.tust.2013.11.012

http://www.sciencedirect.com/science/article/pii/S088677981300196X.

[68] Schetz J.A. "Aerodynamics of high-speed trains." Annu. Rev. Fluid Mech. 2001. 33:371– 414.

[69] "Swissmetro : aerodynamic drag and wave effects in tunnels under partial vacuum", Michele Mossi , Stefano Sibilla, 2015.

[70] . Li Y.F., et al. "Aerodynamic drag analysis of double-deck container vehicles with different structures."J.Cent.South Univ. Technol.(2011181311−1315DOI: 10.1007/s11771−011−0838−8.

[71] International Union of Railways, 2005. Determination of railway tunnel cross sectional areas on the basis of aerodynamic considerations, Paris, France. (http://uic.org).

[72] ''AERODYNAMIC LOADING OF TRAINS PASSING THROUGH TUNNELS'' Dr Fathi Tarada, Forest Row, UK, Ivo Stieltjes

APPENDICES

Appendix I: Specification of ENT Passenger Car and Locomotive

1. Technical Specification for Electric Freight/ Passenger Locomotive 7200 KW AC

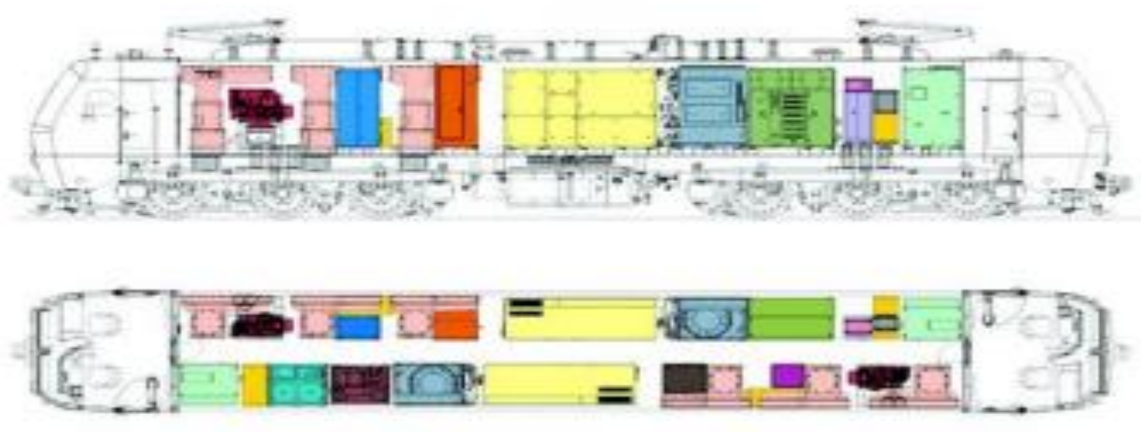

Appendix I-1: HXD1C high power AC drive Six-axle (7200KW) Freight Electric

The following table shows some of the technical specifications of HXD1C locomotive specification.

Appendix I-2: HXD1C locomotive of passenger car

Appendix I-3: Interior layout drawing of passenger train

Appendix II: Drag and Lift convergence history of a passenger train at speed of 120Km/hr [57]

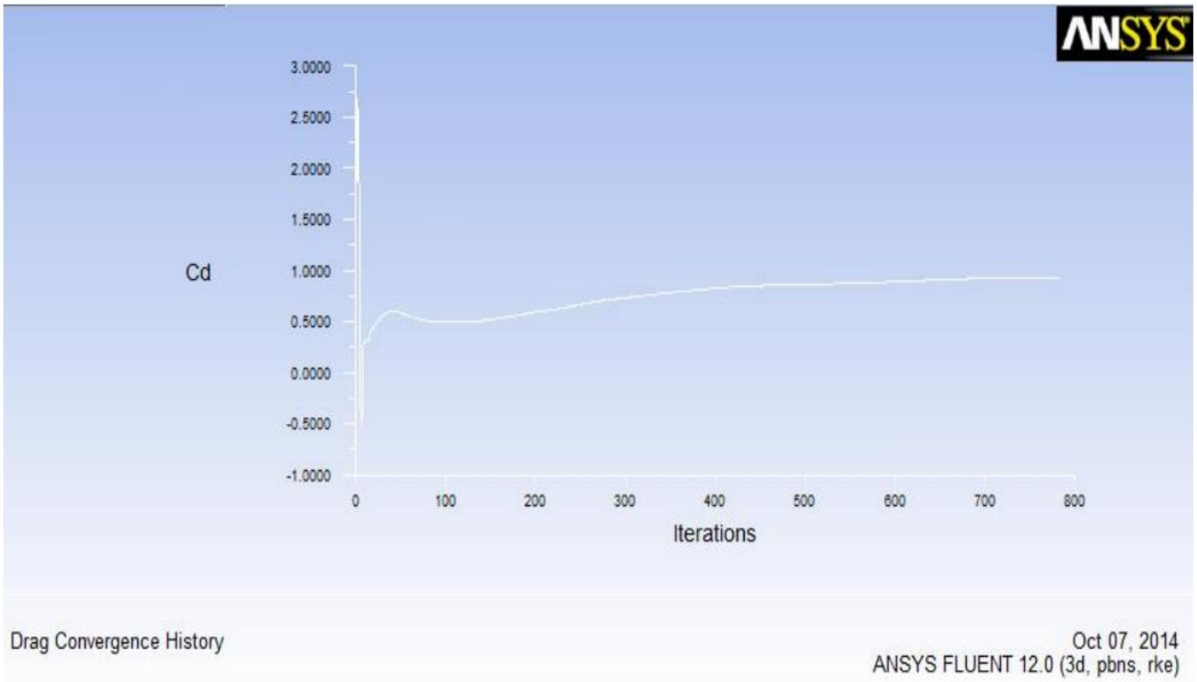

Appendix II-1: Drag convergence history of aerodynamic Simulation of the Train With-out the effect of Cross-wind (α=0) at train speed of 120 km/hr (34m/s) [57]

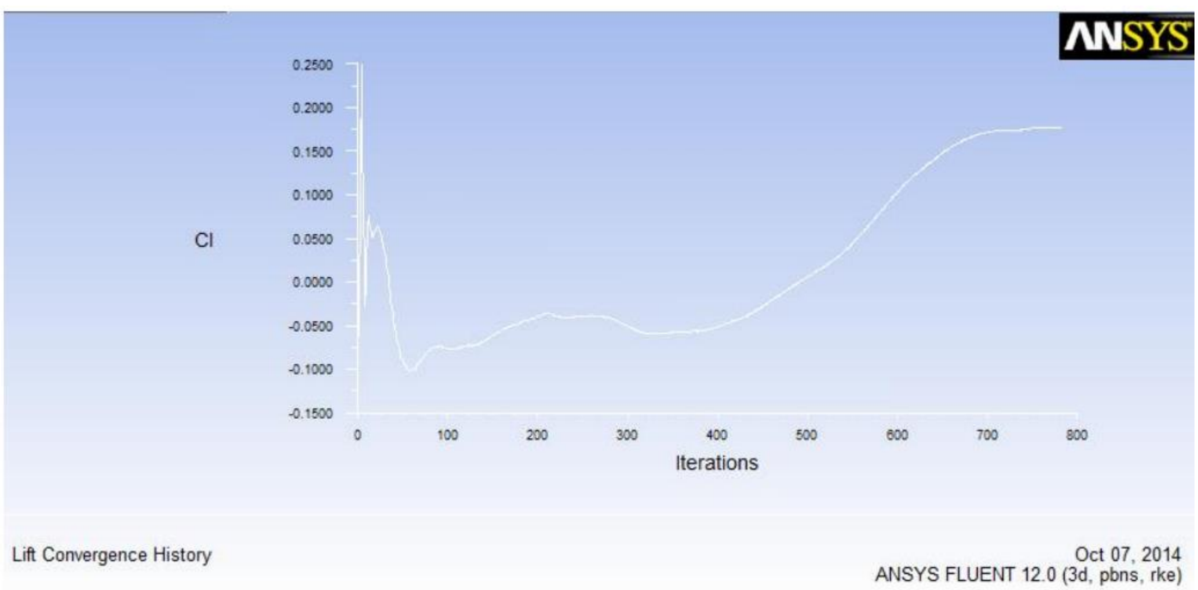

Appendix II-2: Lift convergence history of aerodynamic Simulation of the Train With-out the effect of Cross-wind (α=0) at train speed of 120 km/hr (34m/s) [57]

Appendix III: Simulation result of Pressure Variation along the train body on different train position relative to tunnel [43]

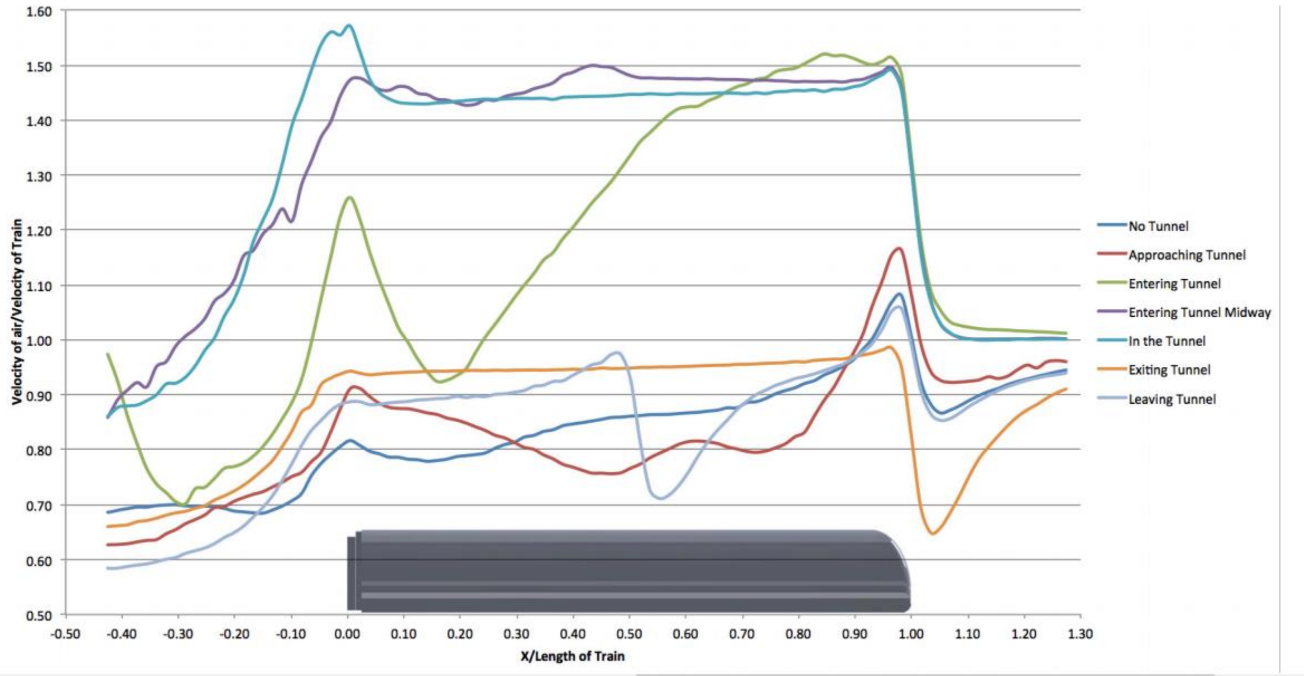

Appendix III: Simulation result of Pressure Variation along the train body on different train position relative to tunnel, at a train velocity of 38.9 m/s (140km/h), tunnel length of 50m and blockage ratio of 36.88% [43].